Design and Evaluation of Solar and Geothermal Energy Systems Integrated with Cu-Cl Cycle

by

Mert Temiz

A thesis submitted to the
School of Graduate and Postdoctoral Studies in partial
fulfillment of the requirements for the degree of

Master of Applied Science in Mechanical Engineering

Faculty of Engineering and Applied Science
University of Ontario Institute of Technology (Ontario Tech University)
Oshawa, Ontario, Canada
September 2020

Thesis Examination Information

Submitted by: **Mert Temiz**

Master of Applied Science in **Mechanical Engineering**

Thesis title: Design and Evaluation of Solar and Geothermal Energy Systems Integrated with Cu-Cl Cycle

An oral defense of this thesis took place on August 13, 2020, in front of the following examining committee:

Examining Committee:

Chair of Examining Committee	Prof. Dr. Martin Agelin-Chaab
Research Supervisor	Prof. Dr. Ibrahim Dincer
Examining Committee Member	Prof. Dr. Bekir Sami Yilbas
Examining Committee Member	Dr. Ahmad Barari
Thesis Examiner	Dr. Sayyed Ali Hosseini

The above committee determined that the thesis is acceptable in form and content and that a satisfactory knowledge of the field covered by the thesis was demonstrated by the candidate during an oral examination. A signed copy of the Certificate of Approval is available from the School of Graduate and Postdoctoral Studies.

Abstract

This thesis study proposes solar and geothermal based three multigeneration systems. System 1 consists of a bifacial photovoltaic (BiPV) plant, multi-effect distillation (MED) desalination unit and, proton exchange membrane (PEM) electrolyzer. Systems 2 and 3 additionally consist of the copper chlorine (Cu-Cl) thermochemical hydrogen production cycle integrated with a concentrated solar power (CSP) and supercritical geothermal systems, respectively. Electricity, freshwater, hydrogen, and space heating are produced as useful outputs for the communities in Gokcebayir in Turkey, Geyser in the United States, and Shinozaki in Japan. All of the proposed systems are designed, modeled, and analyzed with hourly sensitive annual simulations. According to the results, the highest overall energy efficiency is calculated for system 2 as 27.4%, and the highest overall exergy efficiency is calculated for system 3 as 18.6%. Integration of the Cu-Cl cycle with solar and geothermal based systems is led to prevent waste production and achieve sustainability goals.

Keywords: solar; geothermal; hydrogen; Cu-Cl cycle; exergy

Author's Declaration

I hereby declare that this thesis consists of original work of which I have authored. This is a true copy of the thesis, including any required final revisions, as accepted by my examiners.

I authorize the University of Ontario Institute of Technology (Ontario Tech University) to lend this thesis to other institutions or individuals for the purpose of scholarly research. I further authorize University of Ontario Institute of Technology (Ontario Tech University) to reproduce this thesis by photocopying or by other means, in total or in part, at the request of other institutions or individuals for the purpose of scholarly research. I understand that my thesis will be made electronically available to the public.

MERT TEMIZ

Statement of Contributions

Part of the work described as multigeneration system 1 is published as:

Temiz M, Dincer I. Techno-Economic Assessment of Bifacial Photovoltaic and Geothermal Based Multigeneration System for Cleaner Communities. Journal of Cleaner Production 2020;275:122879. doi:10.1016/j.jclepro.2020.122879.

Acknowledgements

First of all, I wish to express my deepest gratitude to my supervisor, Prof. Dr. Ibrahim Dincer for his endless support, guidance, and tolerance. His extraordinary dedication played a critical role as a motivation source and it influenced me to try my best for my research and studies.

I would like to thank my entire family and friends. Their endless support and encouragement is one of the major driving forces to pursue my studies. It is hard to describe their massive contributions and value for me.

I would like to express my gratefulness to my former supervisor Dr. Nader Javani and former employer Prof. Dr. Haluk Ors. Their insightful guidance prepared me and illuminated my path for my further studies and works.

Also, I would like to thank all my friends and colleagues from Ontario Tech who always trusted and supported me during my journey. Every single person in ACE 3030B was very helpful, friendful, and very supportive during my time at Ontario Tech.

Table of Contents

List of Tables

List of Figures

Nomenclature

E	total energy (kJ)
ex	specific exergy (kJ/kg)
$\dot{E}x$	exergy rate (kW)
F	Faraday constant (C/mol)
G	Gibbs free energy (J)
g	gravitational acceleration (m s^{-2})
h	specific enthalpy (kJ/kg)
LHV	lower heating value (kJ/kg)
$\dot{m}$	mass flow rate (kg/s)
$\dot{N}$	molar flow rate (mol/s)
P	pressure(kPa)
Q	heat (kJ)
$\dot{Q}$	heat rate (kW)
S	total entropy (kJ /K)
s	specific entropy (kJ/kg K)
$\dot{S}$	entropy rate (kW/K)
T	temperature (^{o}C)
V	overpotential (V)
w	water, work
$\dot{W}$	power generation rate (kW)
X	mass ratio of component

Subscripts

c	compressor
com	community
cv	control volume
d	destruction
El	electrolysis
f	fresh

gen	generation
Gh	Greenhouse
GH	Global Horizontal
Hy	hydrolysis
HX	heat exchanger
i	inlet
MC	mixing chamber
o	outlet
P	pump
s	saline
T	turbine
TL	thermolysis
TV	throttling valve
W	water

Greek Letters

γ	specific heat ratio
η	efficiency
Δ	difference

Acronyms

AC	alternative current
BAPV	building attached photovoltaic
BIPV	building integrated photovoltaic
BIPV/T	building integrated photovoltaic/thermal
BiPV	bifacial photovoltaic
CdTe	Cadmium telluride
Comp	compressor
CSP	concentrated solar power
Cu-Cl	Copper chlorine
DC	direct current
EES	engineering equation software

EGS	enhanced geothermal system
HVAC	heating, ventilating and air-conditioning
Csa	hot-summer Mediterranean climate
HOMER	hybrid optimization model for multiple energy resoucrs
IDDP	Iceland Deep Drilling Project
IEC	International Electrochemical Commission
LCOE	levelized cost of electricity
MC	mixing chamber
MED	multi-effect distillation
NASA	National Aeronautics and Space Administration
NASA-SSE solar energy	National Aeronautics and Space Administration surface meteorology and
NREL	National Renewable Energy Laboratory
ORC	organic Rankine cycle
PTC	parabolic trough collector
PV	photovoltaic
PV/T	photovoltaic/thermal
PV-DCBM	photovoltaic-direct current building module
PEM	proton exchange membrane
SAM	System Advisor Model

Chapter 1. Introduction

1.1 Energy and Environmental Issues

Fossil fuels and industrialization have led to achieving countless challenges and have made remarkable improvements such as mobility and illumination to our civilization for over 200 years. The existence of rich energy has resulted in enhanced agricultural activities, improved transportation, rapid industrialization, therefore, urbanization and better quality of life [1]. In 1859, commercial fossil oil was established for the first time, and the energy industry entered a new era where internal combustion engines started to dominate as the prime mover from human labor, animals, waterwheels, and turbines, windmills, steam engines, and steam turbines. At that time, commercial fossil oil utilization was seen even as an environmentally benign establishment, since fossil oil can substitute the whale oil, therefore, whales and the environment have had benefits as a result of the tightened whaling industry and whale hunting [2]. But thereafter, climate change became one of the major issues, not only for the whales but this time for the entire planet earth. Fossil fuels and industrialization are the major contributors to greenhouse gas (GHG) emissions which lead to retain more heat than regular by Earth's atmosphere.

GHG emissions have resulted in remarkable anthropogenic contributions. CO_2 from fossil fuel and industrial processes represent 65% of the annual anthropogenic greenhouse gas emissions. The atmospheric concentration of CO_2 has risen at an accelerated rate for over 200 years. During the ice ages and interglacial periods, CO_2 concentrations were getting low and high. However, its previous historic peak was around 300 ppm [3]. In 2018, CO_2 concentration has reached 407.2 ppm and it keeps rising.

Energy utilization behavior has been affected by climate change. Air temperature and humidity are the main drivers of air conditioning usage. Therefore, an increase in the air temperature is reflected as growing cooling demand [4]. Likewise, drought periods will be reflected as rising irrigation demand, especially during growing seasons. Climate change related energy demand is expected to grow by 25-58% if there is no adaptation by around 2050 [5].

Also, socioeconomic factors have a remarkable impact on the energy usage behavior. Human society tends to have a larger population, better life quality, a larger economy, and greater mobility. This tendency leads to inevitably growing global energy demand [1].

In 2018, world's primary energy demand reached its highest annual amount by growing 2.3% since 2010. World's largest energy consumers, namely, China, the United States, and India contribute nearly 70% towards the global energy growth. In order to look at the global energy production from 2000 to 2018, the share of fossil fuels has risen from 80% to 81% and renewables with hydro have doubled its production capacity [6].

On the other hand, climate change possesses a threat to energy security. The coastal energy infrastructures are at risk due to melting ice and rising sea and ocean levels. While climate change reducing water availability and increasing temperatures, thermoelectric power plants are suffering reduced cooling efficiency by cause of the relatively high ambient temperatures and reduced water flow by cause of the water scarcity. Even electric power transmission systems are at risk since higher temperatures cause less efficient operations and possess a high risk of physical damage. These are basically vulnerabilities in the energy sector [7].

Although renewable energy transition is a necessity, the implementations on this path need tremendous efforts on massive infrastructure changes and integrations [8]. This transition and implementations of developments in the energy industry are not similar to information technology or biotechnology. The time scale is very different in the energy industry likewise the construction sector. Digital transformation has happened in the blink of an eye in contrast with the renewable energy transition. Digital businesses became huge in a very short time since there is no physical infrastructure needed [9].

One of the most challenging hurdles is to make faster renewable energy transition possible while attracting scientists, businesses, and politicians for research, investments, and intensives with state-of-art energy systems.

1.2 Solar Energy

It is unthinkable that any society can maintain its life without solar energy. It is a fundamental energy source, which enable plants to produce all of the food that all humans

and animals need [1]. The utilization of solar radiation started more than 2500 years ago. The ancient Greeks used to face their houses to the south to exploit solar radiation for space heating especially during winter [10]. NASA used solar PV for the first time on its Vanguard satellite, in 1958. It was used for six years having a total capacity of 1-watt. Solar PV was not cost-effective in the beginning, it was mainly used for space missions during the 1960s. The oil crisis in 1973 impacted the solar PV research and developments, which resulted in application of solar PV over small rooftops and for off-grid telecom systems. With higher investments, solar PV cell prices dropped between 1980 and 1990 from 32$/W to 9$/W. Solar PV has gained its popularity with recent policy supports, incentives, and feed-in-tariffs [11]. Recently, solar PV module prices have reduced to 0.21$/W which is highly cost-effective as in Q1 2020 in the United States.

As a renewable energy alternative solar energy has successfully attracted businesses since more solar power plants are added than all nuclear and fossil fuel power plant additions in 2019. In comparison with other renewables, solar energy additions were nearly twice of wind and more than all renewable energy power plants combined in terms of energy capacity. Annual solar power capacity additions were reached 100GW in 2018 and these were 117GW for 2019. However, solar power is still representing a small share in comparison with other types of power generation systems. In 2015, the total share of solar power generation was only 1% of total power generations and it was more than doubled in 2018 where the solar power generation share was 2.2%. Today, over 630GW solar capacity have installed globally, which represents 2.6% of total power generation capacity [12].

Solar energy conversion can be made via PV plants and CSP plants. Generally accepted concentrating solar power plant types are parabolic through, central receiver power tower, linear Fresnel reflector, and parabolic dish. CSP plants convert solar energy to thermal energy for direct or indirect operation. The upside of CSP technology is its compatibility with thermal energy storage systems. While CSP technology offers easy integration with thermal energy storage systems, therefore, flexibility and dispatchability requirements of grids can be achieved in contrast with solar PV technology. However, solar PV technology possesses highly cost-competitive market availability. Therefore, solar PV

plants were mainly dominated the solar energy generation as 592TWh electricity generation in 2018, on the contrary, CSPs were generated 12TWh electricity during 2018.

In terms of availability, the nature of solar radiation possesses intermittency due to periodic and aperiodic conditions and weather circumstances. Therefore, solar energy can not be used as a single supply solution in continuous demands. When the need arises, deficit power should be compensated via alternative flexible energy generation system; moreover, in case of solar power generation plant produces excess electricity, utilization of excess power can be made via an energy storage medium.

1.3 Hydrogen Energy

Currently, the majority of hydrogen demand is occurring for chemical process where hydrogen is used as processing agents. However, hydrogen energy systems possess an effective solution for intermittent renewable energy, therefore, environmentally benign and sustainable hydrogen as a fuel can be replaced with fossil-based fuels [13].

The conversion process of available energy into hydrogen fuel is mainly occurring via fossil-based methods nowadays, such as steam reforming or coal gasification. In terms of greenhouse gas emissions, the natural gas steam reforming process emits 11,888 g CO_2 equivalent per kg of net produced hydrogen [14]. Moreover, coal gasification methods emit double CO_2 in comparison with steam reforming processes [15].

In order to produce hydrogen in an environmentally benign and sustainable manner, recovered energy, low carbon methods or renewable energy resources should be utilized with suitable methods.

According to the International Energy Agency, hydrogen production and transportation costs will achieve feasibility and sustainability goals. Green hydrogen as a fuel source will be more cost-competitive both from production and transportation aspects. Figure 1.1 shows the estimated production and transportation costs of hydrogen. Carbon capturing methods possesses a commercially viable alternative hydrogen production method. Also, off-grid renewable methods possess an environmentally benign alternative.

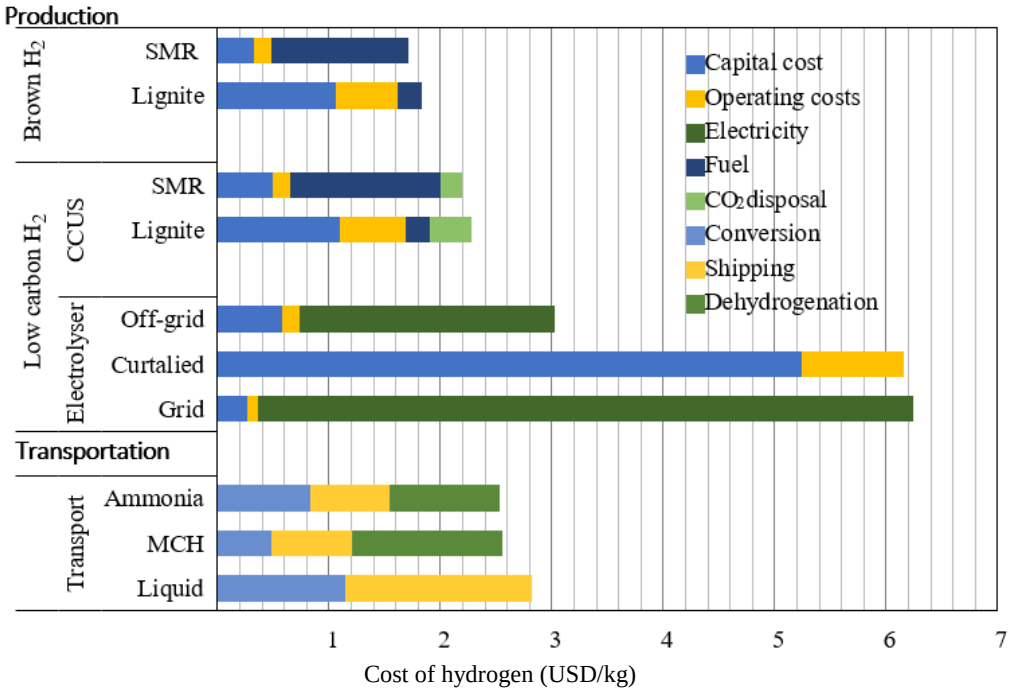

Figure 1.1 Estimation of hydrogen production and transportation costs from Australia to Japan in 2040 (data from [16])

On the transportation side, ammonia possesses a good hydrogen carrier among other alternatives. On the other hand, the hydrogen economy has momentum. Figure 1.2 shows the fast development of hydrogen as a fuel especially between 2030 and 2040 where 10 times growing is projected to occur.

Hydrogen has various roles in order to decarbonize processes and sectoral applications. No GHG emissions occur during the hydrogen combustion. It stores a high energy per unit mass in comparison with other fuels and energy storage methods. It can be used as a feedstock or chemical substance in different applications. There are available applications for hydrogen usage as an energy source in the industry such as iron and steel production [17].

1.4 Geothermal Energy

Geothermal energy has contributed to global electricity generation with 90TWh of annual production in 2018, which represents 0.33% of the total global electricity generation [6]. However, it is a common practice to employ geothermal energy for heating. While 0.32% of heat consumption is met by geothermal in 2012, 0.62% of the total energy consumption

for heat is met in 2018. 82% growth occurred from 2013 to 2018 in geothermal share at the total energy supply for heat, which is the biggest growth among all the renewables [11].

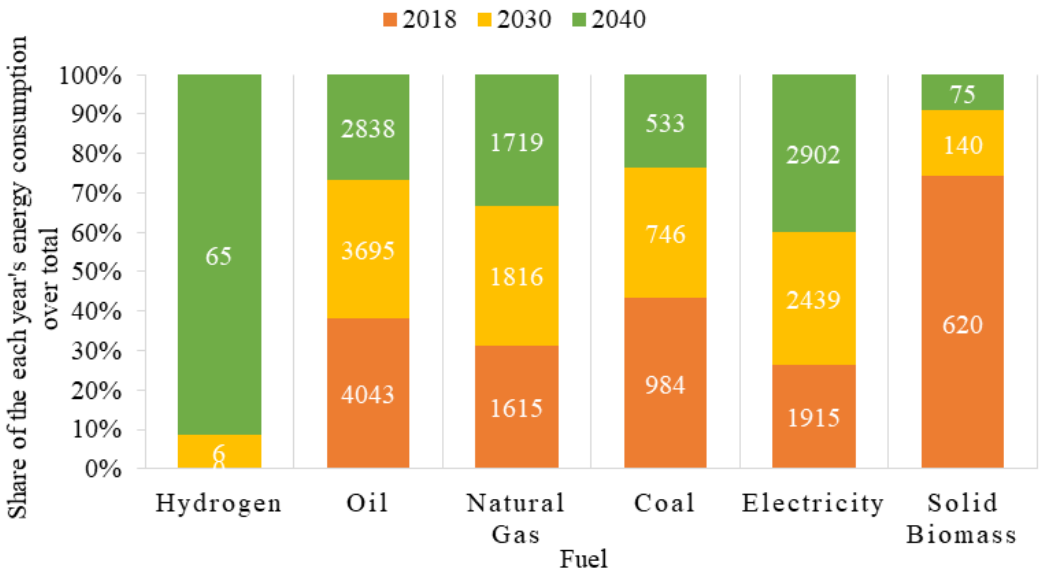

Figure 1.2 Final energy consumption by fuel (amount of fuel in Mtoe) (data from [6])

1.5 Motivation

Energy-related issues are one of the most challenging hurdles for today's society. Although energy is one of the main drivers of modern society, fossil-based fuel combustion causes anthropogenic climate change and possesses energy security risks. Research for alternate energy options shows that there is no single solution to surmount all of the energy-related hurdles. Renewable sourced energy generation systems produce environmentally benign and sustainable energy. However, the commercial viability of these systems is questionable. Intermittent availability of renewables is one of the major challenges which possesses negative effects on grid flexibility which prevents to meet the desired energy on time. Current storage systems are not in the desired state in terms of feasibility and commercial viability for large-scale applications.

For the aforementioned reasons, it is very crucial to develop multigeneration systems. Multigeneration systems utilize renewable resources to produce and to store useful outputs until whenever these useful outputs desired from the demand side for consumption. In this aspect, the Cu-Cl thermochemical cycle is a potential alternate fuel production method by utilizing high-grade thermal energy which can be gained from solar, geothermal, or nuclear

resources. However, the commercial viability of these systems is not in the desired condition. In terms of enhancing the feasibility and commercial viability of the Cu-Cl cycle, integrating and assessing various techniques is very crucial.

1.6 Objectives

This thesis study primarily focuses on the integration of the Cu-Cl thermochemical hydrogen production cycle with solar and geothermal sources. The three proposed systems consist of different thermal energy incorporation methods for the Cu-Cl cycle and different hydrogen production methods.

In this regard, the specific objectives of this thesis study are following:

- To design multigeneration systems that utilize renewable resources. Proposed multigeneration systems utilize solar, geothermal and sea resources to produce hydrogen, electricity, space heating, and freshwater as useful outputs via BiPV plant, supercritical geothermal system, multi-effect distillation (MED) desalination unit, and Cu-Cl thermochemical hydrogen production cycle subsystems.
- To propose renewable high-grade heat supply systems for thermal requirements of the Cu-Cl cycle. Supercritical geothermal system and parabolic trough CSP plant are used for their high-grade heat supply capabilities.
- To analyze the proposed multigeneration systems realistically. Thermodynamic analyses are conducted both energetically and exergetically. PVsyst, Aspen Plus, and hybrid optimization model for multiple energy resources (HOMER) Pro simulation programs are used to obtain detailed data for each subsystem and each load from the demand side. Hourly analyses have been simulated for a year to reach more realistic results.
- To conduct cost comparison methods for each useful output in the proposed systems.
- To apply different operating conditions to find their effects on subsystems and overall system performances. Parametric studies are performed for some of the subsystems and overall system.

Chapter 2. Literature Review

A detailed literature review is provided about green hydrogen production methods especially thermochemical cycles, solar photovoltaics, and concentrated systems, geothermal systems particularly enhanced geothermal systems (EGS), ammonia trilateral Rankine cycle.

Dincer [18] comprehensively discussed future energy use and related environmental issues and presented potential alternatives to the current environmental issues such as renewables.

Dincer and Acar [19] investigated clean energy solutions for better sustainability. They discussed opportunities and comparatively assessed various energy sources by considering their technical, economic and environmental potential and performance. They also presented and discussed multigeneration systems. They confirmed the advantages of integrated systems with multiple outputs by cause of reduced energy demand, reduced emissions, lower system cost, and reduced waste of energy and exergy.

Solar photovoltaic systems are the fastest growing photovoltaic technology amongst others [6]. Joshi et al. [20] reviewed the photovoltaic and photovoltaic thermal systems. They classified the photovoltaic systems in accordance with their applications. They analyzed the performances of photovoltaic and photovoltaic thermal systems electrically, thermally, energetically and exergetically.

Zhang et al. [21] reviewed CSP plant technologies and have presented methodologies to predict hourly direct irradiations from the available monthly averages data. The potential of the CSP plants was presented in order to provide accurate design background.

Bifacial solar photovoltaic technology is one of the recent technologies thatis available recently as commercial solar PV module type with its cost-effective state on the global PV market. Bifacial solar photovoltaic technology was examined comprehensively by Guerrero-Lemus et al. [22]. They investigated research and development opportunities and contributions of bifacial solar photovoltaic technology to the rapidly growing global solar market. Improved conversion efficiencies as a result of front and back side energy harvesting, module reliability, improved cell efficiencies were emphasized. They

suggested a standardized certification procedure in order to expend the applications and to assure enhanced performance.

Branker et al. [23] investigated the evaluation method of photovoltaic projects, namely, the levelized cost of electricity, in order to provide clarity on proper calculations. They focused on justifications, assumptions, and completeness degrees to avoid varying and contradictory results while comparing technologies, therefore, they aimed to provide a more reliable comparison method while PV becoming an economically advantageous renewable source of electricity.

Fuqianq et al. [24] investigated CSPs particularly parabolic trough CSPs, comprehensively. They focused on common heat transfer fluids, comprehensive derivation process, and heat transfer methods. They listed and reviewed current and future parabolic through collector CSP projects.

In order to reach the flexibility and dispatchability goals of grid systems, or to surmount intermittency hurdles, thermal energy storage systems have the key role for the energy storage options of the CSP systems. Gonzalez - Roubaud et al. [25] investigated steam accumulator, molten salts, and reviewed their applications in commercial thermal energy storage systems. They provided particular economical comparison methods for each thermal energy storage system, separately. They focused to compare thermal energy storage system options by calculating their levelized cost of electricity in a 100MW Rankine cycle with different plant and storage options which varies between 1h and 9h of operation capacity.

Prieto et al. [26] reviewed the CSP storage option, thermochemical storage technology. Different thermochemical storage technologies were reviewed, summarized, and compared. They focused on three redox reactions, perovskite-type hydrogen production, sulfur-based cycles, metal oxide non-redox cycles.

EGS is the recent geothermal technology that enhances energy efficiency. Especially large-scale applications of EGS possesses better efficiency in comparison to convetional techniques. Breede et al. [27] systematically reviewed EGSs and their both commercial and research applications. They showed that geothermal system projects are not typical due to

environmental conditions therefore, there are various potential financial risks and challenges for different geothermal system projects. They showed that the current status of the EGS is still on a learning curve.

Olasolo et al. [28] presented a general overview of EGSs from its start point to today's status. They analyzed the development of an enhanced geothermal plant, seismic challenges on fluid injection processes, optimization methods, and other aspects. They listed existing literature, projects, and methods both for current and future.

Efforts are started from the 19th century on the utilization of heat to obtain power by Carnot [29], Clausius [30], and Rankine [31]. Smith [32] presented fundamental considerations for the development of the trilateral cycles. Recovering power from low-temperature hot liquid streams was analyzed in detail. Smith and Silva [33] investigated the power output and effect of fluid mixtures for the development of the trilateral cycles. They listed several classes of mixtures in order to find suitable working fluid and have considered in several aspects such as toxicity and cost-effectiveness. Smith et al. [34] studied high-efficiency two-phase screw expanders. Development of the trilateral flash cycle systems with the right working fluid and expander choices were presented due to their long period and comprehensive investigation.

Fischer [35] compared trilateral and organic Rankine cycles. Optimized systems were considered with water for the trilateral and pure working fluids for the organic Rankine cycle systems. A comprehensive literature review was presented and optimized case studies were performed.

Zamfirescu and Dincer [36] performed a thermodynamic analysis of the trilateral Rankine cycle with ammonia and water mixture with a positive displacement expander. They investigated the opportunity and have presented the benefits of the proposed system. They compared the proposed optimized cycle with organic Rankine and Kalina cycles.

In order to pursue renewable energy transition, intermittency of renewable sources and transportation of collected and transformed energy hurdles should be surmounted. Hydrogen is a potential energy carrier medium alternative. However, major global demand of hydrogen is related with its usage as a chemical substance. Hydrogen demand for fuel

purposes is behind the chemical substance purposes. Whether for the chemical substance demand or for the fuel demand, hydrogen production is mainly derived by steam reforming or coal gasification processes which have the high CO_2 emission rates. As a potential alternative, green methods for hydrogen production were discussed by Dincer [13]. Several methods were analyzed and assessed in order to compare these processes. Methods and practical applications were studied with case studies.

Dincer and Acar [37] examined different hydrogen production methods and compared them due to their environmental impact, economic factors, and energy efficiency and exergy efficiency. They also presented the relations between economic and environmental factors via the social cost of carbon concept. They presented thermochemical cycles especially hybrid ones as one of the most promising potential solutions in environmental and economic aspects.

Rosen [38] reviewed thermochemical hydrogen production methods. Recent developments in non-fossil driven hydrogen production methods were described, not comprehensively but particularly highlighted selected methods and focused on them. Among the other thermochemical methods, the Cu-Cl thermochemical cycle was emphasized. A case study was conducted for the Cu-Cl thermochemical cycle.

2.1 Integrated Solar Energy Systems

1973 oil crisis was initiated the seeking of alternative energy, thereafter, Three Mile Island and Chernobyl accidents, and public opinion against the nuclear was led to a trend of the development of solar energy utilization [11]. Currently, the main motivation of solar energy development is to maintain energy security and to reach the zero-emission energy production goal in order to prevent climate change [7].

Photovoltaic cells absorb the sunlight; therefore, photons excite the electrons in the semiconducting material and convert them into negative-positive electron-hole pairs. These electron-hole pairs induce to separate; therefore, electrons shift to one of the electrodes and holes move the other electrode. Therefore, the electric current can be generated [39]. Crystalline silicon cells are dominating the global PV market in virtue of its cost-effectiveness.

Thermodynamic efficiency for the ideal solar cell is around 31%. Currently, available PV modules in global PV market have around 19% efficiency. Although either mono or poly, crystalline silicon cells are dominating the PV industry, amorphous silicon, nanocrystalline silicon, procrystalline silicon; and non-silicon, such as cadmium telluride (CdTe), copper indium selenide solar cells are other types of PV technologies that sharing the global PV market [40].

In order to exploit excess energy, photovoltaic/thermal (PV/T) and BiPV module technologies are enhancing the electrical energy production. There are studies available, which aims the performance assessment of photovoltaic thermal modules. Kumar and Rosen [41] reviewed photovoltaic-thermal solar collectors for air heating purposes. They discussed the technology and recent developments, particularly for air heating applications. They presented findings which, photovoltaic thermal systems can increase the electrical output up to 10% in comparison with photovoltaic modules, besides the increased electrical output, generated heat is another useful output of photovoltaic thermal systems, some types of photovoltaic thermal hybrid systems can produce up to 300% more thermal energy than equivalent electrical energy, photovoltaic thermal systems emits less carbon as a hybrid system rather than two separate systems.

Joshi et al. [42] studied hybrid PV/T systems. They reached 33 to 45% energy efficiencies. They showed that their proposed system have up to 45% energy efficiency increment in comparison with commercial PV modules. In terms of exergy efficiency, they presented their findings as from 11% to 16% range of exergy efficiency. Since the thermal system integration allows cooling and utilization of excess heat, both PV electrical conversion and total energy conversion efficiencies are increasing.

Joshi et al. [43] compared glass-to-tedlar and glass-to-glass PV modules for their hybrid photovoltaic thermal systems. The thermal performance of both systems were analyzed and compared. They presented their findings in which overall thermal efficiency was found up to 47% for glass to glass and up to 45% for other systems. In terms of thermal and electrical combined efficiency, the glass-to-glass system showed a better performance, which was around 2% increased efficiency in contrast with the glass-to-tedlar system.

Rosell et al. [44] integrated low solar concentration technologies with PV/T system. Linear Fresnel concentrator was coupled with PV/T collector. Low concentration rates were applied for the proposed system. In comparison with up to 20% commercial solar PV module solar energy conversion efficiency, 60% overall energy efficiency is achieved with the proposed system when the concentration ratio is above six suns.

Zhao et al. [45] studied both non-concentrated and concentrated PV/T system. Silicon solar cell-based photovoltaic module and direct absorption collector are integrated. A genetic algorithm was used to determine optimum solar radiation spectrum and concentration. Working fluid properties were also optimized in order to reach both maximum transmission of the visible light and the maximum absorption of the solar infrared radiation. Their findings showed that optimized working fluid is able to absorb 92% of the solar infrared radiation and to transmit 89% of the visible light. They showed that the overall efficiency is around 60% to 67% at the optimized concentrated photovoltaic thermal system where solar irradiance is increased from 800 W/m^2 to 8000 W/m^2. Their system was generated 196°C working fluid and exergetic efficiency has been increased from 12% to 22%.

Agrawal and Tiwari [46] integrated photovoltaic thermal system with building in order to exploit potential renewable energy generation in metropolitan areas. The proposed building integrated photovoltaic thermal system was produced 16209kWh annual electrical exergy and 1531 kWh annual thermal exergy on the $65m^2$ effective rooftop area at 53.7% average overall thermal efficiency.

In order to exploit excess solar energy and convert it to useful output in any form, BiPV technology is a recent technology that received remarkable attention both from commercial and research organizations. The main feature of BiPV modules is to absorb the solar irradiance not only from the front but also from the rear side. Double glass frameless technology provides several advantages such as high durability, better cooling, more resistance to a corrosive environment, etc. Besides its theoretical energy gain, a practical application in Hokuto City, Japan has showed that the 21.9% energy gain has occurred in comparison with conventional monofacial PV power plants [47].

Castillo-Aguilella and Hauser [48] presented the results of various test conditions for bifacial modules. In comparison to conventional PV plants, there are some variables that crucial for the BiPV plant design such as module height, tilt, and the albedo of the ground. BiPV plants were produced from 12.3% to 30% more electricity in comparison with conventional monofacial PV plants in their study. Furthermore, they developed a best fit empirical model according to measured test data.

Stein et al. [49] studied the outdoor performance of the BiPV modules and systems. Their objective was to report BiPV installations and their performance in order to obtain a performance model to predict the energy gain of bifacial plants. They showed that the bifacial gain has been varied especially due to the tilt angle and height of the module. At maximum gain, BiPV plants were produced 27.1% more electricity than the commercial PV plants at 1.8m height and 45° tilt angle, while bifacial gain was 11.7% at its minimum for 30° tilt angle and 0.4m height.

Chudinzow et al. [50] investigated the currently available energy yield models and have determined the areas for development, in order to determine the appropriate energy yield of BiPV plants in comparison to mono-facial PV plants. They used a new model that calculates eight types of irradiances absorbed from BiPV modules, namely, direct normal irradiance, diffuse horizontal irradiance, ground reflected direct normal irradiance and ground reflected diffuse horizontal irradiance both from the front and rear sides. They tested in a case study and have compared ground types. Their results showed that the BiPV plant that was built on dry asphalt has gained less than 6% electricity in comparison with the monofacial PV plant that was built on dry asphalt. On the other hand, the BiPV plant that was built on a white membrane ground field was gained 29% of more energy in contrast with the monofacial PV plant.

Wang et al. [51] developed a comprehensive BiPV model that identifies suitable BiPV module applications and markets with the power and energy yield. Modeling the rear side illumination for module height, module tilt, ground albedo, diffuse radiation, and solar position were attempted. They showed that more than 10% of the bifacial gain is possible for the specified system type.

Valdivia et al. [52] developed a computationally-efficient algorithm for the evaluation of BiPV plant energy yield determination. Their bifacial solar panel model was studied for different system design variations. A ray-tracing approach to sum the direct, diffuse, and albedo components of solar irradiance on the front and rear sides of the PV module was used to calculate the energy yield of BiPV modules and compared with mono-facial photovoltaic modules. Their results showed that the BiPV module is produced 18% more electricity in contrast with the monofacial PV module.

Appelbaum [53] investigated the calculation of the solar field with bifacial panels deployed in multiple rows. Annual incident irradiation on BiPV collectors deployed in rows with an optimal tilt angle was calculated. Two types of deployments as facing south on the east-west direction and facing east on the north-south direction was studied. South facing BiPV modules at an optimum tilt angle were produced 32% more electricity in comparison with vertical east-facing PV modules. Guo et al. [54] investigated vertically mounted BiPV modules and globally compared between BiPV modules facing east-west and mono-facial modules mounted conventionally. They found that the latitude, the local diffuse fraction, and the albedo are strong effects on the radiation received by the PV modules. The albedo requirements were compared with the measured global albedo distribution. A map was developed, which shows the more beneficial configuration as a vertically mounted bifacial module or conventionally mounted mono-facial module for a specific location.

Deline et al. [55] evaluated multiple BiPV plant deployment scenarios with employed data from practical applications and simulations. They provided the expected amount of irradiance in detail. A proposed international standard for the measurement procedure for bifacial modules was motivated their study. They showed that, comparison of outdoor bifacial field measurements with proposed methodologies agreed within 1%-2% for characterization of bifacial modules with the use of conventional laboratory and production-line measurement equipment.

Castillo-Aguilella and Hauser [56] presented the best-fit model that uses the module’s minimum height ratio, tilt angle, and ground albedo to predict the annual energy output of the BiPV plant. For the off-south facing applications, the azimuthal correction

factor for the bifacial energy model was adapted to expand the application area of the proposed model. Their results showed that the difference between modeled results and the third-party data within the range between 2% and 10% in terms of variable uncertainty, between 3% and 4% in terms of accuracy of accepted irradiance models for PV, and between 8% and 15% for the direct normal irradiance component.

In order to increase collected solar radiation, tracking systems are structural solutions for PV plants. Orienting each panel for the daily movement on the north-south axis as east-west motion and for the seasonal movements on the east-west axis as changing tilt angle increases the amount of direct solar radiation. There are two major types of tracking systems as single-axis and two-axis systems. Single-axis systems also have two major application types as horizontal single-axis and tilted single-axis tracking systems. Drury et al. [57] investigated the regional performance of fixed and tracking PV systems in the United States. They studied the relative competitiveness of tracking systems with the fixed and tracking PV price range and evaluated this by region. Their results showed that horizontal single-axis structures can increase electricity generation of PV plants between 12% and 25% in comparison with fixed-tilt systems. Two-axis tracking systems were shown a performance increment between 30% and 45% in comparison with a fixed structure. They showed that tracker systems are cost-effective solutions since tracking PV plants have lower LCOEs in many US regions. Al-Rousan et al. [58] technically reviewed the tracking systems. State-of-the-art tracking systems were compared due to their tracking types, efficiency, performance, and advantages. They categorized the different tracking systems based on the type, technology, and driving methods. Active and passive solar tracking systems were investigated and compared. Kaur et al. [59] presented a low cost active dual-axis solar tracker system and built a lab-scale prototype for further tests. Their results showed that an average power gain occurred as 13.44% compared to a fixed structure PV system. Their low-cost proposed system was used servomotors and cost-effective auxiliary components. In the controlling unit, an inexpensive Arduino Uno was used in their study. Their developed solar tracker was possessed a cost-effective double-axis active tracker system. Another cost-effective Arduino based tracking system prototype was developed by Moron et al. [60]. Their developed prototype was gained 18% energy in comparison with fixed oriented structure. However, some of the tracker structures were

faced with serious incidents that can destroy a PV plant due to the stress created by dangerous winds. Ferroudji et al. [61] presented a new two-axis solar tracker system and simulated and analyzed with the finite element method. Their design satisfied the design requirements at 130 km/h wind speed with 1.18mm maximum displacement and 74.43MPa maximum equivalent stress.

The most common application of the rapidly growing solar industry is the photovoltaic plants. However, terrestrial PV plants require field, therefore occupy a large area of land. On the other hand, a large amount of water bodies are unexploited. Therefore, floating photovoltaic plants are the potential solution to the land requirements of solar energy systems. Sahu et al. [62] reviewed floating PV applications, present status, and various design options. Oceans, lakes, lagoons, reservoirs, irrigation ponds, wastewater treatment plants, wineries, fish farms, dams, and canals were listed as potential water bodies to install floating PV plants to conserve valuable land. Ground-mounted, rooftop canal top, offshore applications were compared with floating solar applications. Among the land conservation, water conservation due to prevent evaporation, performance increase due to the cooling effect of water bodies, less dust effect and improved water quality are other benefits of the floating application. However, floating structure is not durable as ground structures and there are more threats available such as high tides, storms, and waves. They showed that the floating structure increases solar energy gain and reduces water evaporation. Trapani and Santafe [63] reviewed the various floating PV projects. They presented projects from 2009 to 2013 and showed the achievements with megawatt-scale projects. Cazzaniga et al. [64] analyzed the performance of floating photovoltaic systems. Several design solutions were compared in terms of performance and cost-effectiveness. Tracking, cooling, and concentration features of floating PV systems were discussed. The integrated air storage system was discussed as well. Their experimental findings showed that there is an unexploited potential for floating photovoltaic energy gain up to 30%. Liu et al. [65] analyzed the power generation efficiency of floating PV systems and discussed the development of PV technology. Their results showed that cell efficiency is increased between 1.58% and 2% for floating PV systems. They showed that the operating temperatures of floating PV systems can be 3.5°C lower than the terrestrial PV systems. Choi et al. [66] explained the major design elements of a tracking floating PV

system, such as the rotation mechanism of structure, tracking algorithm, the basic concept, and the application plan. They designed the rotation mechanism and tracked the azimuth angle in order to prevent rotation by surface flow. Santafe et al. [67] presented the main design features for floating PV applications on irrigation reservoirs. Prevention of the evaporation from the water reservoir was taken as the main purpose of the floating PV application. Installation costs and performance analysis was presented. Their study showed that 25% of the reservoir's storage capacity was saved in favor of floating PV construction. Temiz and Javani [68] designed and analyzed a hydrogen production system integrated floating photovoltaic system. The main goal of the proposed system is to reduce the unmet electricity of the community. Their results showed that the proposed system is reduced the unmet electricity from 49.34% to 0.57% at $0.612/kWh levelized cost of electricity.

The urban environment is not cost-effective for large scale PV farms. However, there is an unexploited potential whether on the roof of the buildings or at the sidings especially glass sidings. Henemann [69] reviewed the building-integrated photovoltaics (BIPV) method that can be integrated into the external fabric of the buildings. Peng et al. [70] discussed the issues of building integrated photovoltaic systems and architectural designs. Building attached photovoltaic (BAPV) and BIPV systems were compared. They designed a new BIPV structural scheme that allows easy maintenance and replacement. Yoon et al. [71] investigated transparent thin-film amorphous silicon solar cells for the building integrated photovoltaic system design and installation for the windows covering the front side of a building. A practical application in Korea was analyzed with long term performance monitoring for 2 years. Azimuth and shading related reductions were occurred, therefore, useful design parameters were obtained and presented in order to optimize further BIPV applications. Heinstein et al. [72] emphasized the cost-effective social and psychological factors on implementations of BIPV. They showed that the BIPV market share is around 59% for France and 30% for Italy, furthermore, BIPV and BAPV combined market share is 65% for Italy and 70% for France in 2019. In financial aspects, even PV costs falling, it is not reflected the bankability of BIPV projects, therefore, the banks do not usually agree to give a mortgage for investing in such systems. Shukla et al. [73] presented the market potential of BIPV products. Material advancements, international standards, and specifications were highlighted. They compared BIPV market

products from a different manufacturer. Therefore, they showed that 21.2% efficiency was reached by the monocrystalline silicon module. Amorphous silicon solar modules were reached 13.3% efficiencies. Biyik et al. [74] comprehensively reviewed both BIPV and building integrated photovoltaic/thermal (BIPV/T) systems. Energy generation amount, nominal power, efficiency, type, and performance assessments were carried out. New thin-film technologies and cooling techniques were discussed as the objectives that were shown in the literature. They showed that the efficiency values of BIPV systems ranging between 5% and 18%. In order to get higher efficiencies, the shadowing effect, ambient temperature, the direction of the building, and the slope of the PV was shown as the important factors for BIPV systems. Liu et al. [75] proposed an efficient and cost-effective power configuration for BIPV systems. They presented dc-building-module based BIPV systems that have good potential for efficiency improvement. They demonstrated the PV-DCBM-based BIPV system prototype and showed that it exhibits satisfactory performance in terms of validity and feasibility. Yang and Athienitis [76] reviewed air-based, water-based, concentrating, and phase change BIPV/T systems. They provided an overview of the applications, developments, current status, and research. Chae et al. [77] assessed the performance of BIPV windows with a semi-transparent solar cell and investigated electrical and optical parameters. They fabricated semi-transparent amorphous silicon solar cells in various conditions. They assessed the performance of developed BIPV windows in six different climate conditions. Their results showed that their developed semi-transparent cell performance is various in a range between 4.8% and 6.3%. They showed that the annual reduction potential Carbon Equivalent ranges between 12% and 21% among their proposed systems and environments. Proposed BIPV systems can save 30% of the total HVAC energy in comparison with a double-pane clear glass system.

CSPs especially with thermal energy storage systems possess a reliable energy production and storage system with its dispatchability and flexibility for the grid, integration ability between them, and cost-effectiveness. Stein and Buck [78] reviewed advanced power cycles for CSP systems. Especially gas turbine combined cycles are driven by CSP systems were emphasized as the most efficient option available. Pikra et al. [79] developed small scale CSP plant especially for the remote areas that consist population does not have electricity. They presented a conceptual design for a stand-alone power unit

that consists of a parabolic trough CSP plant using an organic Rankine cycle at 10kW installed capacity. Dunham and Iverson [80] reviewed CSP systems with high-efficiency thermodynamic power cycles. They highlighted promising candidates such as regenerated He-Brayton, regenerated CO_2-Brayton, CO_2 recompression Brayton, steam Rankine, and combined CO_2-organic Rankine cycle. Their results showed that steam Rankine cycles may offer higher thermal efficiencies up to 600°C. Beyond these temperatures, current components reach material limits for steam Rankine systems. CO_2 recompression Rankine cycle was performed more than 60% thermal efficiencies at 30MPa and 1000°C.

2.2 Integrated Geothermal Energy Systems

Sub-surface thermal energy can be used for heating, cooling, power, and other purposes with geothermal systems. Especially borders of major plates are viable for geothermal systems. 90TWh of annual electricity is produced via geothermal power plants in 2018 [6]. Carlino et al. [81] technically reviewed a geothermal reservoir in geological, geochemical, geophysical, and stratigraphic aspects. The active volcanic island of Ischia geothermal system was analyzed with multi-disciplinary data. They evaluated the possible temperature and pressure changes in the shallow geothermal reservoir, due to the hot fluid withdrawal for electrical production. Zhai et al. [82] analyzed the influence of working fluid properties on system performance. The organic Rankine cycle was used to produce power from pumped geothermal water. Cycle optimization was performed to maximize work output. Rodriguez et al. [83] investigated the organic Rankine cycle and Kalina cycle for low grade (low temperature) geothermal power plant applications. R-290 working fluid was used for the organic Rankine cycle, and 84% ammonia and 16% water mixture were used for the Kalina cycle, which are the best-performed fluids for each cycle. Their results showed that the geothermal system with the Kalina cycle produced 18% more power than the geothermal system with an organic Rankine cycle. Economical calculations showed that the levelized cost of electricity for the Kalina cycle is 0.18€/kWh and for the organic Rankine cycle, it was calculated as 0.22€/kWh. Fallah et al. [84] performed exergy analyses for a low-grade EGS with Kalina cycle. Their results showed that the highest exergy destruction occurred in the condenser, and it is followed by the evaporator, turbine, low-temperature heat exchanger, and high-temperature heat exchanger. Calise et al. [85] presented a geothermal and parabolic trough solar plant-based multigeneration system for

electricity, thermal, cooling, and freshwater demands. Exergetic and exergoeconomic analyses were conducted. Results showed that 40% to 50% of global exergy efficiencies occurred during the thermal recovery mode and 16% to 20% efficiencies occurred during the cooling mode. Al-Ali and Dincer [86] studied an integrated solar geothermal system that produces electrical power, cooling, space heating, hot water, and heat for industrial use. Energy and exergy analysis were assessed for single-generation, cogeneration, trigeneration, and multigeneration systems. Operating conditions and environmental parameters were used in the parametric study to evaluate their influence on efficiencies. Their results showed that energy efficiencies were calculated as 16.4% for single-generation and 78% for multigeneration; exergy efficiencies were calculated as 26.2% for single-generation and 36.6% for multigeneration.

High-grade geothermal systems are located at depths near or below the brittle-ductile transition zone. Supercritical geothermal energy was utilized for more than 100 years. It was employed for a thermochemical heat source in the current study. Energy reserve to a depth of 10 km from the surface is around $1.3x10^{27}$J, which is equal to the global energy demand for 6 million years [87]. Lu [88] reviewed 18 significant EGS fields and technologies in Europe, Japan, South Korea, Australia, and the United States. Global EGS status and economics were discussed. The potential of the EGS was shown and the installed capacity estimation forecast was done as 70GWe by 2050. Reinsch et al. [89] reviewed supercritical geothermal systems, past studies, and ongoing projects. Deep wells drilled geothermal fields such as The Geysers, Salton Sea, Hawaii, Kakkonda, Larderello, Krafla, Los Humeros, and Menengai were discussed. Elders et al. [90] studied Iceland Deep Drilling Project (IDDP) and presented the implications for global upcoming projects. They emphasized three important approaches as cost reductions for drilling and other activities to complete wells, cascading the utilization of the excess water therefore excess heat for heating in the residential or industrial area, to utilize supercritical fluids for increasing geothermal power output to reduce the number of wells. Fridleifsson and Elders [91] presented the Iceland Deep Drilling Project-2 and its results where ~426°C temperatures and 340bar fluid pressures are measured. They presented that the well is drilled to 4.5km deep to reach supercritical conditions. From seismic studies, the brittle/ductile boundary is expected around 6km depth, where basaltic rocks are located at 600°C to 700°C

temperatures. Asmundsson et al. [92] presented the achievements made by the High-Temperature Instruments (HiTI) for supercritical geothermal characterization and exploitation funded by the European Union. The project was established out in order to develop well equipment that functional between 300°C to 400°C temperatures, to identify new Na/Li ratios that valid at high temperatures, to test tracers against organic isomers that can resist high temperatures, and to investigate basalt rock deformation and petrophysical properties at high temperature and pressure conditions. Shnell et al. [93] investigated the development of ocean floor supercritical geothermal systems which are never applied before. They emphasized the importance of such application due to the availability of most significant supercritical geothermal reservoirs are under the ocean floor. Supercritical hydrogen production, desalination process, and extraction of minerals were discussed in their study. Scott et al. [94] presented numerical simulations of supercritical geothermal resource formation for the first time. Primary geologic factors such as the brittle-ductile transition temperature, the host rock permeability, and the intrusion depth of how to control the extent and thermo-hydraulic structure of supercritical geothermal reserves was demonstrated. Stimac et al. [95] reviewed the exploitable supercritical geothermal resources at Geysers, Salton Sea, and Coso geothermal fields. Challenges and costs were addressed in order to reach the brittle-ductile transition layer and the critical point of water. Costs of deep drilling, high-temperature drilling, and uncertainties were discussed. Similar efforts that were recently performed in other countries were discussed as well. Tsuchiya et al. [96] investigated the granite-porphyry system as a natural process that has similarities with supercritical geothermal heat harnessing. Therefore, similarities between lithostatic and hydrostatic pressure regimes were studied to provide guidance and useful information to adapt supercritical geothermal systems such as the creation of fracture clouds. Radulovic and Castaneda [97] investigated the behavior of selected zeotropic mixtures, namely R-143a/R-125 and R143a/R-C318 in the supercritical Rankine cycle. Energy efficiency and exergy efficiency were calculated to identify the optimal operational parameters. Selected zeotropic mixtures were assessed due to their behaviors in order to find their potential. Optimization was performed in order to determine optimum pressure and temperature at the turbine inlet for the best thermal and exergetic performance. R-143a/R-124

combination was shown as the most promising candidate. CO_2 injection rather than water is an option that exploits supercritical CO_2 for geothermal systems.

2.3 Integrated Hydrogen Energy Systems

If hydrogen is generated from renewable resources and used as a fuel, it is a promising environmentally benign energy carrier medium. Currently, it is mainly produced by the steam methane reforming process from natural gas, and it is mainly used as a chemical substance. However, there are efforts available for environmentally clean and sustainable hydrogen production and utilization both for commercial and research purposes. Turner [98] described that environmentally clean hydrogen can address sustainability, environmental emissions, and energy security issues. Replacing fossil fuel-based energy carriers with sustainable fuel was described as one of the key pieces of today's society must address while identifying and building a sustainable energy system. Acar and Dincer [99] assessed the environmental impacts of hydrogen production methods either renewable or not. Natural gas steam reforming, coal gasification, solar and wind-driven water electrolysis, biomass gasification, Cu-Cl, and S-I thermochemical hydrogen production cycles and high-temperature electrolysis were compared due to their performance and were assessed due to their social, economic, and environmental impacts. They also investigated the impact of the installed capacity of hydrogen production plant on the unit price of the produced hydrogen. Nuclear based thermochemical Cu-Cl cycle was possessed as the lowest global warming potential and the lowest social cost of carbon, hydrogen production option. Wind electrolysis was performed as the lowest acidification potential hydrogen production option, which followed by nuclear-based thermochemical Cu-Cl and S-I hydrogen production cycles. In terms of the unit cost of hydrogen, the biomass gasification method was performed as the lowest hydrogen unit cost option among the others. Coal gasification and natural gas steam methane reforming were followed the biomass gasification in terms of the unit cost of hydrogen. In terms of energetic and exergetic efficiencies, biomass gasification was performed as the best hydrogen production option, followed by Cu-Cl and S-I nuclear-based thermochemical hydrogen production cycle. The acidification potential of the biomass gasification hydrogen production method was emphasized as one of the focus areas in order to expand this option as a promising hydrogen source. Bolton [100] reviewed the solar photoproduction option to produce hydrogen.

Photochemical systems, semiconductor systems, photobiological systems, and hybrid and other systems were investigated their performance, improvement potential, and long-term functionality. Photovoltaic driven hydrogen production, photoelectrochemical cells with semiconductor electrodes, photobiological systems, and photodegradation systems were emphasized as promising candidates for future work in hydrogen production methods. Turner et al. [101] reviewed hydrogen production from renewable resources. Electrolysis technology, biomass gasification methods, thermolysis process in solar-driven thermochemical hydrogen production methods, photolysis process in photoelectrochemical hydrogen production methods, and photobiological water splitting were discussed. Holladay et al. [102] reviewed hydrogen production processes from renewable and fossil fuel-based resources and techniques. Electrolysis from renewable resources was emphasized as the near-term low emission alternative. Biohydrogen, thermochemical hydrogen production methods, and photo-electrolysis were highlighted as longer-term technologies. For smaller-scale distributed production, electrolysis was highlighted as the cost-competitive alternative. Sherif et al. [103] discussed hydrogen production, storage, distribution and utilization technologies, and the hydrogen economy. Wind energy utilization to produce hydrogen was discussed with possibilities to enhance wind power competitiveness with hydrogen usage.

High grade excess thermal energy utilization, especially from nuclear energy, solar energy, or geothermal energy, can provide environmentally benign, relatively efficient hydrogen production method namely thermochemical hydrogen production cycles. Efforts started with alternative fuel requirements especially in remote fields such as military bases in remote battlefields. Wentorf and Hanneman [104] investigated thermochemical hydrogen production methods. Three closed thermochemical cycles were investigated. Their results showed that 40% to 60% thermal efficiencies were achieved. Steinfeld [105] reviewed solar-driven thermochemical hydrogen production methods. They reviewed studies about examining concentrated solar radiation utilization as the energy source of high-temperature process heat for thermochemical processes. Naterer et al. [106] reviewed nuclear hydrogen production and the thermochemical Cu-Cl cycle program of Canada. They emphasized a supercritical water reactor with hydrogen production. Experimentation, modeling, simulation, thermochemistry, safety, reliability, economics, and advanced

materials were discussed. Funk [107] reviewed thermochemical hydrogen production initiatives such as Energy Depot, THEME, Ispra Mark chemical cycles, CRISTINA, JAERI, UT-3, and MASCOT. The renewable usage and requirement for comparisons in terms of efficiencies, capital costs, and irreversibilities were emphasized. Beghi [108] reviewed the efforts at the Joint Research Centre Ispra for thermochemical hydrogen production experiments. Mark 1 process and variants, iron-chlorine processes, and the sulfur family were discussed. Ozbilen et al. [109] assessed the four-step Cu-Cl thermochemical hydrogen production cycle thermodynamically, economically, and environmentally with exergy, cost, exergoenvironmental, exergoeconomic, and life cycle analyses. They showed that the hydrolysis reactor of the Cu-Cl thermochemical hydrogen production cycle was possessed the highest environmental impact and it is the most expensive component. The unit cost of hydrogen was calculated as $3.36/kg. In the second part of their study, Ozbilen et al. [110] performed multi-objective optimization. According to their results, exergy efficiency is increased by 0.8% and 4.5% lower cost was achieved in comparison with baseline parameters. In terms of environmental impact, exergy efficiency is increased by 0.5% and 30% lower environmental impact was achieved.

Other environmentally friendly methods such as steam reforming of ethanol, biogas, biomass, nuclear for hydrogen production are available in the literature. Guo et al. [111] reviewed hydrogen production from agricultural waste by dark fermentation. They emphasized the advantage of biohydrogen production from agricultural waste since this waste is abundant, cheap, renewable, and highly biodegradable. They especially focused on dark fermentation from such as crop residues, livestock waste, and food waste.

Solar and geothermal based hydrogen production methods are available in the literature. Yilmaz et al. [112] evaluated the exergetic cost of flash-binary geothermal driven hydrogen production. 200°C liquid geothermal water resource was employed to produce power, thereafter, electrical power was employed in the water electrolysis process. Exergy efficiencies were calculated as 46.6% for the power plant and 45.8% for the overall system. Unit exergetic costs were calculated as $0.04/kWh for the electricity and $3.14/kg for the produced hydrogen. Yuksel and Ozturk [113] assessed energy and exergy analyses of a multigeneration system powered by geothermal resource. Electricity, hydrogen, domestic

hot water, space heating, and cooling were presented as the useful outputs of their proposed multigeneration system. PEM electrolyzer, organic Rankine cycle, quadruple effect absorption cooling system were presented as the major technologies used in their proposed system. 47.04% energy efficiency and 32.15% exergy efficiency were calculated. The unit cost of hydrogen was calculated between $4.8/kg to $1.1/kg related to geothermal water temperature. Yilmaz and Kanoglu [114] performed energy and exergy analyses of geothermal driven hydrogen production system where 160°C 100kg/s geothermal resource was employed. For the binary geothermal power plant, 11.4% energy efficiency and 45.1% exergy efficiency were calculated with thermodynamic analysis. For the hydrogen production system, 64.0% energy efficiency and 61.6% exergy efficiency were calculated. 6.7% energy efficiency and 23.8% exergy efficiency were calculated for the overall system. Ratlamwala and Dincer [115] assessed comparatively two solar heliostat based Cu-Cl thermochemical hydrogen production systems namely solar heliostat system integrated with Cu-Cl cycle and Kalina cycle, and solar heliostat system integrated with Cu-Cl cycle, Kalina cycle, and photocatalytic reactor were compared. Their results showed that the hydrogen production rate for 126.9L/s volumetric flow rate is 986kg/day, for 289L/s volumetric flow rate is 2248.6 kg/day. Overall exergy efficiencies are found between 45.6% and 47.79% for the system without photocatalytic reactor and between 54.94% and 56.41% for the system with photocatalytic reactor.

2.4 Main Gaps in the Literature

Many researchers studied the Cu-Cl thermochemical hydrogen production cycle due to its relatively lower temperature (≈500°C) heat requirements in comparison to other thermochemical hydrogen production cycles such as S-I (≈900°C) or Ca-Br (≈750°C). Few researchers studied multigeneration system integration with the Cu-Cl thermochemical cycle.

Photovoltaic systems have a big momentum among the energy generation systems globally due to its relatively fast cost decline and its high commercial viability. There are many studies available on photovoltaic technologies, however, there are few researchers available who focused on floating PV or BiPV plants and their performance assessments.

Supercritical geothermal systems were actively studied by many researchers. Especially there are many applications and their studies with worldwide deep drilling projects. In contrast with conventional or low-grade geothermal systems, high-grade geothermal systems or supercritical geothermal systems have more commercial viability. However, there are very few studies focused on supercritical geothermal sources with integrated systems. And again, very few studies available on supercritical geothermal system integration with thermochemical hydrogen production systems.

As mentioned before, hydrogen is an energy carrier medium that potential alternative environmentally benign fuel to fossil-based fuel if it is produced by renewables. This study focused on novel Cu-Cl thermochemical hydrogen production cycle integrations with geothermal and solar-based multigeneration systems.

Chapter 3. Developments of Systems

In this section of the thesis, overall and subsystems are presented, evaluation methods, simulation programs are described. Three multigeneration systems are proposed as follows:

- Multigeneration system 1: Bifacial and geothermal based multigeneration system
- Multigeneration system 2: Parabolic trough CSP and geothermal based multigeneration system with Cu-Cl thermochemical hydrogen production cycle and trilateral ammonia Rankine cycle
- Multigeneration system 3: Enhanced geothermal and bifacial based multigeneration system with Cu-Cl thermochemical hydrogen production cycle

All of these proposed systems have similarities, common features, and contrasts. In terms of similarities, all of these systems are driven by renewable energy resources, particularly solar and geothermal. Availability of solar and geothermal resources differ by location on earth, broadly speaking, solar radiation availability mainly depends on the solar radiation angle to the horizontal ground surface and weather conditions, and geothermal resources can be reached from almost anywhere especially with EGSs, however, feasibility factors such as source quality and cost differ. Mainly, highly feasible geothermal sources are located around major plate boundaries, especially there will be a high possibility of feasible geothermal applications where a major plate movement occurred.

Feasibility is an important parameter for the investment decision of these particular plants. In order to obtain high feasibility, location determination has been made carefully due to the major energy source type. In multigeneration system 1, a combination of both sources is considered for location determination. 39°78’N latitude, 26°26’E longitude is selected for multigeneration system 1, which locates in Gokcebayir, Aegean Region, Turkey. There is already a geothermal power plant is actively producing electricity near this field and three commercial solar photovoltaic power plants are built and activated in 2018 and 2019. The synergy between geothermal and solar availability makes this location relatively feasible for multigeneration system 1.

One of the major contrasts of the multigeneration system 1 does not consist of the Cu-Cl thermochemical cycle. Cu-Cl thermochemical cycle requires high-temperature heat

sources at least around 500°C. However, it is not feasible to produce any heat source in the field where the BiPV plant is planned and 180°C geothermal source availability. Thereupon, different locations are determined for multigeneration systems 2 and 3. In geothermal systems, very high temperature geothermal working fluids are not a common practice, therefore EGSs, in other words, engineered geothermal systems (EGS) are considered for multigeneration system 3. Notwithstanding, desired temperatures are rarely available among the high-temperature EGS fields. Therefore, the EGS field in northern Japan is selected for multigeneration system 3 location. Moreover, its solar availability is also relatively feasible especially in comparison to Iceland where another location that meets high-temperature EGS field requirements, particularly the fields in the Iceland Deep Drilling Project.

Another aspect of their differences is the type of community and the reason for the existence of such systems. In multigeneration system 1, components are applicable for small scale applications and there is no need for large investments. However, concentrated solar and supercritical EGSs can catch the feasibility goals with large scale investments. Therefore, large scale systems are developed where the concentrated solar and supercritical enhanced geothermal used for multigeneration systems 2 and 3.

Furthermore, location determination for the second project was more related to solar availability than geothermal, since the high-temperature heat requirements of the Cu-Cl thermochemical cycle meet via solar source. In order to reach desired temperatures, CSP systems are considered due to their ability to produce high temperature working fluid. One of the advantages of the Cu-Cl thermochemical hydrogen production cycle among the other thermochemical hydrogen production cycles is its relatively low-temperature requirements. While more than 900°C temperatures have been needed for sulfur-iodine (S-I) thermochemical hydrogen production cycle or 750°C temperatures have been needed for calcium-bromine (Ca-Br) thermochemical cycles, around 500°C temperatures have been needed for Cu-Cl thermochemical cycle. That makes CSP technology with the parabolic trough collectors viable for multigeneration system 2. On the contrary case, a power tower system with heliostats would be the only viable CSP technology, due to its ability to produce relatively higher temperature working fluid. Parabolic trough CSP technology is

more mature in comparison to solar tower systems. Besides, while there should be a large-scale capacity are needed for commercially feasible solar tower systems, relatively smaller scales are applicable and feasible for parabolic trough systems. Accordingly, distributed small implementations are possible, therefore, investments should not be giant for parabolic through systems.

All of the proposed multigeneration systems have similarities and differences in terms of components. Similarities have mainly occurred relatively near to the end-user, in other words, near to the outputs. Components have been varied near to the inputs or sources and mid processes. MED desalination units have been kept as same in all of the multigeneration systems. While the hydrogen production system has been based on a PEM electrolyzer, dryer, and compressor in multigeneration system 1; the Cu-Cl thermochemical hydrogen production cycle is used for the multigeneration systems 2 and 3. Mainly, the hydrolysis reactor, thermolysis reactor, electrolyzer are the major components with auxiliary components such as dryer, separators, and heat exchangers. The main contrasts of multigeneration system 2 have occurred near to the solar and geothermal source inputs. Parabolic trough CSP plant and integrated molten salt storage systems at the solar input side; trilateral ammonia Rankine cycle system at the geothermal input side are the main contrasts of multigeneration system 2 in terms of components. The main contrast of multigeneration system 3 is Cu-Cl thermochemical hydrogen production cycle has been integrated with EGS. BiPV plant is kept at the solar side. Some of the component groups are considered as subsystems. PV subsystem consists BiPV modules and inverters; the solar electrical hydrogen subsystem consists PEM electrolyzer, PEM fuel cell, hydrogen dryer, compressor, and hydrogen tank; Cu-Cl hydrogen subsystem consists hydrolysis reactor, thermolysis reactor, electrolyzer, and auxiliary components; geothermal power subsystem consists low- and high-pressure steam turbines, flash separators, and auxiliary components; ammonia subsystem consists volumetric expanders, heat exchangers and pump. Geothermal heat pump, multi-effect distillation desalination systems can be considered as other subsystems.

BiPV modules are considered in photovoltaic plants in multigeneration systems 1 and 3. Backface radiation collection availability allows BiPV modules to enhance energy

yield. Field enhancements and array orientations make the bifacial feature more significant in terms of energy gain. BiPV plant development differs in contrast to conventional PV plant development due to several factors. Since the reflected sunlight is an important parameter, array design parameters such as type of the PV construction, pitch distance between PV modules, height above ground, shed total width, and phi angle. The importance of the array design can be seen in Figure 3.1.

Although ground albedo is a natural parameter, the current study and another linked study is using albedo parameter as a design parameter as a result of practical field enhancement method. In practice, white chipping stones or white marble chips have relatively high reflectivity. Even, painted chipping stones with road marking paints make this field enhancement a cost-effective energy gain solution since road marking paints have reflective composition. Bifacial and conventional PV plants are simulated with enhanced and regular albedo fields to determine the energy gain and cost-effectiveness of such systems with and without enhanced albedo. There are natural albedo enhancements that exist, such as fresh snow enhanced albedo up to 90%. In the current study, the artificial field has been used with an 80% albedo assumption. The regular field is considered as 20% albedo.

The frameless structure of BiPV modules gives indirect gains. Such as, transparency of BiPV modules is another important parameter since the PV cells are not covering all PV module surface, transparent empty spaces would allow to reflected radiation by the surface and collected radiation by the next sheds. Usually, 10% of transparency is reached by frameless double glass BiPV modules. Moreover, there are other factors that enhance the energy yield, such as the frameless BiPV modules allow to slide dust or snow which are one of the most important solar blockers for a PV plant, especially if the PV plant is constructed in a dusty or snowy environment.

Speaking of environment, all of the proposed multigeneration systems are assumed to be near any salty water source. That creates a corrosive environment that can decrease the durability of PV modules. Although the majority of the PV modules are able to be certified by International Electrotechnical Commission (IEC) 61701 for severity level 6 which claims the corrosive resistance of PV module, frameless PV modules have better

ability to survive with the corrosive environment, since their only interaction with the environment is the glass. Therefore, frameless technology enables long term use with enhanced durability, especially in a highly corrosive environment. The temperature coefficient can create significant losses in the energy yield especially in high-temperature environments. Relatively lower temperature coefficients are provided with frameless PV modules since they have no frame or cover, only the glass surface directly transfers heat to the air. Another beneficial gain of the bifacial structure is relatively higher settlement therefore space between PV modules and ground allows better cooling. Contrarily, the cost raise has occurred due to several factors. Since PV modules and construction are the major costs of a PV plant, building a BiPV plant creates increasements both module and construction costs. In the worldwide PV market, BiPV modules are around 10% expensive in comparison with conventional PV modules. Besides, special clamps and assembly tools should be used to mount the PV modules to the structure of either a fixed or tracker system.

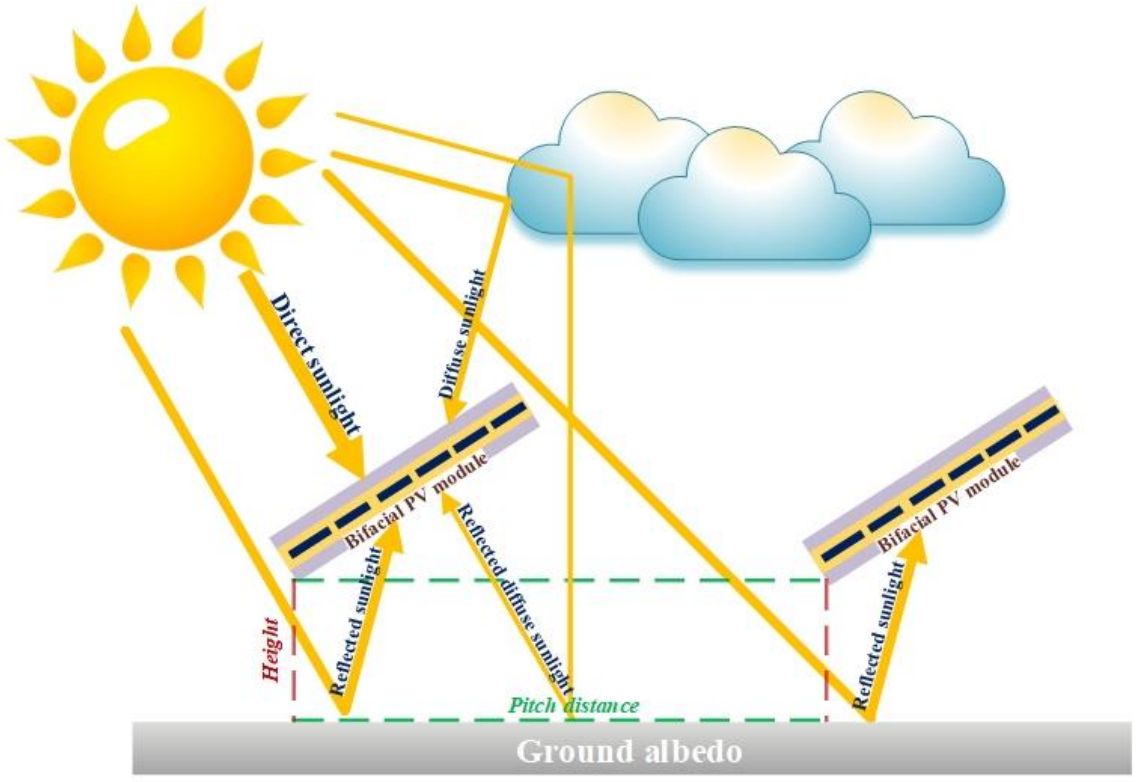

Figure 3.1 Direct and reflected sunlight collected by BiPV modules

Another structural cost increment can be reflected as a specific design since the bifacial system requires not blocked space between ground and PV modules, conventional

structures may be re-designed for this requirement. Moreover, the relatively higher distance between PV modules and ground in bifacial systems, causes increased structural components, especially main profiles will be longer, therefore, costly due to height requirements.

NASA Surface Meteorological and Solar Energy Program database and Meteonorm 7.2 database are employed for the meteorological data, such as global horizontal irradiation and ambient temperature. Meteonorm consists of measurements from about 2500 ground stations and satellites for the selected locations. It interpolates 10 to 30 years of monthly averages from the 3 nearest ground station data for the selected location. If there is no sufficient data, it uses satellite data. NASA-SSE uses satellite data with 1° to 1° sensitivity for 10 years. Furthermore, obtained monthly meteorological data have been artificially generated to hourly meteo data via PVsyst software for hourly sensitive simulations.

For multigeneration systems that consist BiPV plant, four different scenarios are applied for each of the specified locations. Single-axis horizontal trackers have been used through its beneficial combination with BiPV modules. Conventional and bifacial monocrystalline silicon-based 72 cell PV modules are assumed in every scenario. In terms of obtaining a more reliable comparison between four scenarios, a conventional PV module is generated from BiPV module specifics only difference is assumed as the back-face radiation collection ability. In practice, the approach that turns BiPV modules into conventional, can be made via to cover the back faces of PV modules.

Parabolic trough CSP plant is employed in multigeneration system 2. The main purpose of this subsystem is to provide the heat requirement for the Cu-Cl thermochemical hydrogen production cycle. Molten salt storage is integrated to provide the heat requirement continuously as a thermal energy storage system. Hitec solar salt is employed as the heat transfer fluid which has the 238°C as minimum operating temperature and 593°C maximum operating temperature values. The selection of heat transfer fluid is crucial since the concentrated solar system is directly connected with the Cu-Cl thermochemical cycle where high-grade heat is required. Thermal energy storage is designed for 13 hours of storage capacity. Hot storage tank heater temperature is designed for 550°C due to the high-temperature requirements of the connected Cu-Cl cycle. The

cold tank is set at 260°C. System Advisor Model software from NREL is employed for all concentrated solar systems and thermal energy storage system design, simulation, and analyses.

Ammonia trilateral Rankine cycle subsystem is employed in multigeneration system 2. The main purpose of this subsystem is to produce power and to provide the heat requirement for the evaporator of the residential heat pump system.

Cu-Cl thermochemical hydrogen production cycle subsystem is employed in multigeneration systems 2 and 3 instead of the electrical hydrogen production system in multigeneration system 1. The main purpose of this subsystem is to provide hydrogen fuel for the community. Aspen Plus software is employed for the design of the reactors, streams, and simulation of the reactions. Figure 3.2 and Figure 3.3 shows the Aspen Plus layout and general layout of the Cu-Cl cycle.

Table 3.1 Summary of the proposed systems

Details	**Multigeneration System 1**	**Multigeneration System 2**	**Multigeneration System 3**
Location	Gokcebayir in Turkey	Geysers in the United States	Shinozaki in Japan
Main focus	Self-consumption	Agricultural activities, self-consumption	Industrial scale hydrogen production
Resources	Sea, Geothermal, Solar	Sea, Geothermal, Solar	Sea, Geothermal, Solar
Electricity production	BiPV, Steam turbines	Ammonia trilateral Rankine cycle	BiPV, Steam turbines
Heat production	Heat pump, heat exchangers	PTC with TES, Heat pump, heat exchangers	Heat pump, heat exchangers
Hydrogen production	PEM electrolyzer	Cu-Cl cycle	Cu-Cl cycle
Water production	MED	MED	MED
Solar intensity	>1200 kWh/m^2 GHI	>1600 kWh/m^2 GHI	>1200 kWh/m^2 GHI
Geothermal temperature	>120°C	>120°C	>450°C

3.1 Development of Multigeneration Systems

In this section, the developments of three multigeneration systems are presented. As above mentioned, each multigeneration system has different characteristics in demand, consumption, commercial goals, and grid connection types. Table 3.1 shows the brief details of each system.

In contrast to multigeneration systems 2 and 3, multigeneration system 1 has fewer components, therefore, it does not require large scale investments. This allows distributed small-scale implementations of multigeneration system 1 in a broader range of system capacity and consumer type.

Multigeneration system 2 is particularly designed for large-scale implementation, since the profitability goals can be met with larger scales, therefore, larger investments. A big-scale greenhouse system is implemented, where higher thermal energy is required. System 3 is assumed as an industrial-scale hydrogen production plant located in a small community. Auxiliary systems supply energy requirement with useful commodities for the small community.

All of the components and units are proposed with a production in a green manner goal. Therefore, emissions and byproducts are very low in comparison to other production systems. However, there are still available. Heat exchangers, pumps, turbines, and other components are causing heat losses therefore thermal pollutions. Some of the systems are built in a sea environment that possesses a threat to aquatic creatures. Especially high pumping rates can cause the deaths of underwater creatures.

Byproducts are available in all of the proposed systems. MED desalination unit produces more brine than the freshwater. Reinjection of the brine which is the seawater with high concentrations of salt can be harmful to sea creatures again but locally in the reinjection area. However, salt concentrations of the sea are not getting affected by reinjection since there is an enormous scale difference. Chemical byproducts can be seen not theoretically but with implementations in the Cu-Cl unit. After thermolysis and hydrolysis reactions, unreacted byproducts can cause cumulations in the lower sections of the reactors.

R-134a is employed due to its wide usage. It is an ozone-friendly refrigerant however, it has a global warming potential. The leakage of this refrigerant can possess harmful effects on the environment. MED desalination unit produces more brine than the freshwater. Reinjection of the brine which is the seawater with high concentrations of salt can be harmful.

On the other hand, geothermal systems are employed in all of the proposed multigeneration systems. However, underground reservoirs may contain various minerals and gases, which causes environmental impacts. All of the proposed systems are closed-loop geothermal system; therefore, all of the pumped water is reinjecting into reinjection wells, hence emissions and other harmful environmental effects can be surpassed. Filter implementations are important to prevent harmful effects such as mercury filters that should be implemented if there is availability in the specific geothermal field.

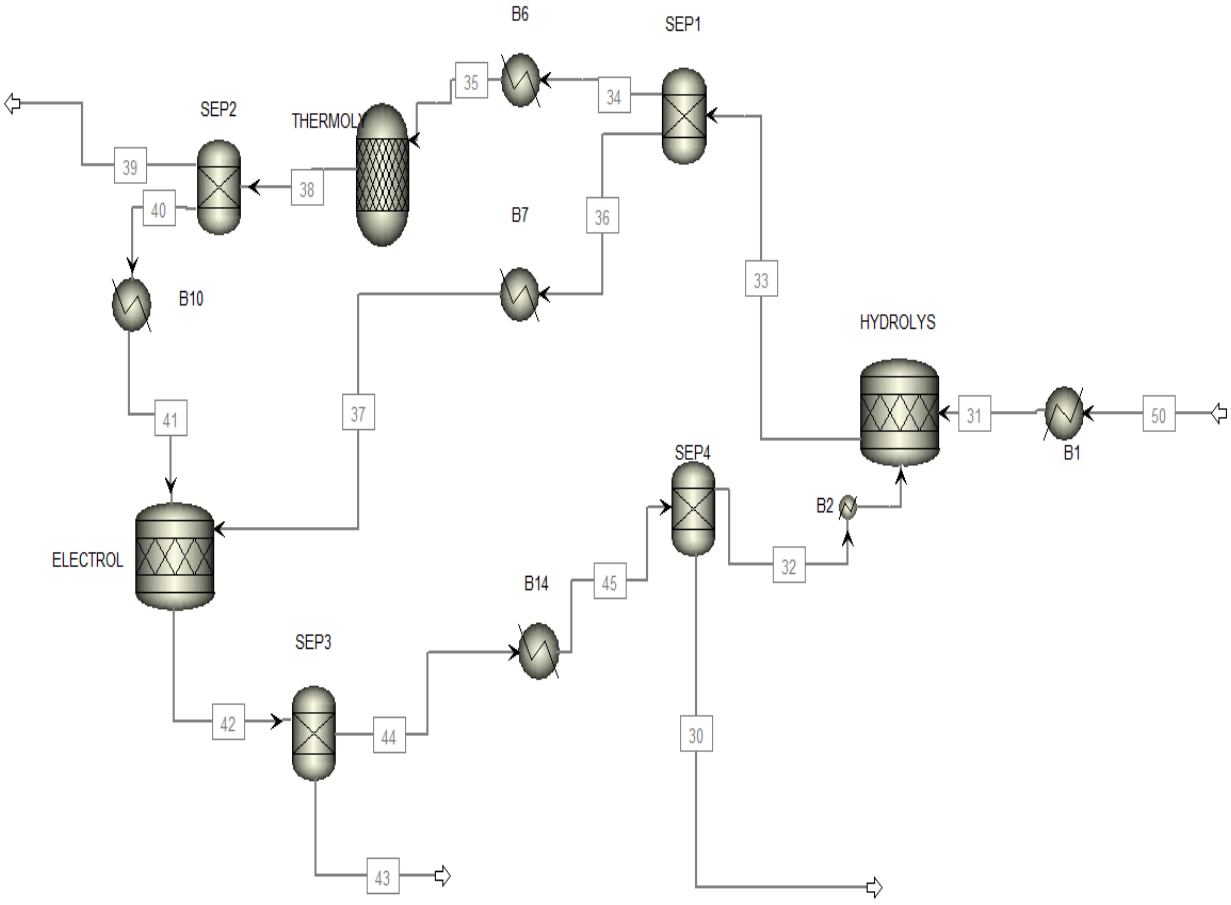

Figure 3.2 Layout: Thermochemical Cu-Cl hydrogen production

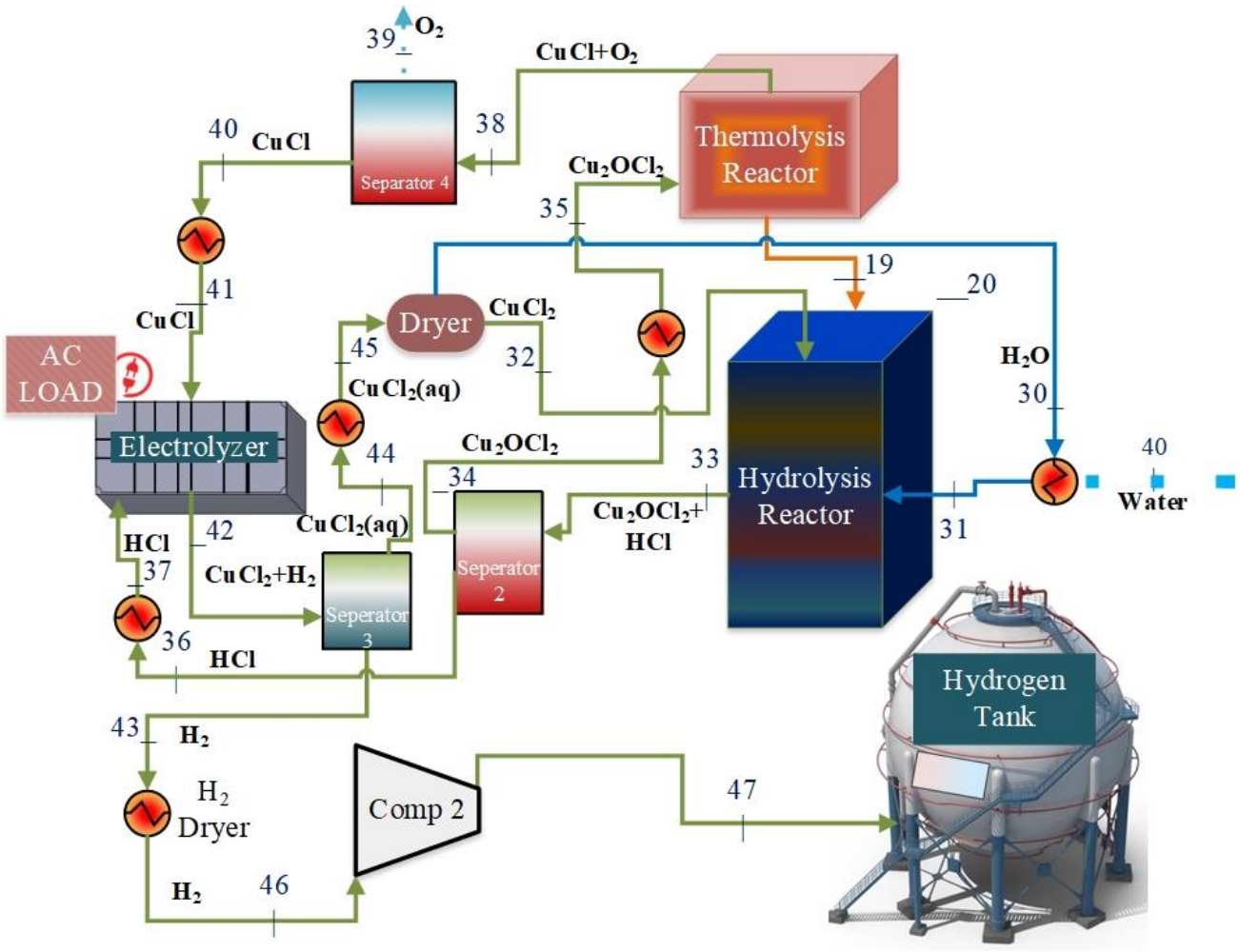

Figure 3.3 Layout: Thermochemical Cu-Cl hydrogen production and utilization

3.1.1 Development of Multigeneration System 1

Multigeneration system 1 integrates multiple subsystems, namely a BiPV plant, residential geothermal heat pump, geothermal power generation system, MED desalination unit, electrical hydrogen subsystem. Natural resources, particularly, solar, geothermal, and sea resources are considered.

Relatively small-scale systems are integrated to produce electricity, heat, hydrogen, and freshwater. Since the natural resources are the only considered resources of multigeneration system 1, resource availability and system feasibility depend on the location. Due to the proposed subsystems, there is no need for extreme conditions. A medium temperature geothermal resource, particularly from 100°C to 200°C resources are

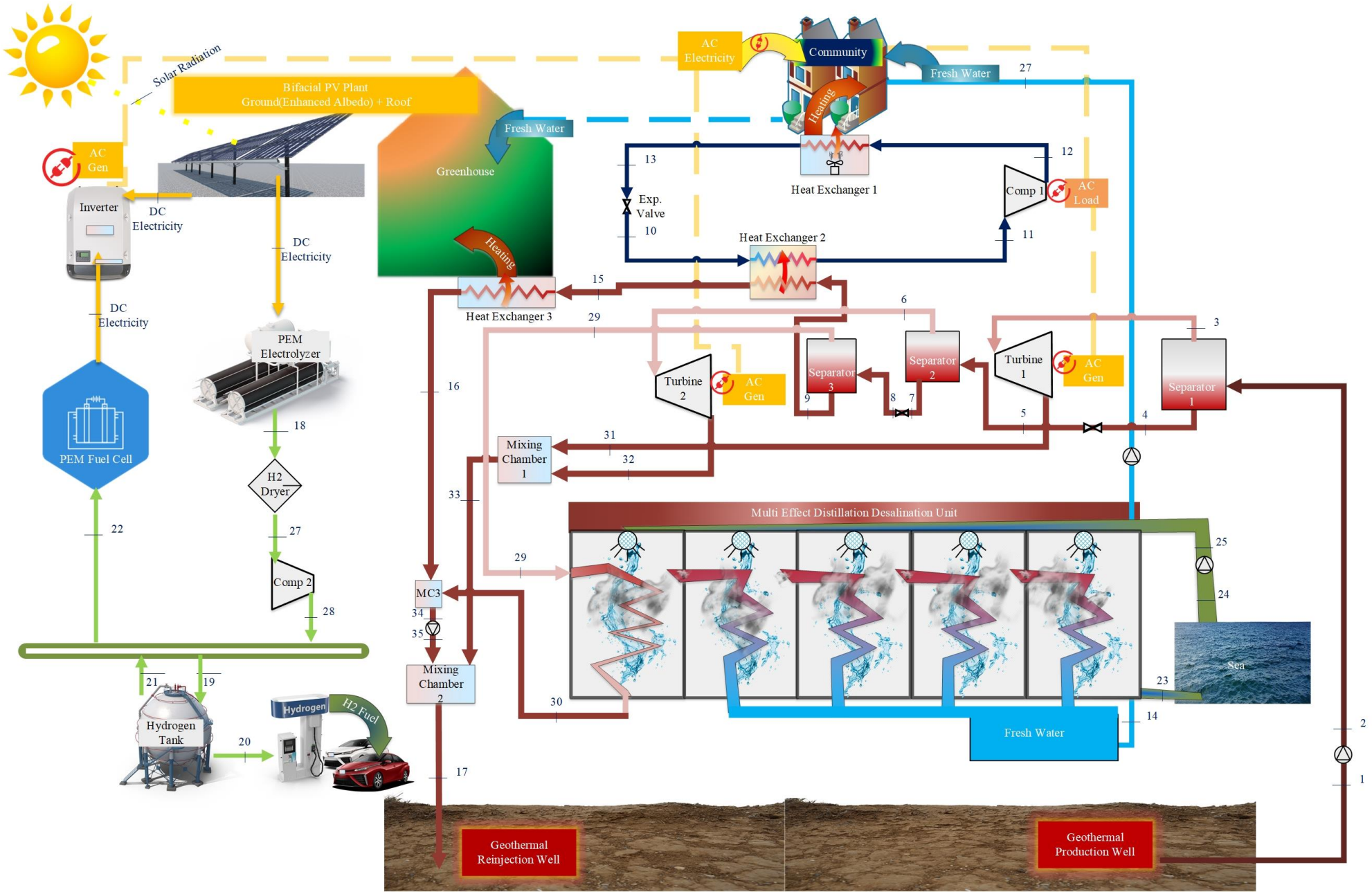

Figure 3.4 Layout of multigeneration system 1

suitable for multigeneration system 1. In terms of solar energy, more than 1200 kWh/m^2 global horizontal irradiation is relatively suitable for multigeneration system 1. Furthermore, the proposed system should be near to the sea, ocean, or any other salty water resources. Gokcebayir in Turkey is the selected location for multigeneration system 1. Near the assumed field, commercial solar PV and geothermal power plants are already actively producing electricity. The assumed field is located a few kilometers away from the Aegean Sea. Therefore, source requirements have been met for the selected location.

BiPV plants collect the solar radiation from two novel layouts and convert it to electrical energy. Primarily, the BiPV plant feeds the community and auxiliary systems such as the tracker system of the plant. Electrolyzer employs excess electricity for hydrogen production purposes. Dryer and compressor dry and compress the hydrogen for desired conditions. The hydrogen tank stores the produced hydrogen either for fuel requirements or to utilize for electricity via the PEM electrolyzer. On the geothermal side, geothermal fluid goes into the separator and two flash power generation system produces electricity. Excess brine goes into the residential heat pump and greenhouse heat exchanger for space heating of residential area and greenhouse. Therefore, another part of separated brine from the geothermal separated in another flash separator and obtained steam goes into the MED desalination unit for freshwater production. All processes can be seen in the layout in Figure 3.4.

3.1.2 Development of Multigeneration System 2

Multigeneration system 2 integrates multiple subsystems, namely a parabolic through CSP, residential geothermal heat pump, geothermal driven ammonia trilateral Rankine cycle subsystem, MED desalination unit, Cu-Cl thermochemical hydrogen production subsystem. Natural resources, particularly, solar, geothermal, and sea resources are employed in order to produce useful outputs as freshwater, electricity, space heating, and hydrogen.

This multigeneration system 2 is proposed to provide electricity, freshwater, hydrogen, and space heating for a big community and a greenhouse system. The estimated

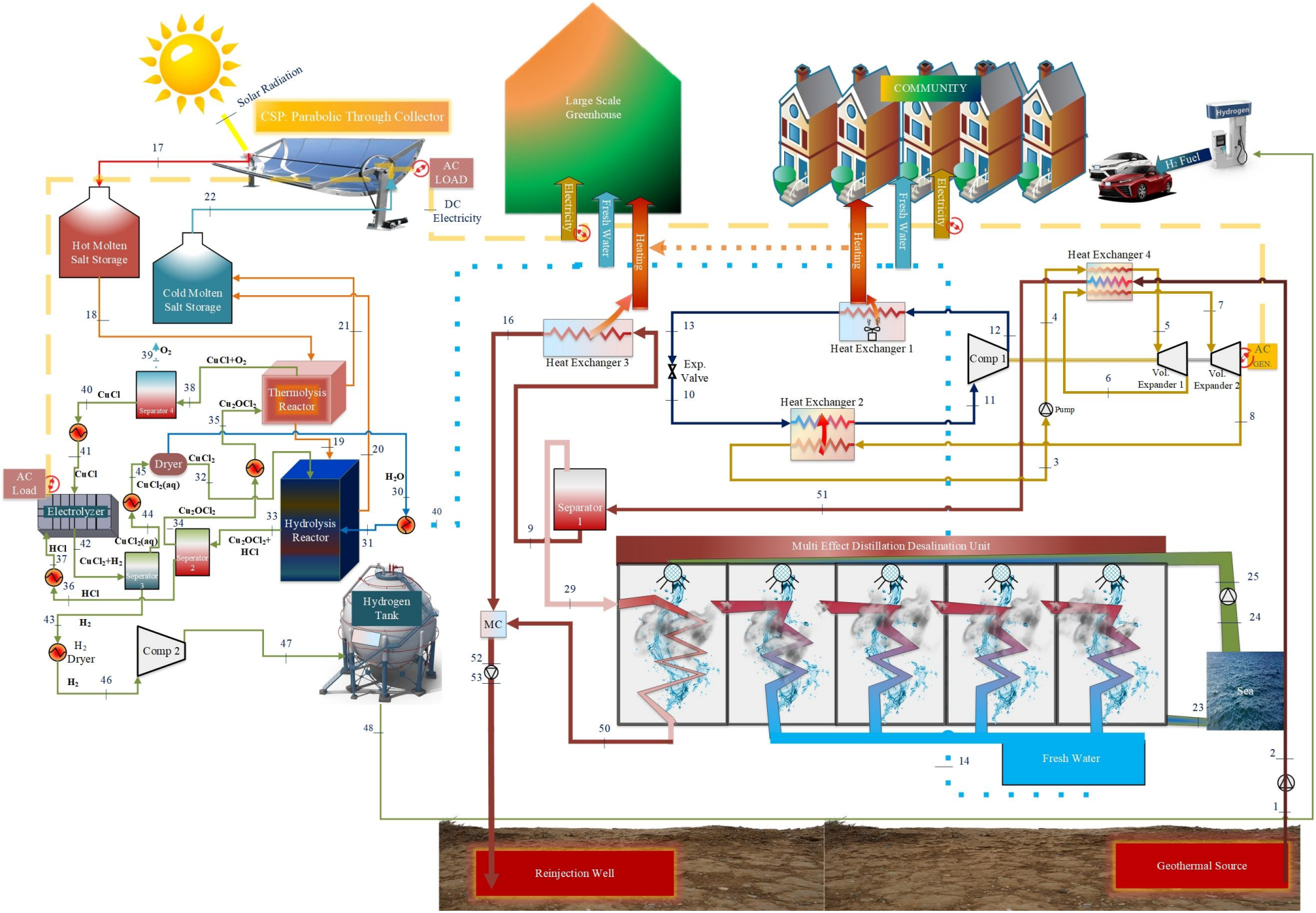

Figure 3.5 Layout of multigeneration system 2

number of households in the community is around 3842. This large community needs more than 47MWh electricity and 452MWh thermal energy. In comparison to multigeneration systems 1 and 2, multigeneration system 2 consists of a larger scale greenhouse. Agriculture is one of the important parts of this community. All produced useful outputs are consumed in the field. Therefore, self-consumption is one of the keywords of multigeneration system 2. There is no grid connection is considered for multigeneration system 2. For multigeneration system 2, solar energy takes charge of critical energy supply in the form of thermal energy. Hydrolysis and thermolysis reactors of the Cu-Cl thermochemical hydrogen production cycle require high-temperature heat supply. Therefore, parabolic collectors concentrate the solar radiation to reach desired temperatures. Although solar radiation is concentrated, global horizontal irradiation should be relatively higher in contrast with other multigeneration systems, due to the requirements. Therefore, more than 1500 kWh/m^2 global horizontal radiation is relatively suitable for multigeneration system 2. On the other hand, there is no such components or subsystems that require high temperature geothermal source. For this reason, a medium temperature geothermal resource is relatively suitable for multigeneration system 2. The salty water resource for the freshwater useful output requires a sea, ocean, or another salty water resource. In terms of location determination, solar availability at high importance and geothermal and sea availability at low importance are considered. Healdsburg, Geysers Geothermal Field, California, United States is selected for multigeneration system 2 due to its high global horizontal irradiation values ($1792kWh/m^2$), geothermal resource availability (the Geysers is the world's largest geothermal field) and infrastructure, and its closeness to the Pacific Ocean in terms of the water resource. Therefore, source requirements have easily met for the considered location. Figure 3.7 is a combined map for the geothermal and solar potential by showing current geothermal plants and global horizontal irradiation. It can be easily seen; the area of California State possesses wealthy resources with a high density of geothermal plants and global horizontal solar radiation.

Basically, CSPs are directly connected with the Cu-Cl cycle, therefore large-scale hydrogen production for the community's hydrogen fuel requirements can be done. The thermal energy storage system as the molten salt storage unit is integrated with the concentrated solar system. Parabolic trough collectors collect the solar radiation and

concentrate the radiation on the receiver. Heat transfer fluid namely Hitec solar salt collects radiation to heat itself. Heat transfer fluid feeds the thermal energy storage tanks in charging states and it feeds the Cu-Cl cycle for heat requirements. The heat requirement for the reactions comes with the heat transfer fluid to the reactors and pre-heating units.

The heating process starts from the highest temperature to the lowest temperature unit. Around at 260°C temperatures, heat transfer leaves the Cu-Cl cycle and goes into the cold molten salt storage tank. Cu-Cl cycle steps can be seen in Table 3.2.

On the other part, geothermal water goes into a trilateral flash cycle to feed the evaporator of the system for thermal energy requirements. In the trilateral flash cycle, the pump pressurizes ammonia and pressurized ammonia receives heat in the evaporator. High-temperature ammonia goes into the first expander to turn its energy into power. Expanded ammonia goes into again the same evaporator for reheating, therefore, reheated ammonia goes into the second expander for another power generation. Expanded ammonia goes into the condenser and transfers its excess heat into the residential heat pump then goes again the cycle. In the residential heat pump, R-134a receives excess heat from ammonia goes into the compressor. Compressed R-134a goes into the heat exchanger to release its heat for space heating purposes. Then the expansion valve expands R-134a and the cycle can start again. Geothermal water after the trilateral cycle goes into the flash separator. Obtained steam goes into 4 stage MED desalination unit. Therefore, fresh water can be produced by sea resources at each stage. Collected freshwater feeds the community, the greenhouse, and the Cu-Cl cycle. Separated brine from the flash separator goes into the greenhouse heat exchanger for direct heat exchange. All steps can be seen in Figure 3.5.

Table 3.2 4 step Cu-Cl thermochemical cycle in multigeneration system 2

#	Step	Equation	Temperature
1	Hydrolysis	$2CuCl_2 + H_2O \rightarrow 2Cu_2OCl_2 + 2HCl$	510 ℃
2	Thermolysis	$Cu_2OCl_2 \rightarrow 2CuCl + 1/2\ O_2$	390 ℃
3	Electrolysis	$2CuCl + 2HCl \rightarrow 2CuCl_2 + H_2$	85 ℃
4	Drying	$CuCl_{2(aq)} \rightarrow \ CuCl_{2(s)}$	85 ℃

3.1.3 Development of Multigeneration System 3

Multigeneration system 3 integrates subsystems which are mainly driven by the geothermal resource and BiPV plant. The geothermal resource is integrated with the Cu-Cl thermochemical cycle, double flash power generation subsystem, multi-effect desalination unit, and residential heat pump.

A suitable location is rare in comparison to other proposed multigeneration systems. Natural resource availability and capability are important for location determination. Solar, geothermal and sea resource availabilities are important likewise multigeneration systems 1 and 2. In contrast to proposed multigeneration systems 1 and 2, geothermal resource capability possesses high importance due to its integration via the Cu-Cl thermochemical hydrogen production cycle. The high temperature thermal energy requirements of thermolysis and hydrolysis reactors is considered to be met by geothermal source. Therefore, high temperature geothermal source existence is essential. Figure 3.7 shows high temperature geothermal systems and global horizontal irradiations. Red plus signs show the high temperature geothermal sources. It is the main constrain since there are not many of them. Shinozaki in Japan is considered for the third multigeneration system. There is already a power plant that works with desired temperatures and pressures in the area. Other high temperature locations are also suitable for multigeneration system 3. However, relatively low solar availability decreases feasibility in Iceland.

The main focus of multigeneration system 3 is to produce industrial-scale hydrogen with fresh water, electricity, and heating for its own usage and small-scale community. Although the largest system is designed, the community is the smallest. Moreover, the area is a remote region; therefore, system 3 is utilized for hydrogen production and small-scale loads such as small community loads, auxiliary system loads.

The supercritical geothermal system connects with a large-scale Cu-Cl cycle unit and feeds it. The heat, required for the reactions, comes from the supercritical geothermal resource. The heating process starts from the highest temperature component and ends at the lowest temperature unit. After the Cu-Cl cycle, geothermal fluid leaves the cycle and goes into a two-step power generation unit. Steps in the Cu-Cl cycle can be seen in Table 3.3.

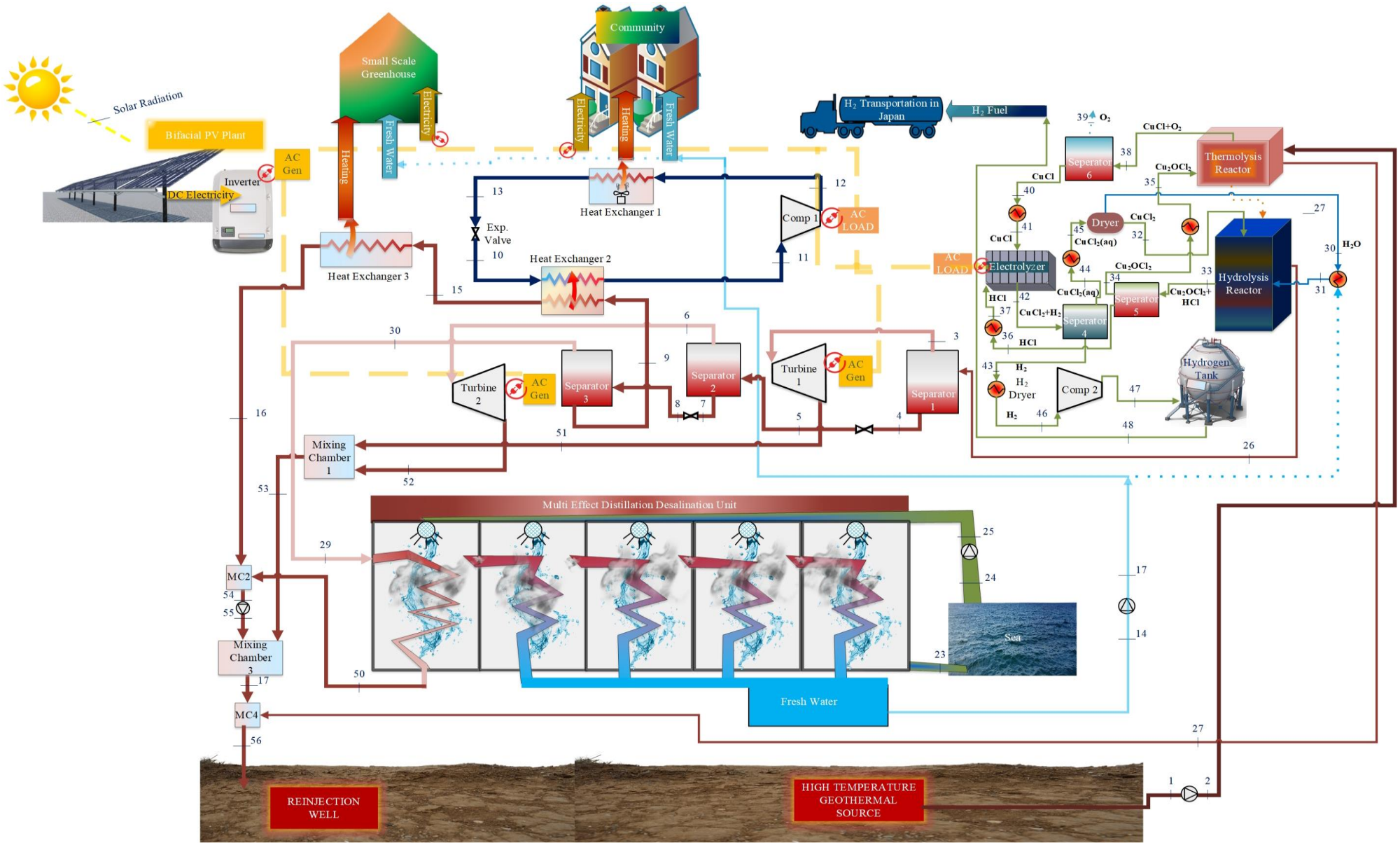

Figure 3.6 Layout of multigeneration system 3

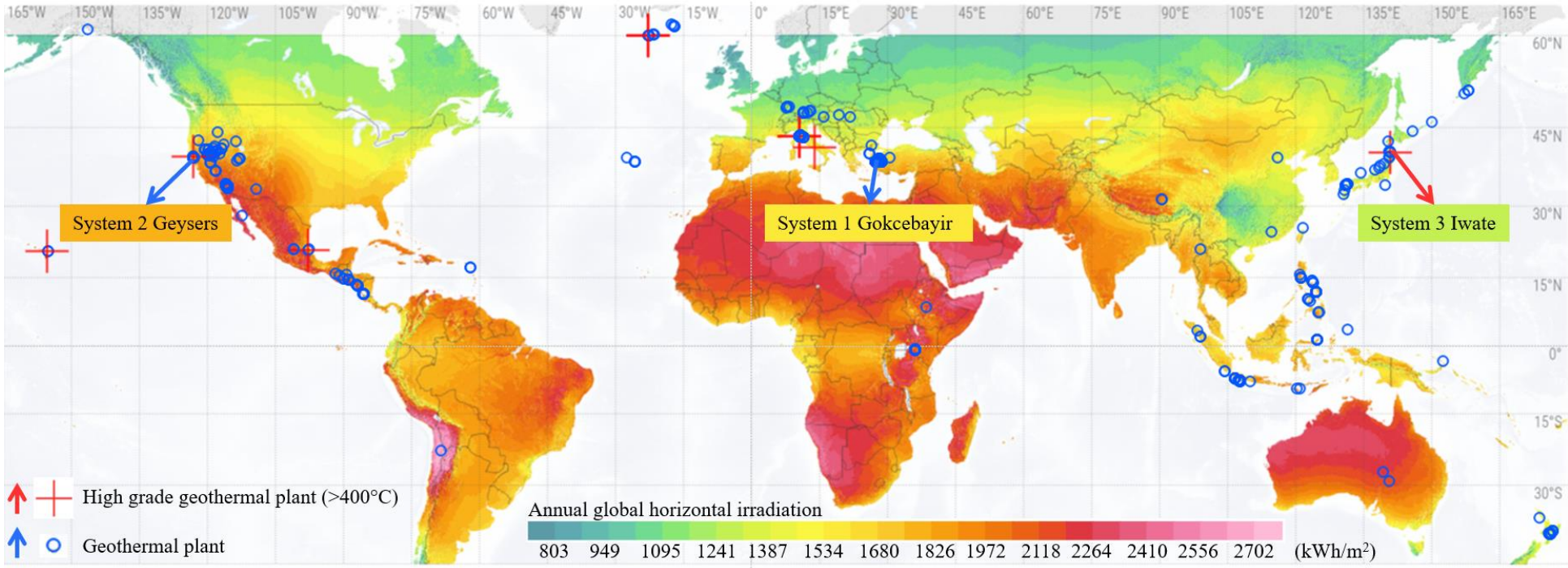

Figure 3.7 Combined high grade and regular geothermal plants and global horizontal irradiation (data from [117] background solar map [118])

Table 3.3 Thermophysical properties of the Cu-Cl cycle in multigeneration system 3

	Step	Equation	Temperature
1	Hydrolysis	$2CuCl_2 + H_2O \rightarrow 2Cu_2OCl_2 + 2HCl$	515℃
2	Thermolysis	$Cu_2OCl_2 \rightarrow 2CuCl + 1/2\ O_2$	380℃
3	Electrolysis	$2CuCl + 2HCl \rightarrow 2CuCl_2 + H_2$	23℃
4	Drying	$CuCl_{2(aq)} \rightarrow \ CuCl_{2(s)}$	85℃

Thereafter, geothermal fluid goes into a two-stage power generation unit to produce electricity for a small community and auxiliary systems. One part of the excess brine goes into a residential heat pump and greenhouse heat exchanger for space heating purposes. Another part of excess brine goes into the MED desalination unit for freshwater production. Large scale BiPV plant mainly feeds the Cu-Cl cycle for electricity requirements of the hydrogen production process namely electrolysis. All processes can be seen in the layout in Figure 3.6.

In multigeneration system 3, the BiPV plant is designed at 149MWp capacity to produce the required amount of electricity, but not on time. For this particular reason, the netting model incentive with the national grid is considered for further calculations.

Chapter 4. Modeling and Analysis

Various analyses are conducted for each major component and overall multigeneration systems. Thermodynamic analysis both energetic and exergetic, and parametric studies are performed in order to determine and obtain performances and efficiencies of the components and systems. Subsystems are modeled, analyzed, and integrated with other subsystems to create multigeneration systems. Simulations and feasibility analyses are conducted to obtain detailed results. Engineering equation software (EES) is used especially for its thermophysical property database and built-in functions. BiPV plants are simulated and analyzed via PVsyst software. Feasibility analyses and load generations of overall systems are performed via HOMER Pro software. Cu-Cl thermochemical cycle is simulated and analyzed in Aspen Plus software. CSP plants are modeled, simulated, and analyzed via NREL's SAM software.

The following considerations and assumptions are utilized for all of the proposed multigeneration systems for analyses. The reference environment conditions are taken as T_0 = 296.15K for reference temperature and P_0 = 101.325 kPa for reference pressure. The isentropic efficiency of each turbine is assumed to be 90%. Compressors and pumps are considered as at 85% isentropic efficiencies. The turbines, pumps, compressors, and throttling valves are considered adiabatic. Kinetic and potential energy and exergy changes and pressure losses are neglected.

General mass, energy, entropy, and exergy balance equations for each of the multigeneration systems can be expressed as follows:

According to the principle of mass conservation, the general mass balance equation for each of the multigeneration systems can be written as:

$$\sum_i \dot{m}_i = \sum_o \dot{m}_o \tag{4.1}$$

According to the principle of the thermodynamic version of energy conservation law, in other words, the first law of thermodynamics, general energy balance equation for each of the multigeneration systems can be expressed as:

$$\sum_{net} \dot{Q}_{net} + \sum_{net} \dot{W}_{net} + \sum_i \dot{m}_i \left(h_i + \frac{V_i^2}{2} + gZ_i \right) = \sum_o \dot{m}_o \left(h_o + \frac{V_o^2}{2} + gZ_o \right) \tag{4.2}$$

The general entropy balance equation and entropy generation rate for each of the multigeneration systems can be calculated as:

$$\sum_i \dot{m}_i s_i + \sum_{net} \frac{\dot{Q}_{net}}{T_S} + \dot{S}_{gen} = + \sum_o \dot{m}_o s_o \quad (4.3)$$

For multigeneration system 1, the general exergy balance equation can be written as:

$$\sum_i \dot{E}x_{\dot{Q}_i} + \dot{W}_i + \dot{E}x^{Q} + \sum_i \dot{m}_i\, ex_i = \sum_o \dot{E}x_{\dot{Q}_o} + \dot{W}_o + \sum_o \dot{m}_o\, ex_o + \dot{E}x_d \quad (4.4)$$

Each pump in multigeneration system 1 can be analyzed with following the mass, energy, entropy, and exergy balance equations respectively as follows:

$$\dot{m}_i = \dot{m}_o \quad (4.5)$$

$$\dot{m}_i h_i + \dot{W}_p = \dot{m}_o h_o \quad (4.6)$$

$$\dot{m}_i s_i + \dot{S}_{gen,p} = \dot{m}_o s_o \quad (4.7)$$

$$\dot{m}_i ex_i + \dot{W}_p = \dot{m}_o ex_o + \dot{E}x_{d,p} \quad (4.8)$$

Each turbine in multigeneration system 1 can be analyzed with following the mass, energy, entropy, and exergy balance equations respectively as follows:

$$\dot{m}_i = \dot{m}_o \quad (4.9)$$

$$\dot{m}_i h_i = \dot{W}_t + \dot{m}_o h_o \quad (4.10)$$

$$\dot{m}_i s_i + \dot{S}_{gen,t} = \dot{m}_o s_o \quad (4.11)$$

$$\dot{m}_i ex_i = \dot{W}_t + \dot{m}_o ex_o + \dot{E}x_{d,t} \quad (4.12)$$

Heat exchanger 2 in multigeneration system 1 can be analyzed with following the mass, energy, entropy, and exergy balance equations respectively as follows:

$$\dot{m}_9 = \dot{m}_{15} \text{ and } \dot{m}_{10} = \dot{m}_{11} \quad (4.13)$$

$$\dot{m}_9 h_9 + \dot{m}_{10} h_{10} = \dot{m}_{15} h_{15} + \dot{m}_{11} h_{11} \quad (4.14)$$

$$\dot{m}_9 s_9 + \dot{m}_{10} s_{10} + \dot{S}_{gen,HX2} = \dot{m}_{15} s_{15} + \dot{m}_{11} s_{11} \quad (4.15)$$

$$\dot{m}_9 ex_9 + \dot{m}_{10} ex_{10} = \dot{m}_{15} ex_{15} + \dot{m}_{11} ex_{11} + \dot{E}x_{d,HX2} \quad (4.16)$$

The mixing chamber 1 in multigeneration system 1 can be analyzed with following the mass, energy, entropy, and exergy balance equations respectively as follows:

$$\dot{m}_{31} + \dot{m}_{32} = \dot{m}_{33} \quad (4.17)$$

$$\dot{m}_{31} h_{31} + \dot{m}_{32} h_{32} = \dot{m}_{33} h_{33} \quad (4.18)$$

$$\dot{m}_{31} s_{31} + \dot{m}_{32} s_{32} + \dot{S}_{gen,MC1} = \dot{m}_{33} s_{33} \quad (4.19)$$

$$\dot{m}_{31} ex_{31} + \dot{m}_{32} ex_{32} = \dot{m}_{33} ex_{33} + \dot{E}x_{d,MC1} \quad (4.20)$$

The mixing chamber 2 in multigeneration system 1 can be analyzed with following the mass, energy, entropy, and exergy balance equations respectively as follows:

$$\dot{m}_{35} + \dot{m}_{33} = \dot{m}_{17} \quad (4.21)$$

$$\dot{m}_{35} h_{35} + \dot{m}_{33} h_{33} = \dot{m}_{17} h_{17} \quad (4.22)$$

$$\dot{m}_{35} s_{35} + \dot{m}_{33} s_{33} + \dot{S}_{gen,MC2} = \dot{m}_{17} s_{17} \quad (4.23)$$

$$\dot{m}_{35} ex_{35} + \dot{m}_{33} ex_{33} = \dot{m}_{17} ex_{17} + \dot{E}x_{d,MC2} \quad (4.24)$$

The mixing chamber 3 in multigeneration system 1 can be analyzed with following the mass, energy, entropy, and exergy balance equations respectively as follows:

$$\dot{m}_{16} + \dot{m}_{30} = \dot{m}_{34} \quad (4.25)$$

$$\dot{m}_{16} h_{16} + \dot{m}_{30} h_{30} = \dot{m}_{34} h_{34} \quad (4.26)$$

$$\dot{m}_{16} s_{16} + \dot{m}_{30} s_{30} + \dot{S}_{gen,MC3} = \dot{m}_{34} s_{34} \quad (4.27)$$

$$\dot{m}_{16} ex_{16} + \dot{m}_{30} ex_{30} = \dot{m}_{34} ex_{34} + \dot{E}x_{d,MC3} \quad (4.28)$$

Each throttling valve in multigeneration system 1 can be analyzed with following the mass, energy, entropy, and exergy balance equations respectively as follows:

$$\dot{m}_i = \dot{m}_o \quad (4.29)$$

$$\dot{m}_i h_i = \dot{m}_o h_o \quad (4.30)$$

$$\dot{m}_i s_i + \dot{S}_{gen,tv} = \dot{m}_o s_o \quad (4.31)$$

$$\dot{m}_i ex_i = \dot{m}_o ex_o + \dot{E}x_{d,tv} \quad (4.32)$$

Each compressor in multigeneration system 1 can be analyzed with following the mass, energy, entropy, and exergy balance equations respectively as follows:

$$\dot{m}_i = \dot{m}_o \quad (4.33)$$

$$\dot{m}_i h_i + \dot{W}_c = \dot{m}_o h_o \quad (4.34)$$

$$\dot{m}_i s_i + \dot{S}_{gen,c} = \dot{m}_o s_o \quad (4.35)$$

$$\dot{m}_i ex_i + \dot{W}_c = \dot{m}_o ex_o + \dot{E}x_{d,c} \quad (4.36)$$

The heat exchanger 1 in multigeneration system 1 can be analyzed with following the mass, energy, entropy, and exergy balance equations respectively as follows:

$$\dot{m}_{12} = \dot{m}_{13} \quad (4.37)$$

$$\dot{m}_{12} h_{12} = \dot{Q}_{HX1} + \dot{m}_{13} h_{13} \quad (4.38)$$

$$\dot{m}_{12} s_{12} + \dot{S}_{gen,HX1} = \dot{m}_{13} s_{13} \quad (4.39)$$

$$\dot{m}_{12} ex_{12} = \dot{E}x_{\dot{Q}_{HX1}} + \dot{m}_{13} ex_{13} + \dot{E}x_{d,HX1} \quad (4.40)$$

The heat exchanger 3 in multigeneration system 1 can be analyzed with following the mass, energy, entropy, and exergy balance equations respectively as follows:

$$\dot{m}_{15} = \dot{m}_{16} \quad (4.41)$$

$$\dot{m}_{15} h_{15} = \dot{Q}_{HX} + \dot{m}_{16} h_{16} \quad (4.42)$$

$$\dot{m}_{15} s_{15} + \dot{S}_{gen,HX} = \dot{m}_{16} s_{16} \quad (4.43)$$

$$\dot{m}_{15} ex_{15} = \dot{E}x_{\dot{Q}_{HX2}} + \dot{m}_{16} ex_{16} + \dot{E}x_{d,HX} \quad (4.44)$$

The MED desalination unit in multigeneration system 1 can be analyzed with following the mass, energy, entropy, and exergy balance equations respectively as follows:

$$\dot{m}_{29} = \dot{m}_{30} \text{ and } \dot{m}_{25} = \dot{m}_{14} + \dot{m}_{23} \quad (4.45)$$

$$X_{25}\dot{m}_{25} = X_{14}\dot{m}_{14} + X_{23}\dot{m}_{23} \tag{4.46}$$

$$\dot{m}_{29}h_{29} + \dot{m}_{25}h_{25} = \dot{m}_{14}h_{14} + \dot{m}_{23}h_{23} \tag{4.47}$$

For the PEM electrolyzer in multigeneration system 1, the energy requirement for the hydrogen production reaction can be expressed as:

$$\Delta H = \Delta G + T\Delta S \tag{4.48}$$

where Gibbs free energy is denoted with ΔG and the energy requirement in thermal form is denoted with $T\Delta S$.

Hydrogen production can occur with the following molar flow rate expression for multigeneration system 1:

$$\dot{N}_{H_2,o} = \frac{J}{2F} \tag{4.49}$$

where the current density is denoted with J and Faraday constant is represented with F.

The Electrical energy input rate for the electrolyzer in multigeneration system 1 can be expressed as:

$$\dot{W}_{electric} = JV \tag{4.50}$$

where overpotential of the cell is denoted with V and it can be expressed as:

$$V = V_o + V_{act,a} + V_{act,c} + V_{ohm} \tag{4.51}$$

$$V_o = 1.229 - 8.5x10^{-4}(T_{pem} - 298) \tag{4.52}$$

where activation overpotential is represented as V_{act} and it can be expressed as:

$$V_{act,i} = \left(\frac{RT}{F}\right)\sinh^{-1}\left(\frac{J}{2J_{o,i}}\right), \tag{4.53}$$

where a for anode and c for cathode is denoted as i.

The exchange current density of the electrolysis process in multigeneration system 1 can be written as:

$$J_{o,i} = J_i^{ref}\exp\left(-\frac{E_{act,i}}{RT}\right) \tag{4.54}$$

where a for anode and c for cathode is denoted with i and activation energy is denoted with E_{act}.

For efficiencies:

The energy and exergy efficiencies of the PEM electrolyzer in multigeneration system 1 can be calculated with the following expressions:

$$\eta_{energy,PEM} = \frac{\dot{m}_{H2} \times LHV_{h2}}{\dot{E}_{in}} \tag{4.55}$$

$$\eta_{exergy,PEM} = \frac{\dot{m}_{H2} \times ex_{h2}}{\dot{E}x_{in}} \tag{4.56}$$

where the total mass of collected hydrogen is represented with m_{H2} and energy input to the PEM electrolyzer is represented with E_{in}.

For multigeneration system 1, the overall energy and exergy efficiencies can be expressed as follows:

$$\eta_{en,ov} = \frac{\dot{W}_{El,net} + m_{H_2} LHV_{H_2} + m_{fw} h_{fw} + \dot{Q}_{Res} + \dot{Q}_{Gh}}{I_{GH}\dot{A}_{cell} + (m_1 h_1 - m_{17} h_{17})} \tag{4.57}$$

$$\eta_{ex,ov} = \frac{\dot{W}_{El,net} + m_{H_2} ex_{H_2} + m_{fw} ex_{fw} + \dot{Q}_{Res}(1 - \frac{T_o}{T_s}) + \dot{Q}_{Gh}(1 - \frac{T_o}{T_s})}{I_{GH}\dot{A}_{cell}\left(1 - \frac{T_o}{T_{sun}}\right) + (m_1 ex_1 - m_{17} ex_{17})} \tag{4.58}$$

For the thermochemical Cu-Cl hydrogen production cycle, balance equations can be applied as follows:

For the hydrolysis reactor:

$$\dot{m}_{30} + \dot{m}_{32} = \dot{m}_{33} \tag{4.59}$$

$$\dot{m}_{32} h_{32} + \dot{m}_{30} h_{30} + \dot{Q}_{Hy} = \dot{m}_{33} h_{33} \tag{4.60}$$

$$\dot{m}_{32} s_{32} + \dot{m}_{30} s_{30} + \dot{S}_{gen,Hy} = \dot{m}_{33} s_{33} \tag{4.61}$$

$$\dot{m}_{32} ex_{32} + \dot{m}_{30} ex_{30} + \dot{E}x_{\dot{Q}_{Hy}} = \dot{m}_{33} ex_{33} + \dot{E}x_{d,Hy} \tag{4.62}$$

For the thermolysis reactor:

$$\dot{m}_{35} = \dot{m}_{38} \tag{4.63}$$

$$\dot{m}_{35}h_{35} + \dot{Q}_{TL} = \dot{m}_{38}h_{38} \quad (4.64)$$

$$\dot{m}_{35}s_{35} + \dot{S}_{gen,TL} = \dot{m}_{38}s_{38} \quad (4.65)$$

$$\dot{m}_{35}ex_{35} + \dot{E}x_{\dot{Q}_{TL}} = \dot{m}_{38}ex_{38} + \dot{E}x_{d,TL} \quad (4.66)$$

For the electrolysis reactor:

$$\dot{m}_{41} + \dot{m}_{37} = \dot{m}_{42} \quad (4.67)$$

$$\dot{m}_{41}h_{41} + \dot{m}_{37}h_{37} + \dot{W}_{EL} = \dot{m}_{42}h_{42} \quad (4.68)$$

$$\dot{m}_{41}s_{41} + \dot{m}_{37}s_{37} + \dot{S}_{gen,EL} = \dot{m}_{42}s_{42} \quad (4.69)$$

$$\dot{m}_{9}ex_{9} + \dot{m}_{37}ex_{37} + \dot{W}_{EL} = \dot{m}_{42}ex_{42} + \dot{E}x_{d,EL} \quad (4.70)$$

Each pump in multigeneration system 2 can be analyzed with following the mass, energy, entropy, and exergy balance equations respectively as follows:

$$\dot{m}_i = \dot{m}_o \quad (4.71)$$

$$\dot{m}_i h_i + \dot{W}_p = \dot{m}_o h_o \quad (4.72)$$

$$\dot{m}_i s_i + \dot{S}_{gen,p} = \dot{m}_o s_o \quad (4.73)$$

$$\dot{m}_i ex_i + \dot{W}_p = \dot{m}_o ex_o + \dot{E}x_{d,p} \quad (4.74)$$

Each turbine in multigeneration system 2 can be analyzed with following the mass, energy, entropy, and exergy balance equations respectively as follows:

$$\dot{m}_i = \dot{m}_o \quad (4.75)$$

$$\dot{m}_i h_i = \dot{W}_t + \dot{m}_o h_o \quad (4.76)$$

$$\dot{m}_i s_i + \dot{S}_{gen,t} = \dot{m}_o s_o \quad (4.77)$$

$$\dot{m}_i ex_i = \dot{W}_t + \dot{m}_o ex_o + \dot{E}x_{d,t} \quad (4.78)$$

The heat exchanger 2 in multigeneration system 2 can be analyzed with following the mass, energy, entropy, and exergy balance equations respectively as follows:

$$\dot{m}_8 = \dot{m}_3 \text{ and } \dot{m}_{10} = \dot{m}_{11} \tag{4.79}$$

$$\dot{m}_8 h_8 + \dot{m}_{10} h_{10} = \dot{m}_3 h_3 + \dot{m}_{11} h_{11} \tag{4.80}$$

$$\dot{m}_8 s_8 + \dot{m}_{10} s_{10} + \dot{S}_{gen,HX2} = \dot{m}_3 s_3 + \dot{m}_{11} s_{11} \tag{4.81}$$

$$\dot{m}_8 ex_8 + \dot{m}_{10} ex_{10} = \dot{m}_3 ex_3 + \dot{m}_{11} ex_{11} + \dot{E}x_{d,HX2} \tag{4.82}$$

The mixing chamber 1 in multigeneration system 2 can be analyzed with following the mass, energy, entropy, and exergy balance equations respectively as follows:

$$\dot{m}_{50} + \dot{m}_{16} = \dot{m}_{54} \tag{4.83}$$

$$\dot{m}_{50} h_{50} + \dot{m}_{16} h_{16} = \dot{m}_{54} h_{54} \tag{4.84}$$

$$\dot{m}_{50} s_{50} + \dot{m}_{16} s_{16} + \dot{S}_{gen,MC1} = \dot{m}_{54} s_{54} \tag{4.85}$$

$$\dot{m}_{50} ex_{50} + \dot{m}_{16} ex_{16} = \dot{m}_{54} ex_{54} + \dot{E}x_{d,MC1} \tag{4.86}$$

Each throttling valve in multigeneration system 2 can be analyzed with following the mass, energy, entropy, and exergy balance equations respectively as follows:

$$\dot{m}_i = \dot{m}_o \tag{4.87}$$

$$\dot{m}_i h_i = \dot{m}_o h_o \tag{4.88}$$

$$\dot{m}_i s_i + \dot{S}_{gen,tv} = \dot{m}_o s_o \tag{4.89}$$

$$\dot{m}_i ex_i = \dot{m}_o ex_o + \dot{E}x_{d,tv} \tag{4.90}$$

Each compressor in multigeneration system 2 can be analyzed with following the mass, energy, entropy, and exergy balance equations respectively as follows:

$$\dot{m}_i = \dot{m}_o \tag{4.91}$$

$$\dot{m}_i h_i + \dot{W}_c = \dot{m}_o h_o \tag{4.92}$$

$$\dot{m}_i s_i + \dot{S}_{gen,c} = \dot{m}_o s_o \tag{4.93}$$

$$\dot{m}_i ex_i + \dot{W}_c = \dot{m}_o ex_o + \dot{E}x_{d,c} \tag{4.94}$$

The heat exchanger 1 in multigeneration system 2 can be analyzed with following the mass, energy, entropy, and exergy balance equations respectively as follows:

$$\dot{m}_{12} = \dot{m}_{13} \tag{4.95}$$

$$\dot{m}_{12} h_{12} = \dot{Q}_{HX1} + \dot{m}_{13} h_{13} \tag{4.96}$$

$$\dot{m}_{12} s_{12} + \dot{S}_{gen,HX1} = \dot{m}_{13} s_{13} \tag{4.97}$$

$$\dot{m}_{12} ex_{12} = \dot{E}x_{\dot{Q}_{HX1}} + \dot{m}_{13} ex_{13} + \dot{E}x_{d,HX1} \tag{4.98}$$

The heat exchanger 3 in multigeneration system 2 can be analyzed with following the mass, energy, entropy, and exergy balance equations respectively as follows:

$$\dot{m}_{9} = \dot{m}_{16} \tag{4.99}$$

$$\dot{m}_{9} h_{9} = \dot{Q}_{HX1} + \dot{m}_{16} h_{16} \tag{4.100}$$

$$\dot{m}_{9} s_{9} + \dot{S}_{gen,HX} = \dot{m}_{16} s_{16} \tag{4.101}$$

$$\dot{m}_{9} ex_{9} = \dot{Q}_{HX} + \dot{m}_{16} ex_{16} + \dot{E}x_{d,HX} \tag{4.102}$$

The MED desalination unit in multigeneration system 2 can be analyzed with following the mass, energy, entropy, and exergy balance equations respectively as follows:

$$\dot{m}_{29} = \dot{m}_{50} \text{ and } \dot{m}_{25} = \dot{m}_{14} + \dot{m}_{23} \tag{4.103}$$

$$X_{25} \dot{m}_{25} = X_{14} \dot{m}_{14} + X_{23} \dot{m}_{23} \tag{4.104}$$

$$\dot{m}_{29} h_{29} + \dot{m}_{25} h_{25} = \dot{m}_{14} h_{14} + \dot{m}_{23} h_{23} \tag{4.105}$$

For the electrolyzer in multigeneration system 2, the energy requirement for the hydrogen production reaction can be expressed as:

$$\Delta H = \Delta G + T\Delta S \tag{4.106}$$

where Gibbs free energy is denoted with ΔG and the energy requirement in thermal form is denoted with $T\Delta S$.

For efficiencies:

For the Cu-Cl thermochemical hydrogen production cycle, the conversion efficiency is analyzed as follows:

$$\eta_{\text{conversion,Cu-Cl}} = \frac{\text{LHV}_{H_2}}{\dot{Q}_{\text{net}} + \dot{W}} \tag{4.107}$$

where the lower heating value of hydrogen is represented with LHV_{h2}, the net heat input is represented with $\dot{Q}_{\text{net}}$, and required electrical work is represented with $\dot{W}$.

For multigeneration system 2, the overall energy and exergy efficiencies can be expressed as follows:

$$\eta_{\text{en,ov}} = \frac{\dot{W}_{\text{El,net}} + m_{H_2}\text{LHV}_{H_2} + m_{\text{fw}}h_{\text{fw}} + \dot{Q}_{\text{Res}} + \dot{Q}_{\text{Gh}}}{I_{GH}A_{\text{cell}} + (m_1h_1 - m_{53}h_{53})} \tag{4.108}$$

$$\eta_{\text{ex,ov}} = \frac{\dot{W}_{\text{El,net}} + m_{H_2}ex_{H_2} + m_{\text{fw}}ex_{\text{fw}} + \dot{Q}_{\text{Res}}\left(1-\frac{T_o}{T_s}\right) + \dot{Q}_{\text{Gh}}\left(1-\frac{T_o}{T_s}\right)}{I_{GH}A_{\text{cell}}\left(1-\frac{T_o}{T_{\text{sun}}}\right) + (m_1ex_1 - m_{53}ex_{53})} \tag{4.109}$$

For the thermochemical Cu-Cl hydrogen production cycle in multigeneration system 3, balance equations can be applied as follows:

For the hydrolysis reactor:

$$\dot{m}_{30} + \dot{m}_{32} = \dot{m}_{33} \tag{4.110}$$

$$\dot{m}_{32}h_{32} + \dot{m}_{30}h_{30} + \dot{Q}_{\text{Hy}} = \dot{m}_{33}h_{33} \tag{4.111}$$

$$\dot{m}_{32}s_{32} + \dot{m}_{30}s_{30} + \dot{S}_{\text{gen,Hy}} = \dot{m}_{33}s_{33} \tag{4.112}$$

$$\dot{m}_{32}ex_{32} + \dot{m}_{30}ex_{30} + \dot{E}x_{\dot{Q}_{\text{Hy}}} = \dot{m}_{33}ex_{33} + \dot{E}x_{\text{d,Hy}} \tag{4.113}$$

For the thermolysis reactor:

$$\dot{m}_{35} = \dot{m}_{38} \tag{4.114}$$

$$\dot{m}_{35}h_{35} + \dot{Q}_{\text{TL}} = \dot{m}_{38}h_{38} \tag{4.115}$$

$$\dot{m}_{35}s_{35} + \dot{S}_{\text{gen,TL}} = \dot{m}_{38}s_{38} \tag{4.116}$$

$$\dot{m}_{35}ex_{35} + \dot{E}x_{\dot{Q}_{\text{TL}}} = \dot{m}_{38}ex_{38} + \dot{E}x_{\text{d,TL}} \tag{4.117}$$

For the electrolysis reactor:

$$\dot{m}_{41} + \dot{m}_{37} = \dot{m}_{42} \tag{4.118}$$

$$\dot{m}_{41}h_{41} + \dot{m}_{37}h_{37} + \dot{W}_{EL} = \dot{m}_{42}h_{42} \tag{4.119}$$

$$\dot{m}_{41}s_{41} + \dot{m}_{37}s_{37} + \dot{S}_{gen,EL} = \dot{m}_{42}s_{42} \tag{4.120}$$

$$\dot{m}_{9}ex_{9} + \dot{m}_{37}ex_{37} + \dot{W}_{EL} = \dot{m}_{42}ex_{42} + \dot{E}x_{d,EL} \tag{4.121}$$

Each pump in multigeneration system 3 can be analyzed with following the mass, energy, entropy, and exergy balance equations respectively as follows:

$$\dot{m}_{i} = \dot{m}_{o} \tag{4.122}$$

$$\dot{m}_{i}h_{i} + \dot{W}_{p} = \dot{m}_{o}h_{o} \tag{4.123}$$

$$\dot{m}_{i}s_{i} + \dot{S}_{gen,p} = \dot{m}_{o}s_{o} \tag{4.124}$$

$$\dot{m}_{i}ex_{i} + \dot{W}_{p} = \dot{m}_{o}ex_{o} + \dot{E}x_{d,p} \tag{4.125}$$

Each turbine in multigeneration system 3 can be analyzed with following the mass, energy, entropy, and exergy balance equations respectively as follows:

$$\dot{m}_{i} = \dot{m}_{o} \tag{4.126}$$

$$\dot{m}_{i}h_{i} = \dot{W}_{t} + \dot{m}_{o}h_{o} \tag{4.127}$$

$$\dot{m}_{i}s_{i} + \dot{S}_{gen,t} = \dot{m}_{o}s_{o} \tag{4.128}$$

$$\dot{m}_{i}ex_{i} = \dot{W}_{t} + \dot{m}_{o}ex_{o} + \dot{E}x_{d,t} \tag{4.129}$$

The heat exchanger 2 in multigeneration system 3 can be analyzed with following the mass, energy, entropy, and exergy balance equations respectively as follows:

$$\dot{m}_{9} = \dot{m}_{15} \text{ and } \dot{m}_{10} = \dot{m}_{11} \tag{4.130}$$

$$\dot{m}_{9}h_{9} + \dot{m}_{10}h_{10} = \dot{m}_{15}h_{15} + \dot{m}_{11}h_{11} \tag{4.131}$$

$$\dot{m}_{9}s_{9} + \dot{m}_{10}s_{10} + \dot{S}_{gen,HX2} = \dot{m}_{15}s_{15} + \dot{m}_{11}s_{11} \tag{4.132}$$

$$\dot{m}_{9}ex_{9} + \dot{m}_{10}ex_{10} = \dot{m}_{15}ex_{15} + \dot{m}_{11}ex_{11} + \dot{E}x_{d,HX2} \tag{4.133}$$

The mixing chamber 1 in multigeneration system 3 can be analyzed with following the mass, energy, entropy, and exergy balance equations respectively as follows:

$$\dot{m}_{51} + \dot{m}_{52} = \dot{m}_{53} \tag{4.134}$$

$$\dot{m}_{51}h_{51} + \dot{m}_{52}h_{52} = \dot{m}_{53}h_{53} \tag{4.135}$$

$$\dot{m}_{51}s_{51} + \dot{m}_{52}s_{52} + \dot{S}_{gen,MC1} = \dot{m}_{53}s_{53} \tag{4.136}$$

$$\dot{m}_{51}ex_{51} + \dot{m}_{52}ex_{52} = \dot{m}_{53}ex_{53} + \dot{E}x_{d,MC1} \tag{4.137}$$

The mixing chamber 2 in multigeneration system 3 can be analyzed with following the mass, energy, entropy, and exergy balance equations respectively as follows:

$$\dot{m}_{16} = \dot{m}_{54} \tag{4.138}$$

$$\dot{m}_{16}h_{16} = \dot{m}_{54}h_{54} \tag{4.139}$$

$$\dot{m}_{16}s_{16} + \dot{S}_{gen,MC2} = \dot{m}_{54}s_{54} \tag{4.140}$$

$$\dot{m}_{16}ex_{16} = \dot{m}_{54}ex_{54} + \dot{E}x_{d,MC2} \tag{4.141}$$

The mixing chamber 3 in multigeneration system 3 can be analyzed with following the mass, energy, entropy, and exergy balance equations respectively as follows:

$$\dot{m}_{53} + \dot{m}_{55} = \dot{m}_{17} \tag{4.142}$$

$$\dot{m}_{53}h_{53} + \dot{m}_{55}h_{55} = \dot{m}_{17}h_{17} \tag{4.143}$$

$$\dot{m}_{53}s_{53} + \dot{m}_{55}s_{55} + \dot{S}_{gen,MC3} = \dot{m}_{17}s_{17} \tag{4.144}$$

$$\dot{m}_{53}ex_{53} + \dot{m}_{55}ex_{55} = \dot{m}_{17}ex_{17} + \dot{E}x_{d,MC3} \tag{4.145}$$

Each throttling valve in multigeneration system 3 can be analyzed with following the mass, energy, entropy, and exergy balance equations respectively as follows:

$$\dot{m}_i = \dot{m}_o \tag{4.146}$$

$$\dot{m}_i h_i = \dot{m}_o h_o \tag{4.147}$$

$$\dot{m}_i s_i + \dot{S}_{gen,tv} = \dot{m}_o s_o \tag{4.148}$$

$$\dot{m}_i ex_i = \dot{m}_o ex_o + \dot{E}x_{d,tv} \quad (4.149)$$

Each compressor in multigeneration system 3 can be analyzed with following the mass, energy, entropy, and exergy balance equations respectively as follows:

$$\dot{m}_i = \dot{m}_o \quad (4.150)$$

$$\dot{m}_i h_i + \dot{W}_c = \dot{m}_o h_o \quad (4.151)$$

$$\dot{m}_i s_i + \dot{S}_{gen,c} = \dot{m}_o s_o \quad (4.152)$$

$$\dot{m}_i ex_i + \dot{W}_c = \dot{m}_o ex_o + \dot{E}x_{d,c} \quad (4.153)$$

The heat exchanger 1 in multigeneration system 3 can be analyzed with following the mass, energy, entropy, and exergy balance equations respectively as follows:

$$\dot{m}_{12} = \dot{m}_{13} \quad (4.154)$$

$$\dot{m}_{12} h_{12} = \dot{Q}_{HX1} + \dot{m}_{13} h_{13} \quad (4.155)$$

$$\dot{m}_{12} s_{12} + \dot{S}_{gen,HX1} = \dot{m}_{13} s_{13} \quad (4.156)$$

$$\dot{m}_{12} ex_{12} = \dot{E}x_{\dot{Q}_{HX1}} + \dot{m}_{13} ex_{13} + \dot{E}x_{d,HX1} \quad (4.157)$$

The heat exchanger 3 in multigeneration system 3 can be analyzed with following the mass, energy, entropy, and exergy balance equations respectively as follows:

$$\dot{m}_{15} = \dot{m}_{16} \quad (4.158)$$

$$\dot{m}_{15} h_{15} = \dot{Q}_{HX3} + \dot{m}_{16} h_{16} \quad (4.159)$$

$$\dot{m}_{15} s_{15} + \dot{S}_{gen,HX3} = \dot{m}_{16} s_{16} \quad (4.160)$$

$$\dot{m}_{15} ex_{15} = \dot{E}x_{\dot{Q}_{HX3}} + \dot{m}_{16} ex_{16} + \dot{E}x_{d,HX3} \quad (4.161)$$

The MED desalination unit in multigeneration system 3 can be analyzed with following the mass, energy, entropy, and exergy balance equations respectively as follows:

$$\dot{m}_{29} = \dot{m}_{50} \text{ and } \dot{m}_{25} = \dot{m}_{14} + \dot{m}_{23} \quad (4.162)$$

$$X_{25} \dot{m}_{25} = X_{14} \dot{m}_{14} + X_{23} \dot{m}_{23} \quad (4.163)$$

$$\dot{m}_{29}h_{29} + \dot{m}_{25}h_{25} = \dot{m}_{14}h_{14} + \dot{m}_{23}h_{23} \quad (4.164)$$

For the electrolyzer in multigeneration system 3, the energy requirement for the hydrogen production reaction can be expressed as:

$$\Delta H = \Delta G + T\Delta S \quad (4.165)$$

where Gibbs free energy is denoted with ΔG and the energy requirement in thermal form is denoted with $T\Delta S$.

For efficiencies:

For the Cu-Cl thermochemical hydrogen production cycle, the conversion efficiency is analyzed as follows:

$$\eta_{conversion,Cu-Cl} = \frac{LHV_{H_2}}{\dot{Q}_{net} + \dot{W}} \quad (4.166)$$

where the lower heating value of hydrogen is represented with LHV_{h2}, the net heat input is represented with $\dot{Q}_{net,}$ and required electrical work is represented with $\dot{W}$.

For multigeneration system 3, the overall energy and exergy efficiencies can be expressed as follows:

$$\eta_{en,ov} = \frac{\dot{W}_{El,net} + m_{H_2}LHV_{H_2} + m_{fw}h_{fw} + \dot{Q}_{Res} + \dot{Q}_{Gh}}{I_{GH}A_{cell} + (m_1h_1 - m_{56}h_{56})} \quad (4.167)$$

$$\eta_{ex,ov} = \frac{\dot{W}_{El,net} + m_{H_2}ex_{H_2} + m_{fw}ex_{fw} + \dot{Q}_{Res}(1-\frac{T_o}{T_s}) + \dot{Q}_{Gh}(1-\frac{T_o}{T_s})}{I_{GH}A_{cell}\left(1-\frac{T_o}{T_{sun}}\right) + (m_1ex_1 - m_{56}ex_{56})} \quad (4.168)$$

Table 4.1 shows the main processes in 4 step Cu-Cl cycle. Aspen plus simulations are employed for the analyses of the Cu-Cl cycle.

Cost comparison methods are applied in order to determine the commercial viability of the multigeneration systems, net present value (NPV), internal rate of return (IRR), pay-back period (PBP), and unit cost of useful output are calculated. A 5% interest rate for the bank loan from a Turkish commercial bank is considered. All currencies are considered as United States dollars. Incentive tariffs are considered for the electricity commodity. For

the payback period calculation, residential and commercial tariffs are considered. Regional changes are neglected on tariffs for comparison purposes.

Table 4.1 Equations of 4 step Cu-Cl thermochemical hydrogen production cycle

#	Step	Equation
1	Hydrolysis	$2CuCl_2 + H_2O \rightarrow 2Cu_2OCl_2 + 2HCl$
2	Thermolysis	$Cu_2OCl_2 \rightarrow 2CuCl + 1/2O_2$
3	Electrolysis	$2CuCl + 2HCl \rightarrow 2CuCl_2 + H_2$
4	Drying	$CuCl_{2(aq)} \rightarrow \ CuCl_{2(s)}$

Chapter 5. Results and Discussion

Three multigeneration systems in Turkey, the United States, and Japan with different scenarios are designed, simulated, and analyzed. Several scenarios and parameters are applied to investigate the effect on both subsystems and overall system performances. In the PV subsystem, four different scenarios are applied, namely (i) conventional monocrystalline PV module in 0.2 regular albedo field with tracker structure PV plant, (ii) conventional monocrystalline PV module in 0.8 enhanced albedo field with tracker structure PV plant, (iii) bifacial monocrystalline PV module in 0.2 regular albedo field with tracker structure BiPV plant and (iv) bifacial monocrystalline PV module in 0.8 enhanced albedo field with tracker structure PV plant. Height and pitch distances are designed as 7.2m and 3.0m respectively. Axis height above ground is designed relatively higher than the regular PV plants, however, it is one of the most important parameters for BiPV plants due to the created gap which provides larger space for reflected solar radiation. PV modules with 80% of the bifaciality factor are selected from a Tier-1 company. Inverters are also selected from a Tier-1 company. In contrast with regular PV plants, DC/AC ratio is designed as 1.04 which is relatively lower since the BiPV modules' high-performance expectation. Therefore, inverters are sized for relatively lower DC/AC ratios.

PV plant scenarios have similarities in terms of installed capacity, component quality, and have differences in terms of module type and ground albedo. 20% and 80% albedo fields are simulated with conventional and BiPV modules. Installed capacity is designed as 1.350MWp and 1.3MWac. 400Wp monocrystalline bifacial and monofacial PV modules are utilized with 100kWac inverters. 16 modules in series, 211 strings in parallel, 3376 PV modules are connected to 13 units of inverters. Total cell area and module area are calculated as 6279m^2 and 7135m^2 respectively.

Due to the simulation results for the PV system, in multigeneration system 1, BiPV plants are simulated in Gokcebayir in Turkey location. Specific electricity production is calculated as 1719kWh/kWp/year in the first scenario which consists of 0.2 albedo field with conventional modules. The overall PV plant is produced 2322MWh/year electricity in the first scenario. Conventional PV modules are employed in 0.8 enhanced albedo field in the second scenario. Very similar results are obtained with the first scenario, therefore,

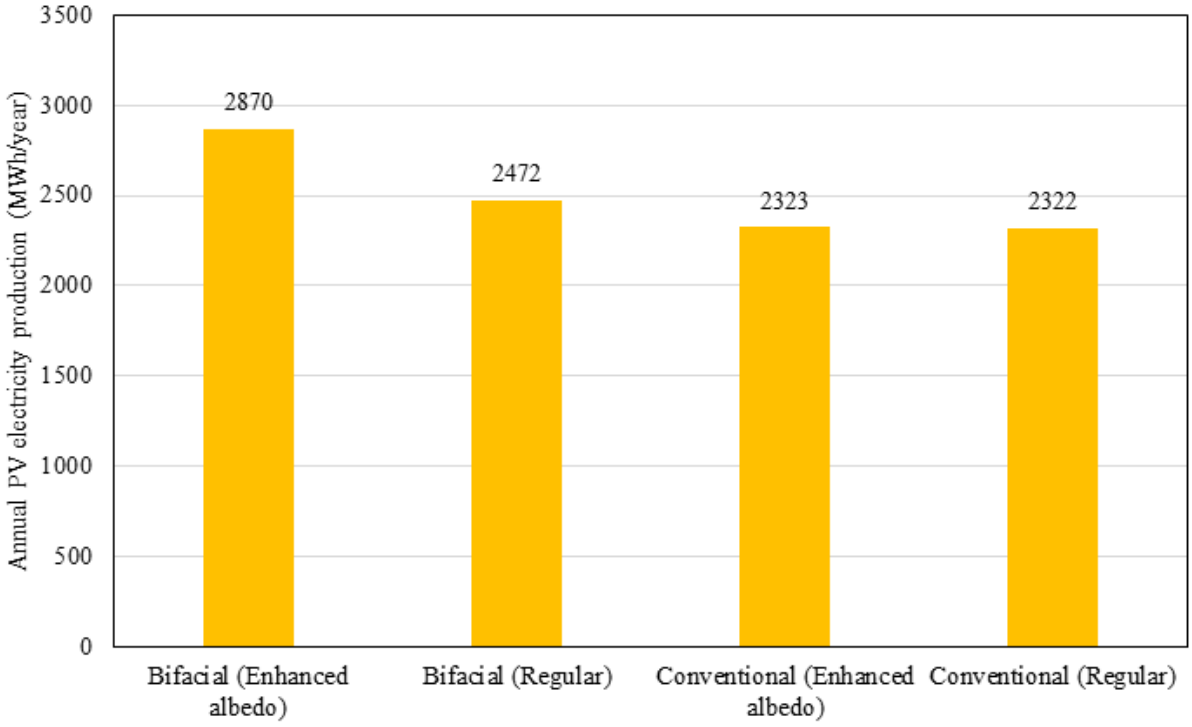

Figure 5.1 PV electricity production by PV plant scenario for Gokcebayir in Turkey

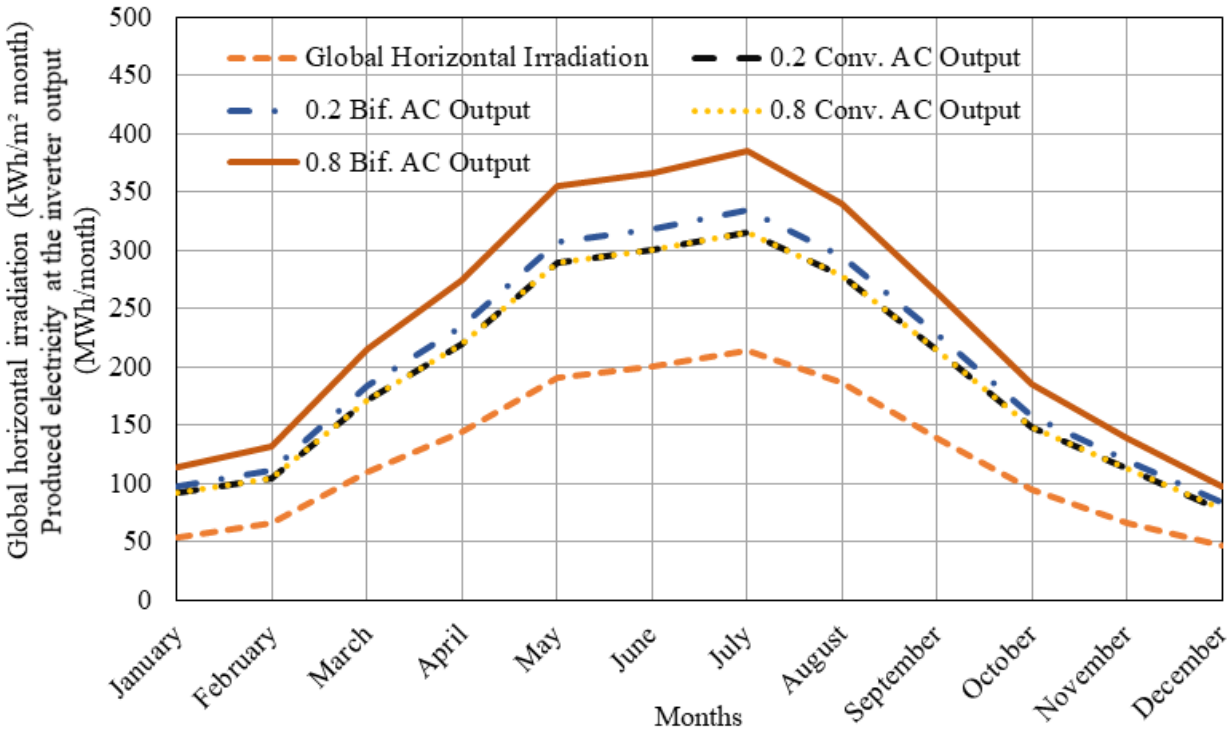

Figure 5.2 BiPV plant electricity production with horizontal global irradiation monthly averages from real data of 2003 to 2013 for Gokcebayir in Turkey (meteorological data from [116])

2323MWh electricity is produced annually at 1720kWh/kWp/year specific production. Only 0.043% of energy gain is calculated between the first and second scenarios where field albedo enhancement is applied. BiPV modules are employed in the third scenario in a regular 0.2 ground albedo field. 2472MWh annual electricity is produced at 1831kWh/kWp/year specific production. Bifacial electricity gain is calculated as 6.4% in comparison with the first scenario. The bifacial PV plant is designed in the fourth and last scenario. BiPV modules are employed in the 0.8 enhanced albedo field. In this last scenario, 2870 MWh annual electricity is produced at 2125 kWh/kWp/year specific production. Bifacial electricity gain is peaked in this BiPV plant where 23.6% of bifacial electricity gain is calculated. PV electricity production for each scenario can be seen in Figure 5.1 for Gokcebayir in Turkey. PV plant productions during the year are shown in Figure 5.2. The effect of ambient temperatures on PV plant performance can be seen in Figure 5.3.

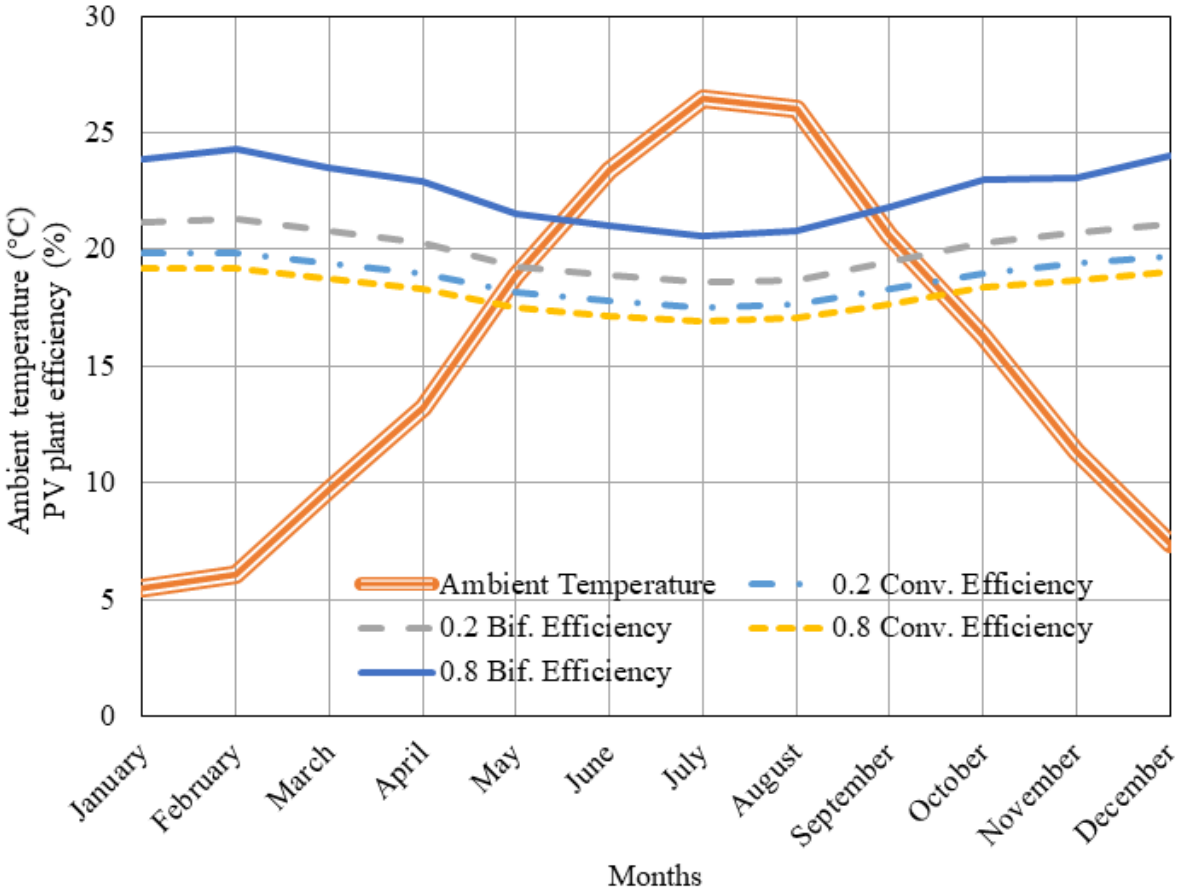

Figure 5.3 BiPV plant performance with ambient temperature monthly averages from real data of 2003 to 2013 for Gokcebayir in Turkey meteorological (meteorological data from [116])

Different amount of energy is produced for different daily global solar irradiation each day. Produced daily electricity by global horizontal irradiation for conventional and bifacial cases in Figures 5.4 and 5.5 respectively.

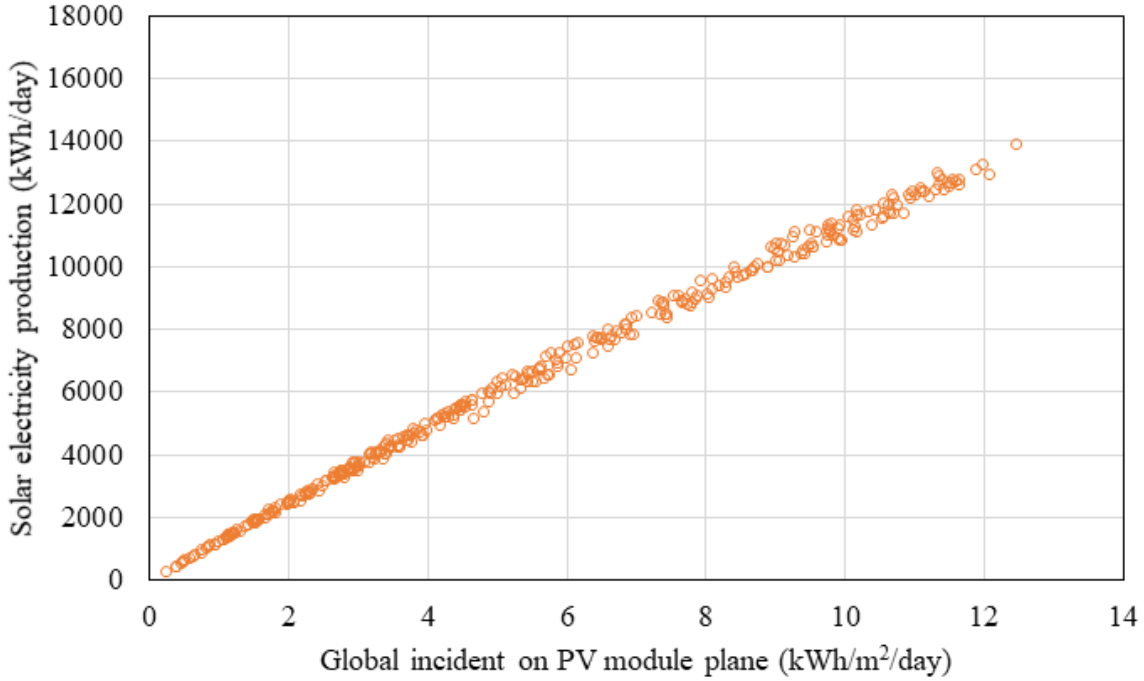

Figure 5.4 Energy injection into the grid by daily global incident in collector plane (Regular albedo mono-facial PV plant in Gokcebayir in Turkey)

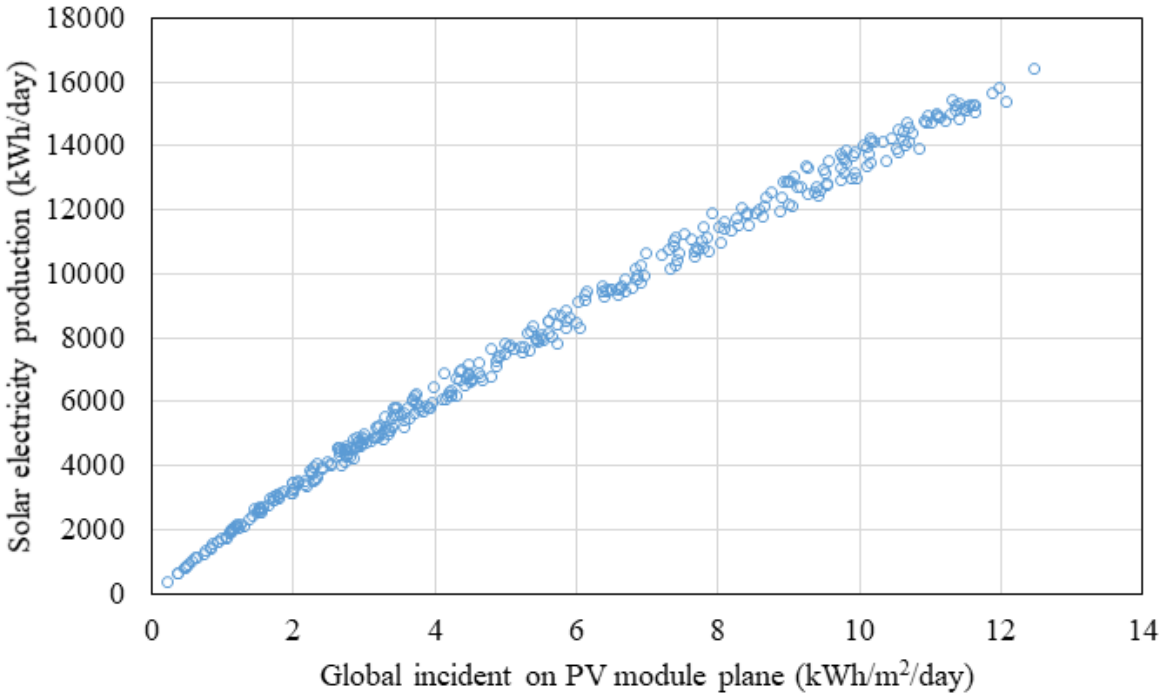

Figure 5.5 Energy injection into the grid by daily global incident in collector plane (Enhanced albedo BiPV plant in Gokcebayir in Turkey)

Although there is no BiPV plant is employed in multigeneration system 2, BiPV plants are simulated for Geysers in the United States location for comparison purposes. PV plant productions during the year are shown in Figure 5.6 for each scenario. Different amount of energy is produced for different daily global solar irradiation each day. Produced daily electricity by global horizontal irradiation for conventional and bifacial cases in Figures 5.7 and 5.8 respectively. Total PV electricity production for each scenario can be seen in Figure 5.9 for Geysers in the United States. Specific electricity production is calculated as 2127kWh/kWp/year in the first scenario which consists of 0.2 albedo field with conventional modules. Overall, the PV plant is produced 2873MWh/year electricity in the first scenario. Conventional PV modules are employed in 0.8 enhanced albedo field in the second scenario. Very similar results are obtained with the first scenario, therefore, 2874MWh electricity is produced annually at 2128kWh/kWp/year specific production. Only 0.047% of energy gain is calculated between the first and second scenarios where field albedo enhancement is applied.

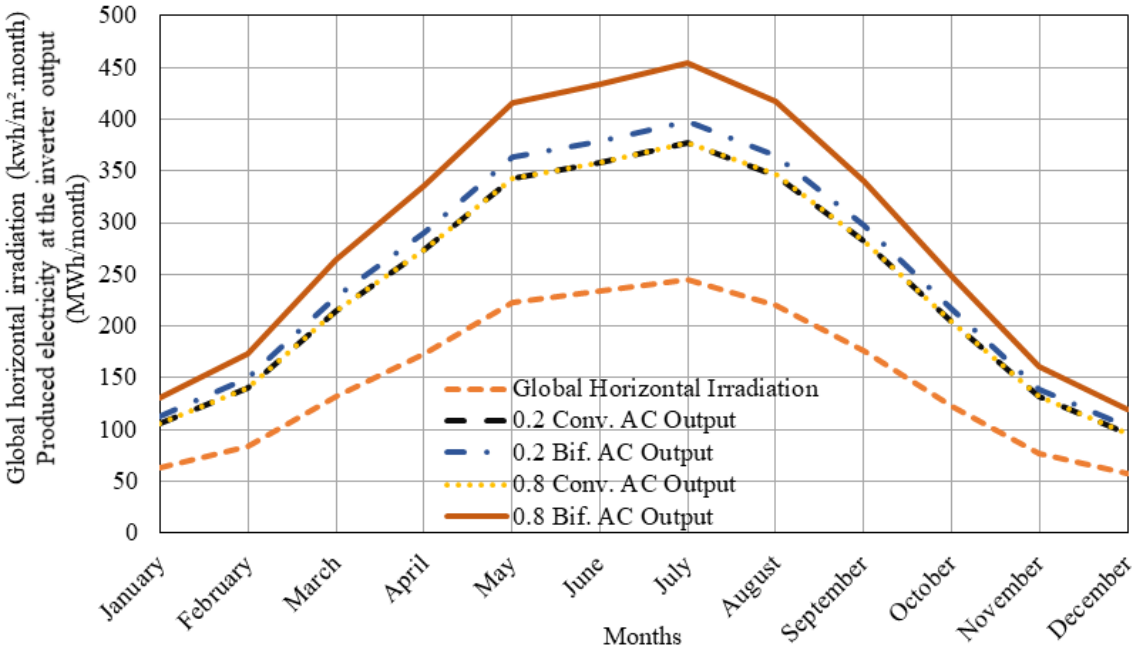

Figure 5.6 BiPV plant electricity production with horizontal global irradiation monthly averages from real data Geysers in the United States (meteorological data from [116])

BiPV modules are employed in the third scenario in a regular 0.2 ground albedo field. 3041MWh annual electricity is produced at 2252kWh/kWp/year specific production. Bifacial electricity gain is calculated as 5.82% in comparison with the first scenario. Another BiPV plant with enhanced albedo is designed in the fourth and last scenario. BiPV

modules are employed in the 0.8 enhanced albedo field. In this last scenario, 3491MWh annual electricity is produced at 2585kWh/kWp year specific production. Bifacial electricity gain is peaked in this BiPV plant where a 21.5% gain is calculated. The effect of ambient temperatures on PV plant performance can be seen in Figure 5.10. Hourly sensitive power output for a year can be seen in Figure 5.11.

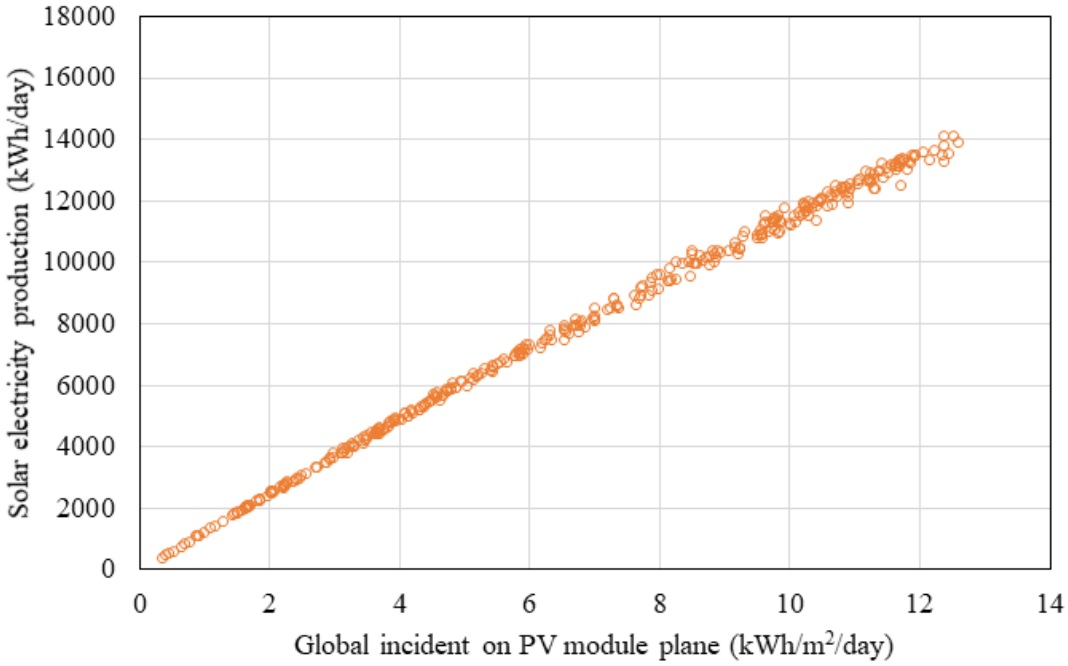

Figure 5.7 Energy injection into the grid by a daily global incident in collector plane (Regular albedo mono-facial PV plant in Geysers in the United States) (meteorological data from [116])

In multigeneration system 3, BiPV plants are simulated in Shinozaki in Japan location. PV plant productions during the year are shown in Figure 5.12 for each scenario. Total PV electricity production for each scenario can be seen in Figure 5.13 for Shinozaki in Japan.

The effect of ambient temperatures on PV plant performance can be seen in Figure 5.14. Hourly sensitive power output for a year can be seen in Figure 5.15. Specific electricity production is calculated as 1429kWh/kWp/year in the first scenario which consists of 0.2 albedo field with conventional modules. The overall PV plant is produced 1930MWh/year electricity in the first scenario. Conventional PV modules are employed in0.8 enhanced albedo field in the second scenario. Very similar results are obtained with the first scenario, therefore, 1931MWh electricity is produced annually at

1430kWh/kWp/year specific production. Only 0.052% of energy gain is calculated between the first and second scenarios where field albedo enhancement is applied.

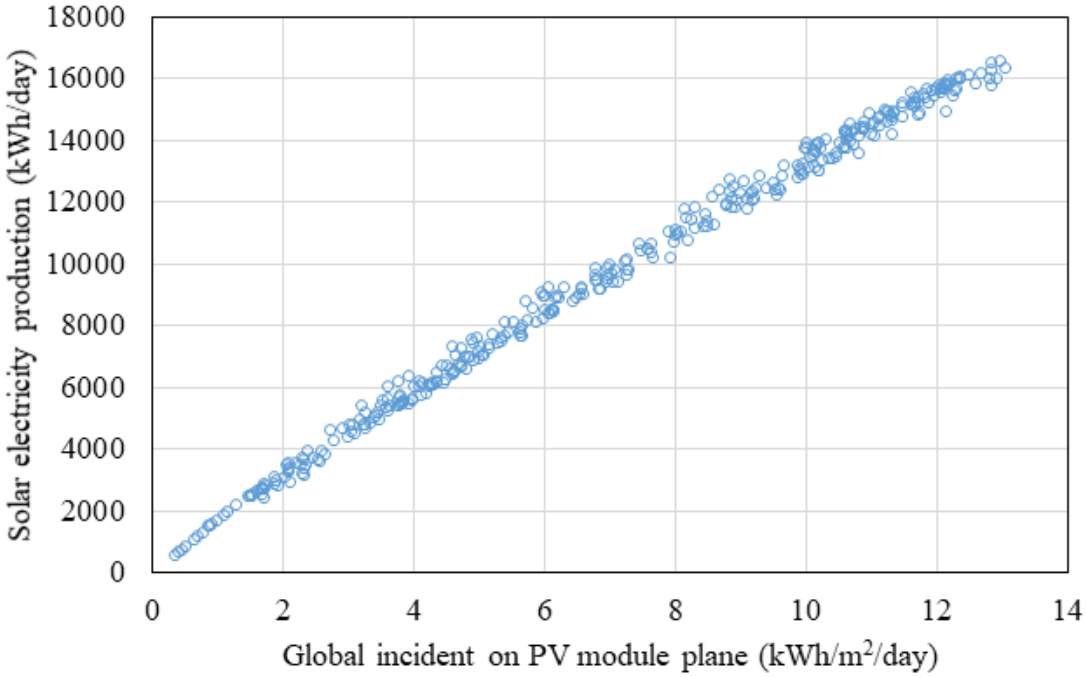

Figure 5.8 Energy injection into the grid by a daily global incident in collector plane (Enhanced albedo BiPV plant in Geysers in the United States)

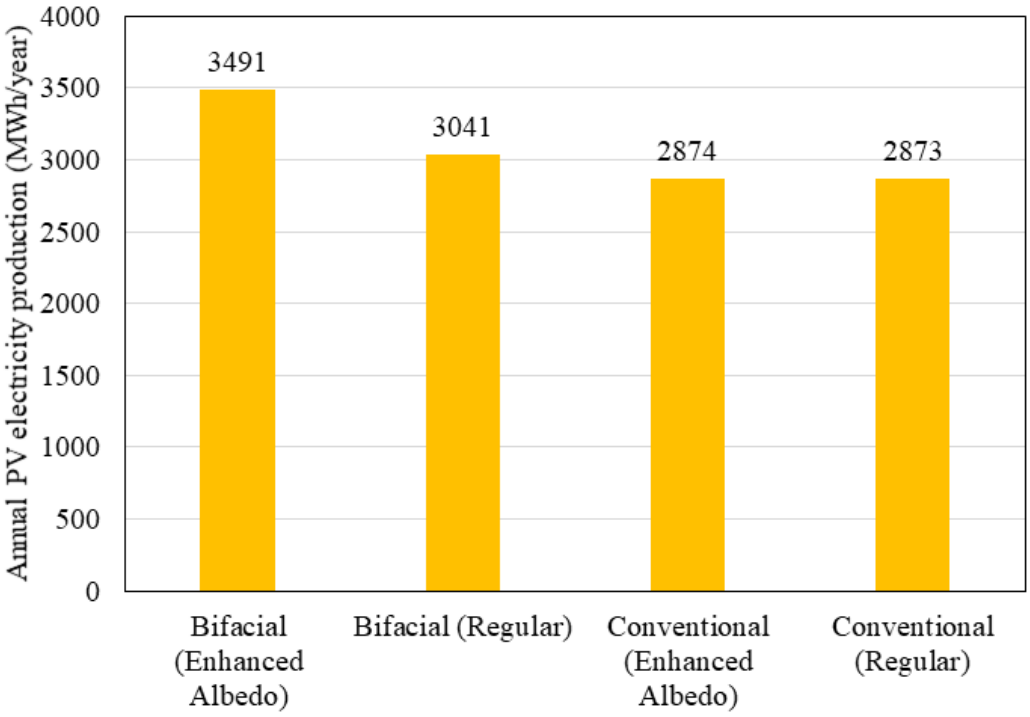

Figure 5.9 PV electricity production by PV plant scenario for Geysers in the United States

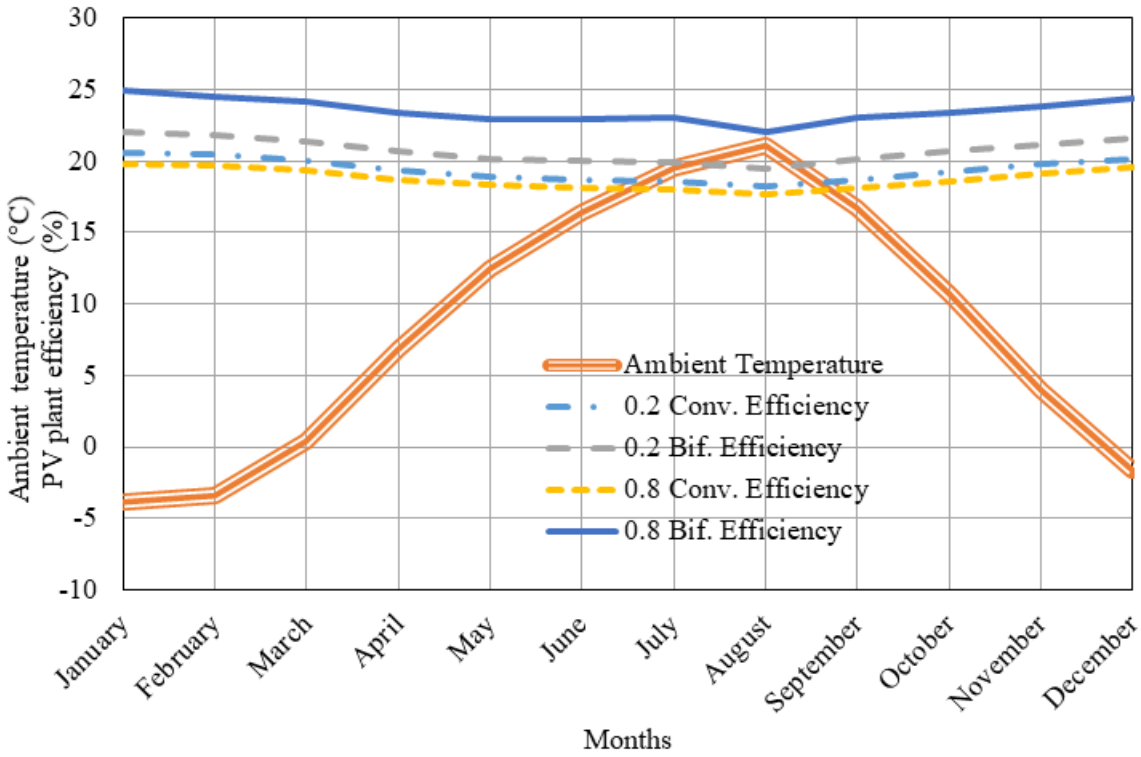

Figure 5.10 BiPV plant performance with ambient temperature monthly averages from real data Geysers in the United States (meteorological data from [116])

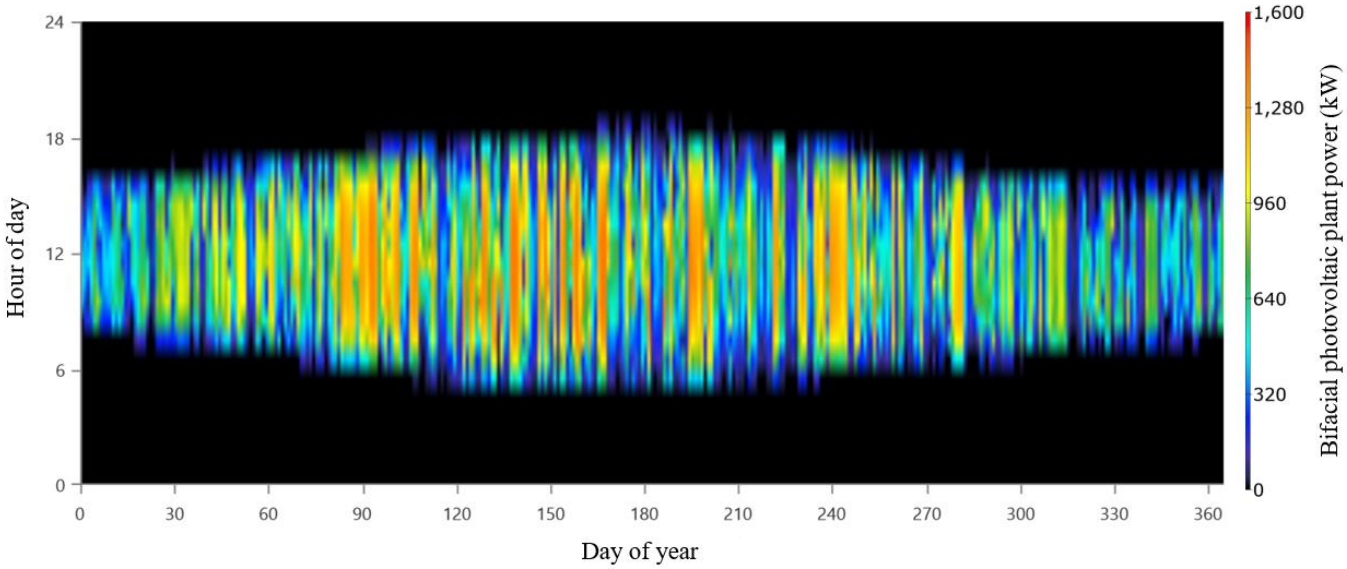

Figure 5.11 BiPV plant production during the year for multigeneration system 2

BiPV modules are employed in the third scenario in a regular 0.2 ground albedo field. 2065MWh annual electricity is produced at 1529kWh/kWp/year specific production. Bifacial electricity gain is calculated as 6.9% in comparison with the first scenario. A novel PV plant is designed in the fourth and last scenario. BiPV modules are employed in the 0.8

enhanced albedo field. In this last scenario, 2422MWh annual electricity is produced at 1794kWh/kWp/year specific production. Bifacial electricity gain is peaked in this BiPV plant where 25.5% of bifacial electricity gain is calculated. Different amount of energy is produced for different daily global solar irradiation each day. Produced daily electricity by global horizontal irradiation for conventional and bifacial cases in Figure 5.16 and 5.17 respectively. Up to 15 MWh daily solar electricity production is occurred in the conventional case. Up to 17 MWh daily electricity production is reached via bifacial case. Shinozaki has the coldest average temperatures in comparison to Gokcebayir and Geysers fields. High array temperatures are led to decreasing energy efficiency. Array temperatures are mostly higher than the ambient temperatures. Bifacial PV module structure enables the higher heat transfer therefore faster cooling due to its frameless body. Even in the coldest field and with bifacial modules, higher array temperature than ambient temperature is inevitable. Due to the simulation results. Up to 55°C array temperatures are occurred. Daily global horizontal irradiation and ambient temperature are the most related parameters with array temperatures. Figure 5.18 shows the operating temperatures by effective irradiance. Operating temperatures are reached until 55°C even in the coldest selected location.

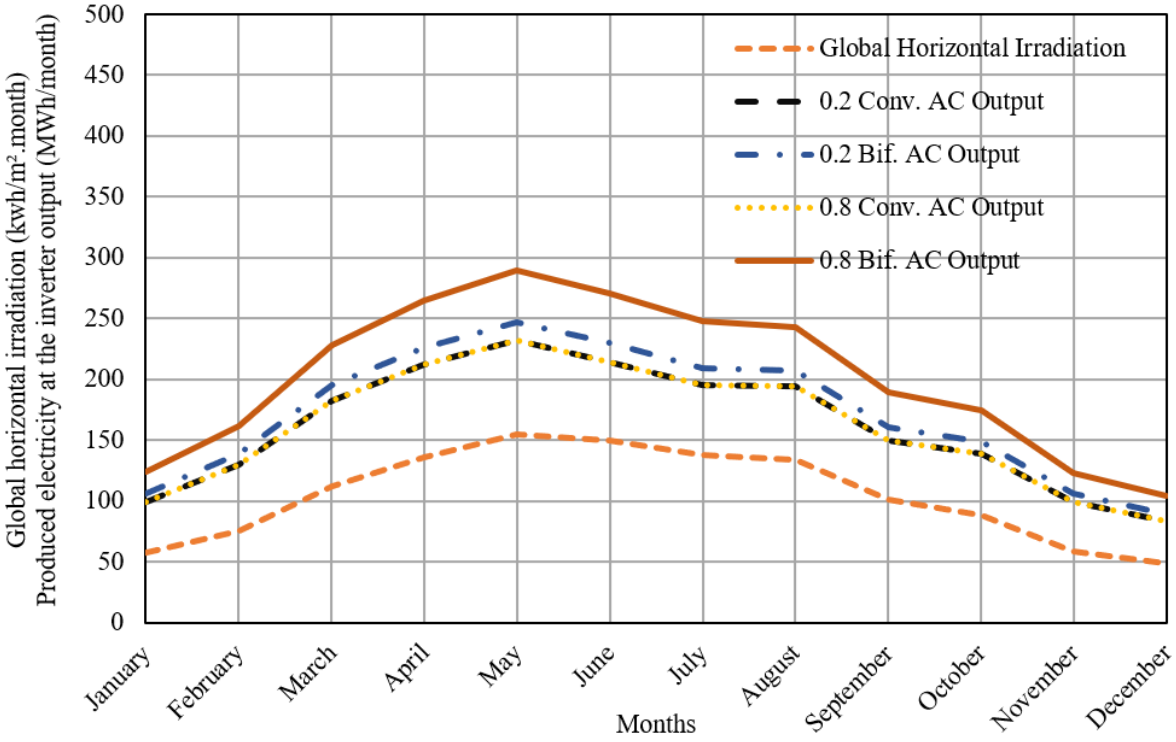

Figure 5.12 BiPV plant electricity production with horizontal global irradiation monthly averages from real data for Shinozaki in Japan (meteorological data from [116])

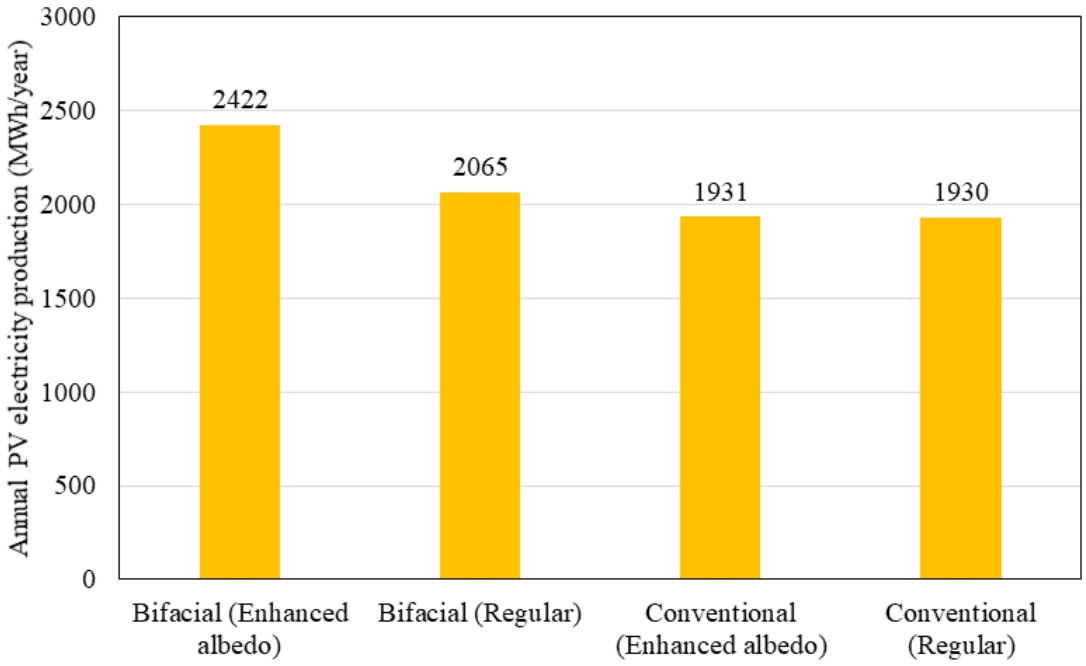

Figure 5.13 PV electricity production by PV plant scenario for Shinozaki in Japan (meteorological data from [116])

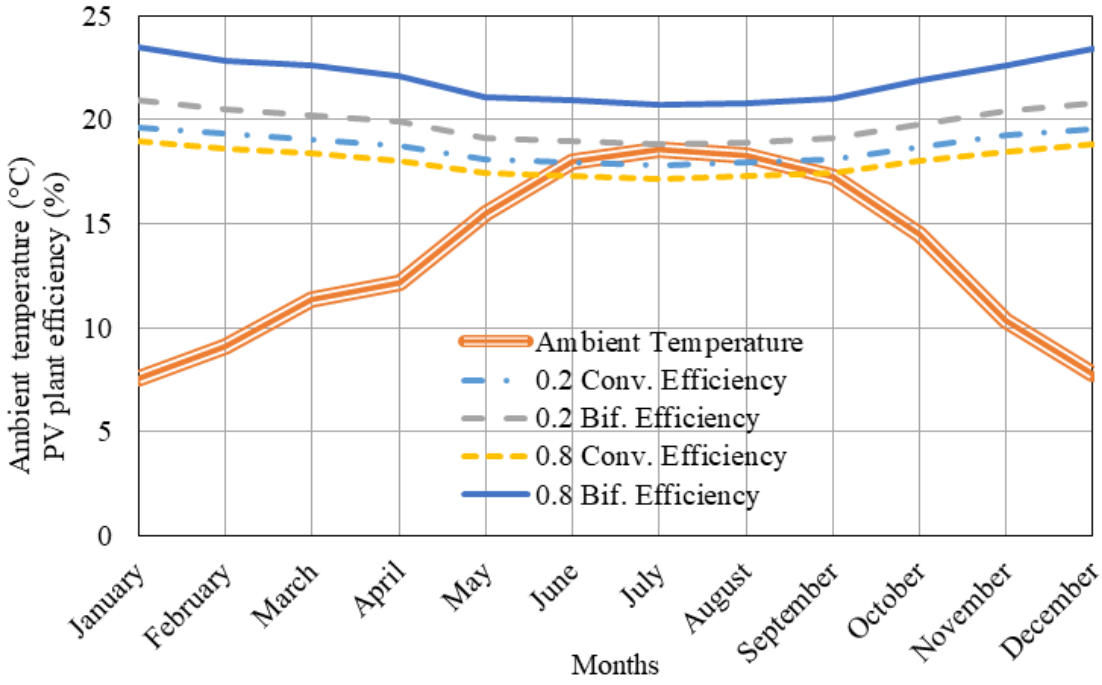

Figure 5.14 BiPV plant performance with ambient temperature monthly averages from real data for Shinozaki in Japan (meteorological data from [116])

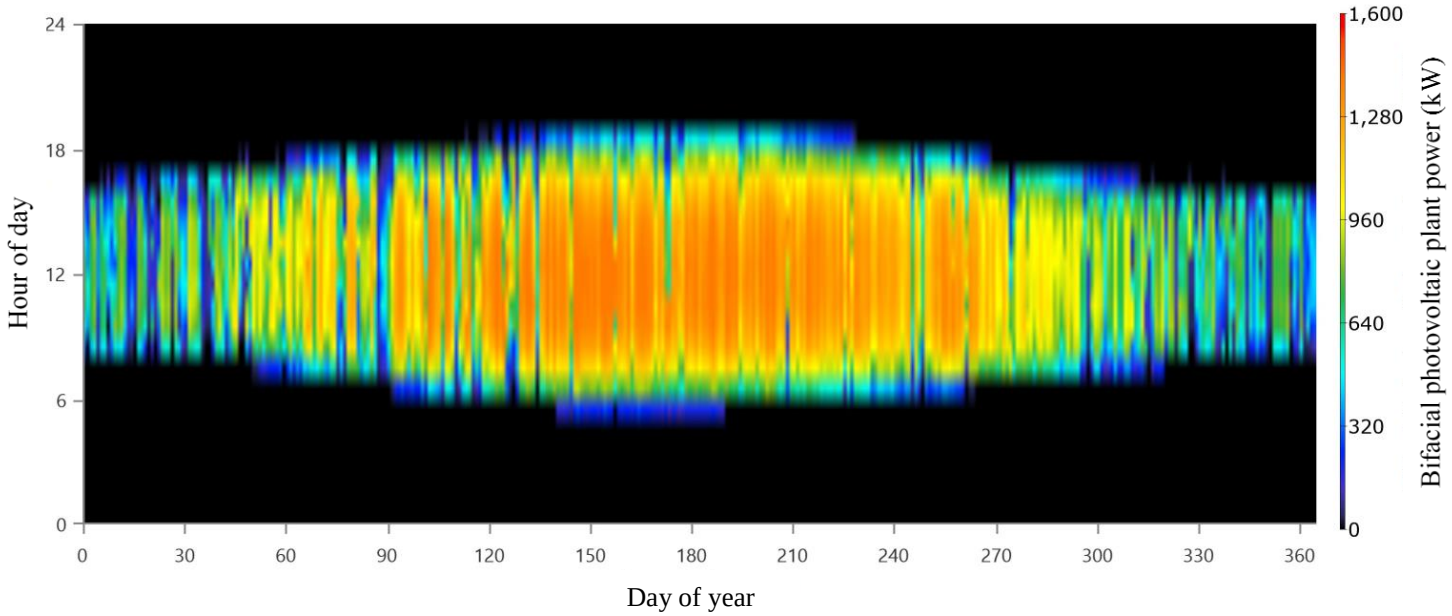

Figure 5.15 BiPV plant production during the year for multigeneration system 3

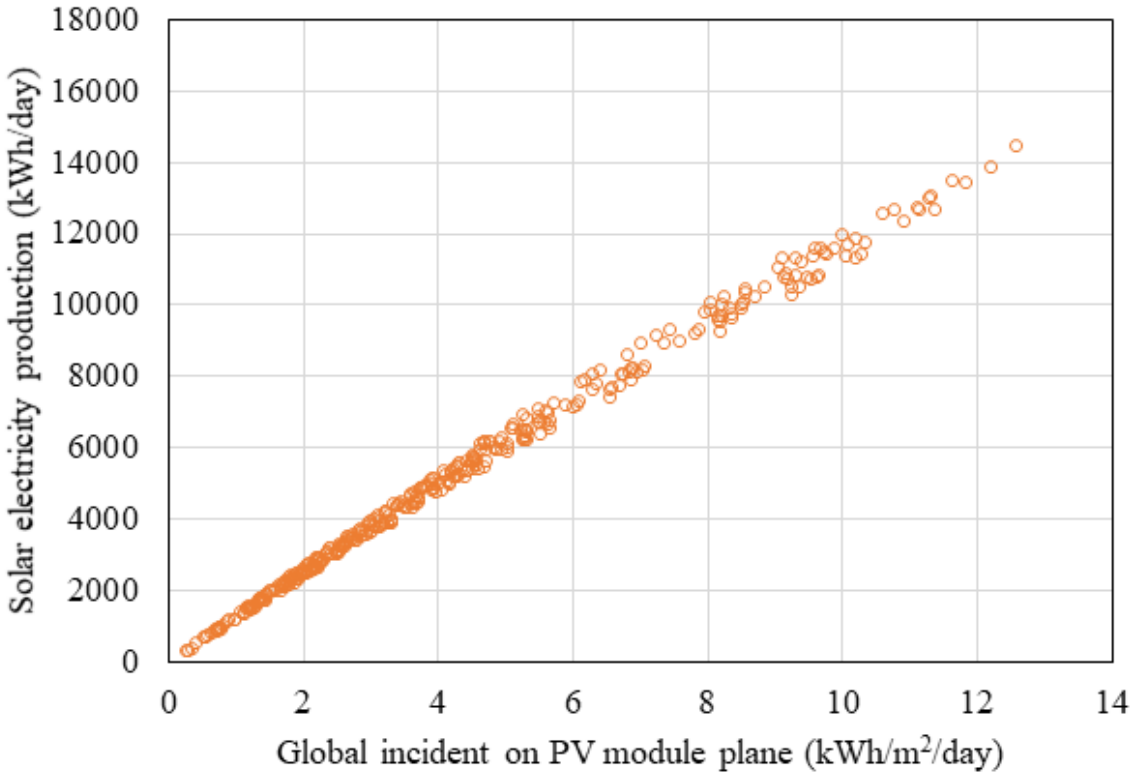

Figure 5.16 Energy injection into the grid by a daily global incident in collector plane (regular albedo conventional PV plant Shinozaki in Japan) (meteorological data from [116])

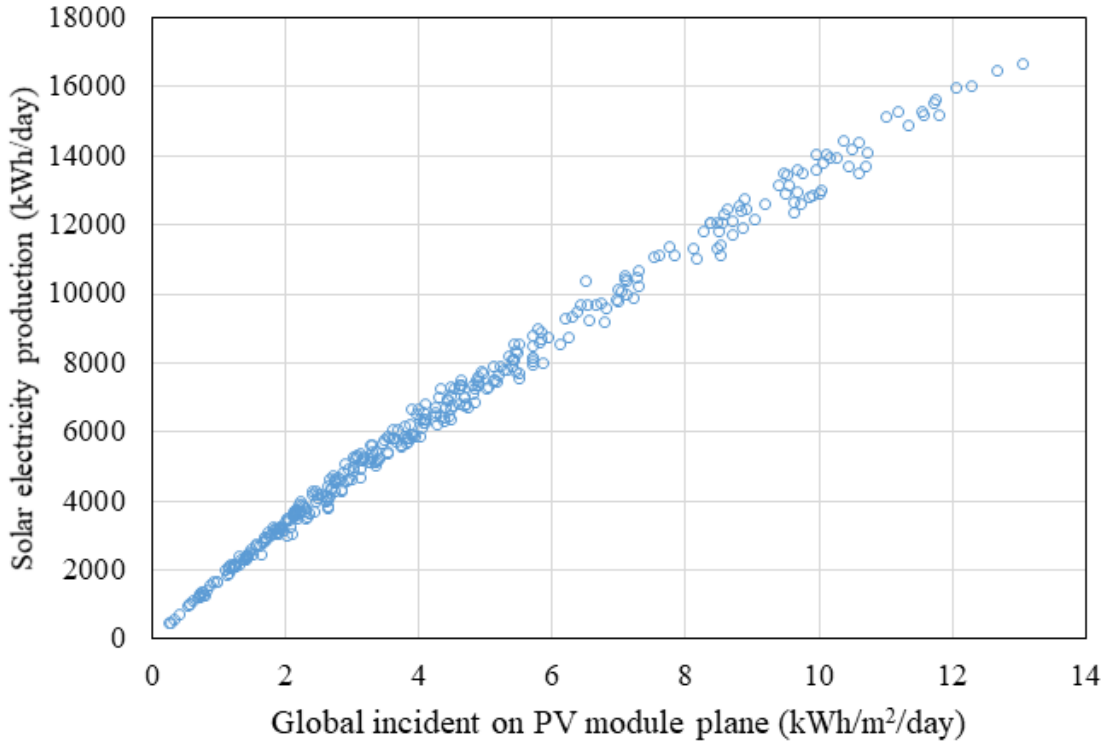

Figure 5.17 Energy injection into the grid by a daily global incident in collector plane (Enhanced albedo BiPV plant in Shinozaki in Japan)

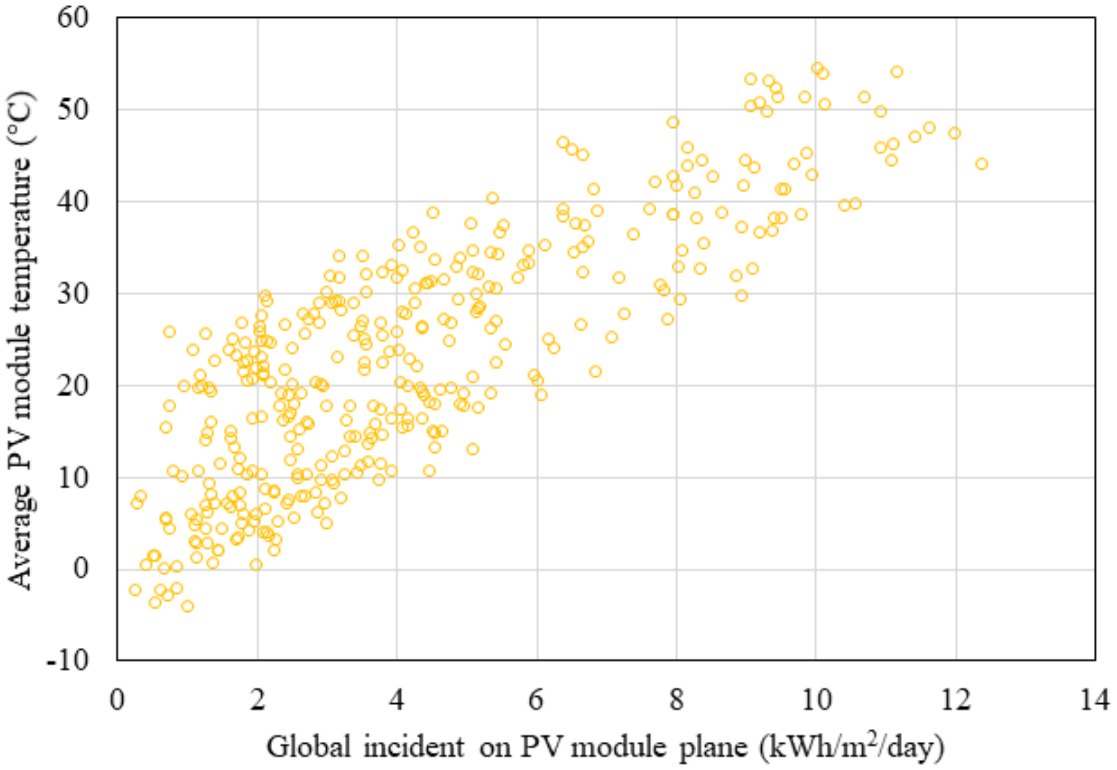

Figure 5.18 PV array temperature by effective irradiance in Shinozaki in Japan

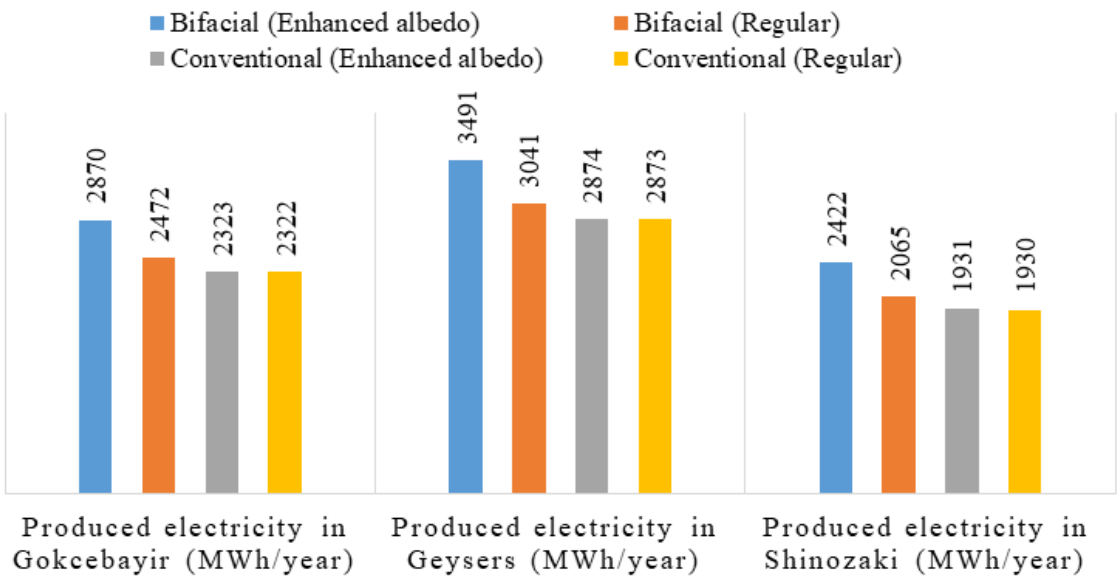

Figure 5.19 Annual electricity production comparison of PV plants

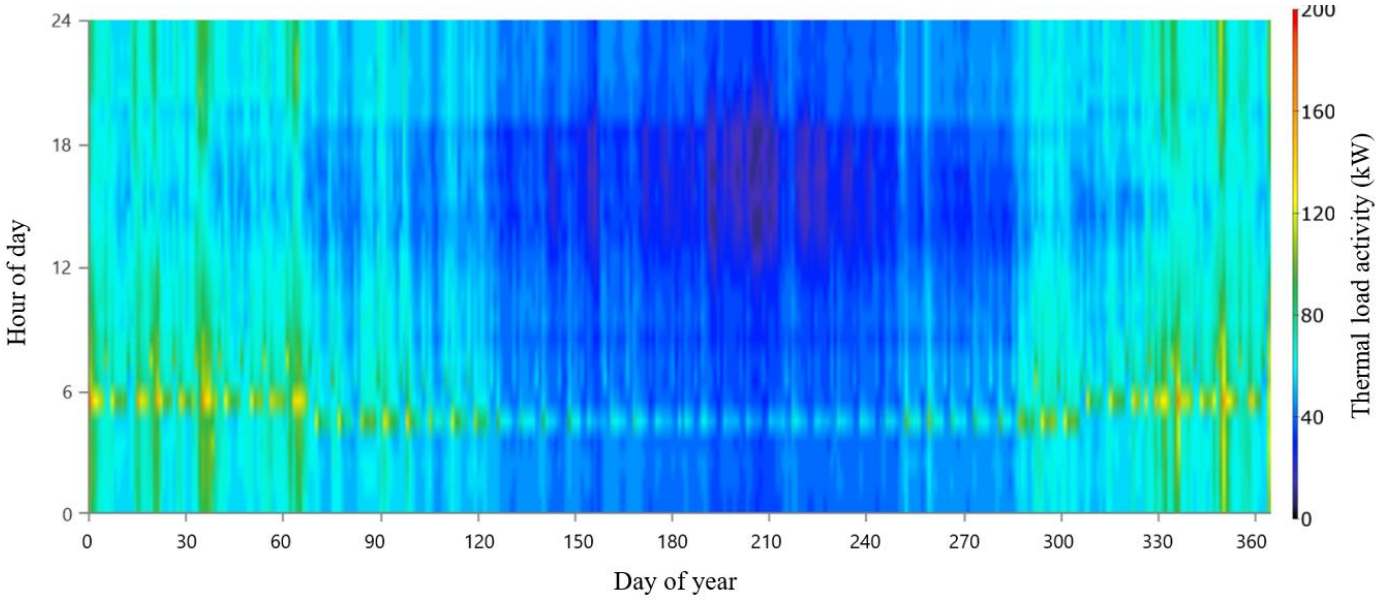

Figure 5.20 Thermal load data during an average year for multigeneration system 1

Four different PV plant scenarios in three different multigeneration system's location are compared in Figure 5.19. Application in Geysers location is performed with the best PV electricity production results. However, the PV plant is not utilized in this location. Since the biggest amount of solar radiation is reached to Geysers in comparison to other proposed locations, the CSP system for the Cu-Cl cycle to produce hydrogen is utilized rather than the PV plant.

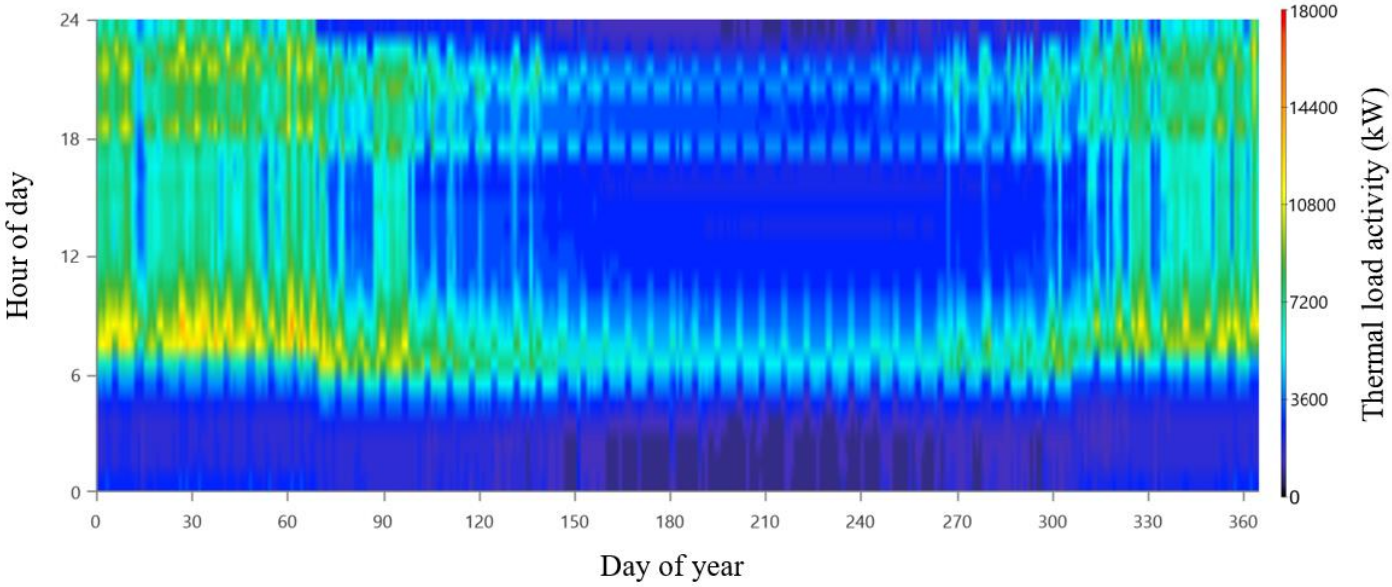

Figure 5.21 Thermal load data during an average year for multigeneration system 2

On the other hand, a 1.3MWp PV plant is scaled up to 21.32MWp PV plant to meet the electrical requirements of industrial hydrogen production in Shinozaki in Japan. As mentioned before, the net metering model with the Japanese national electrical grid is considered for further cost comparison calculations.

For the space heating useful output, heat pump cycle subsystems are employed to meet thermal load requirements. For multigeneration system 1, the residential thermal load is assumed as 446MWh/year. The assumption is made through the location's Köppen–Geiger climatic classification. Figure 5.20 shows the thermal demand for the average year.

For multigeneration system 2, 236,968 MWh/year residential thermal load is assumed as location's Köppen–Geiger climatic classification namely BSh warm semi-arid climate. Figure 5.21 shows the thermal demand for the average year.

For multigeneration system 3, the residential thermal load is obtained as 851MWh/year for its Dfa warm continental climate or humid continental climate class in Köppen–Geiger climatic classification. Figure 5.22 shows the thermal demand for the average year.

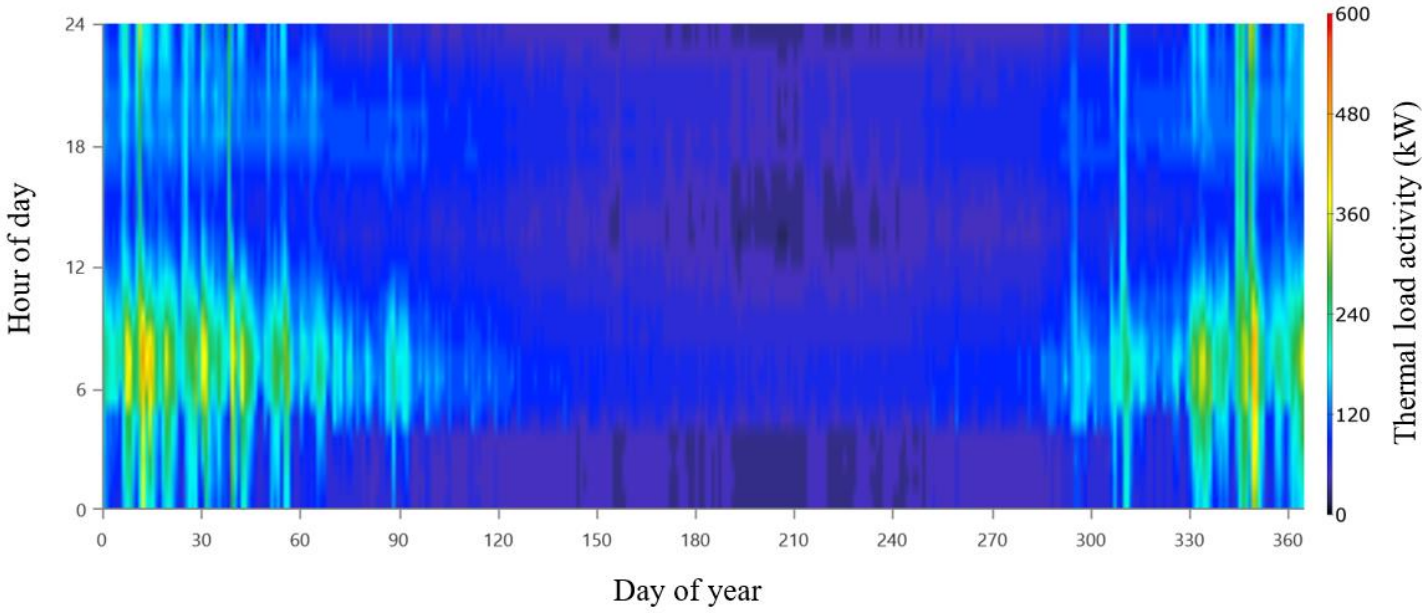

Figure 5.22 Thermal load data during an average year for multigeneration system 3

A CSP integrated with a thermal storage system via a molten salt storage unit is simulated in NREL's SAM software. Due to the results, 19757MWh gross thermal energy and 19370 net thermal energy is produced via parabolic trough CSP. Figure 5.23 shows the receiver's mass flow rate during the year. CSP system is operated at 42.6% capacity for a year. 411MWh electricity is consumed for tracking and auxiliary purposes.

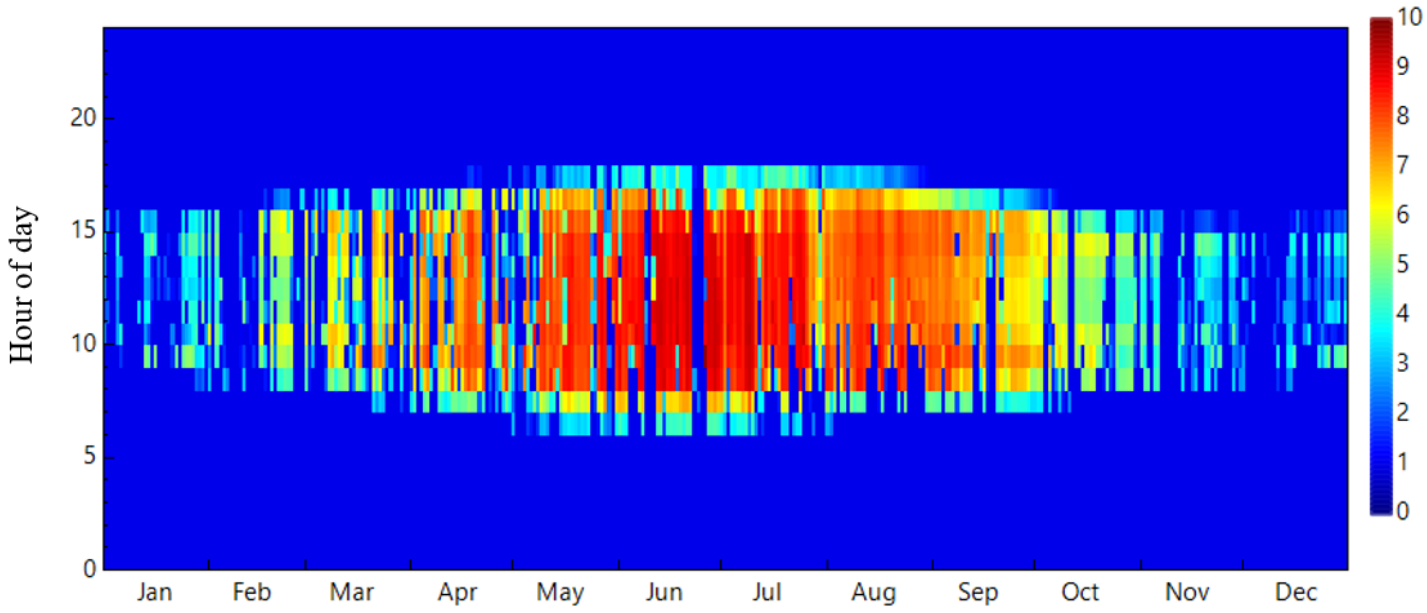

Figure 5.23 Mass flow rate of the heat transfer fluid for solar receiver component during the year (kg/s)

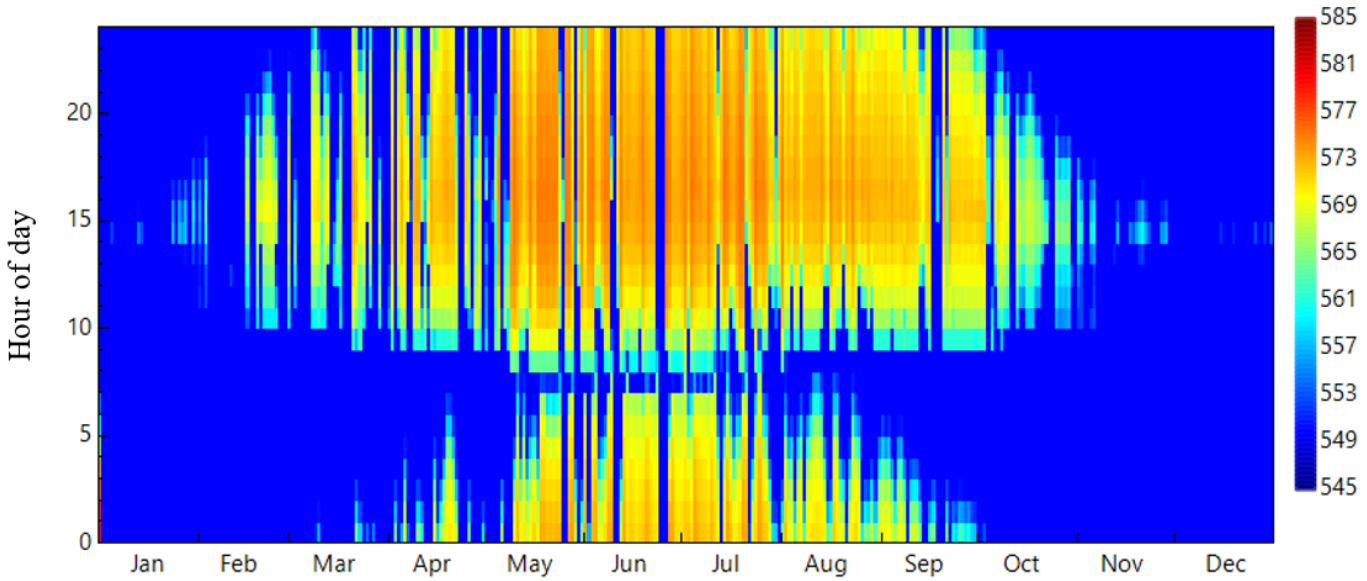

Figure 5.24 Thermal energy storage system hot molten salt storage tank temperature during the year (°C)

A thermal energy storage system is employed for continuous heat supply purposes. In the hot molten salt storage system, Hitec solar salt tried to keep at more than 550°C temperature minimum limit. Figure 5.24 shows the hot molten storage tank temperature during the year. The thermal energy storage system is charged and discharged during the year in order to maintain its desired temperature and feed the thermal load, in this case, the Cu-Cl cycle. Figure 5.25 shows the charge and discharge thermal powers for each month. In order to maintain desired temperatures, the mass flow rate changed during the year. Figure 5.26 and Figure 5.27 show the charge and discharge mass flow rates respectively. Up to 19kg/s mass flow rate is reached especially during the middle of the summer days. Discharges are occurred generally in the mornings up to 13 kg/s mass flow rates. Corners of Figures 5.26 and 5.27 are in dark blue color which represents no-activity. These are also the coldest moments of the entire year. Therefore, thermal energy storage system is unable to supply thermal energy during these moments. One potential solution is to increasing the energy storage capacity of the thermal energy storage system. However, this creates an exponential cost increment.

Figure 5.28 shows the heat losses for the average year. Heat loss occurs during the whole year from the thermal energy storage system. According to the results, heat losses occur between 0.054MWt and 0.064MWt. The ambient temperature and insulation are the

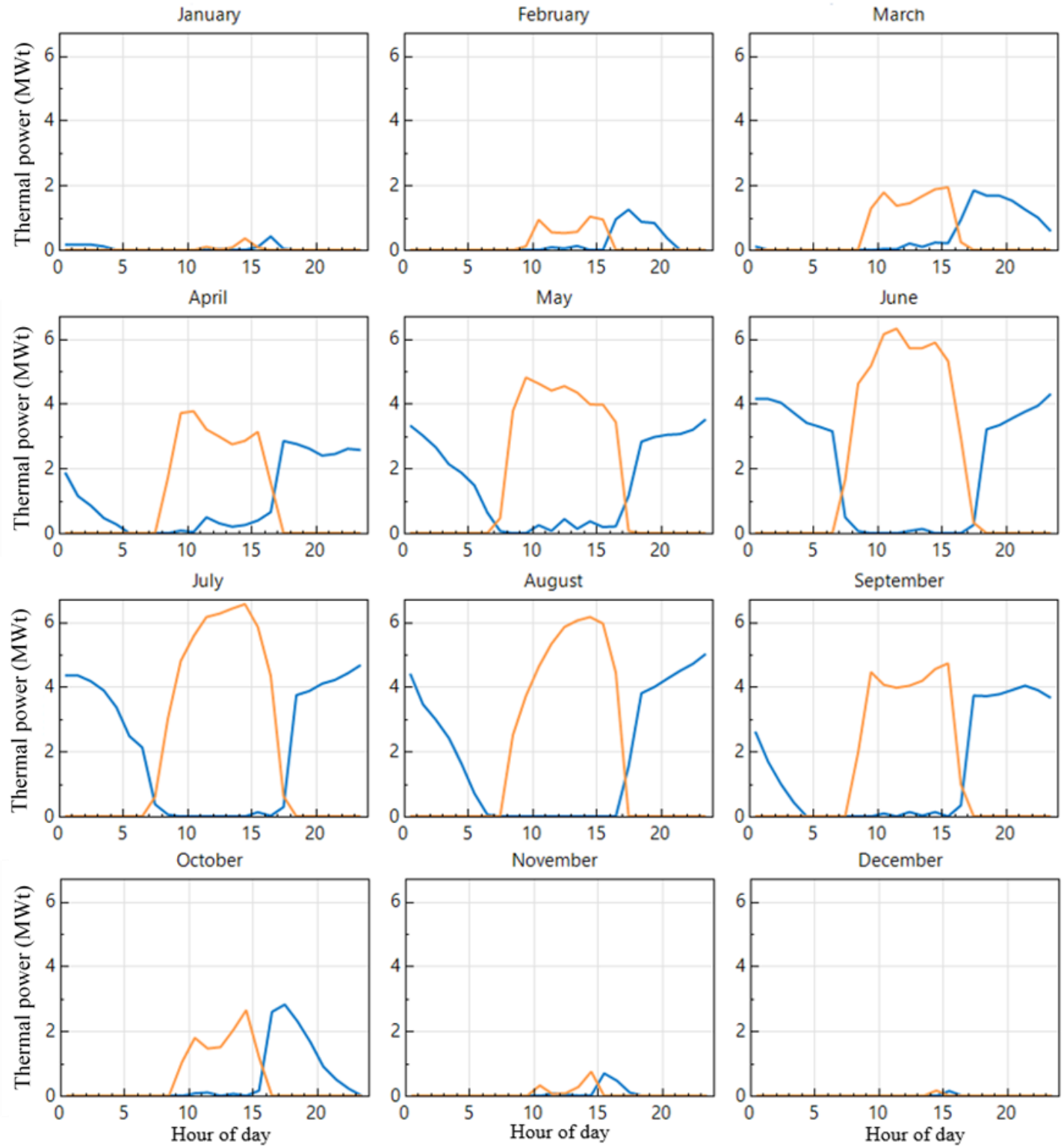

Figure 5.25 Thermal energy storage charging and discharging thermal power (MWt) for each month (blue: charging, orange: discharging)

two important factors that affect the thermal energy storage tank's heat losses during the year. Especially the cold ambient weather temperatures lead the more heat losses particularly during summer nights and other seasons.

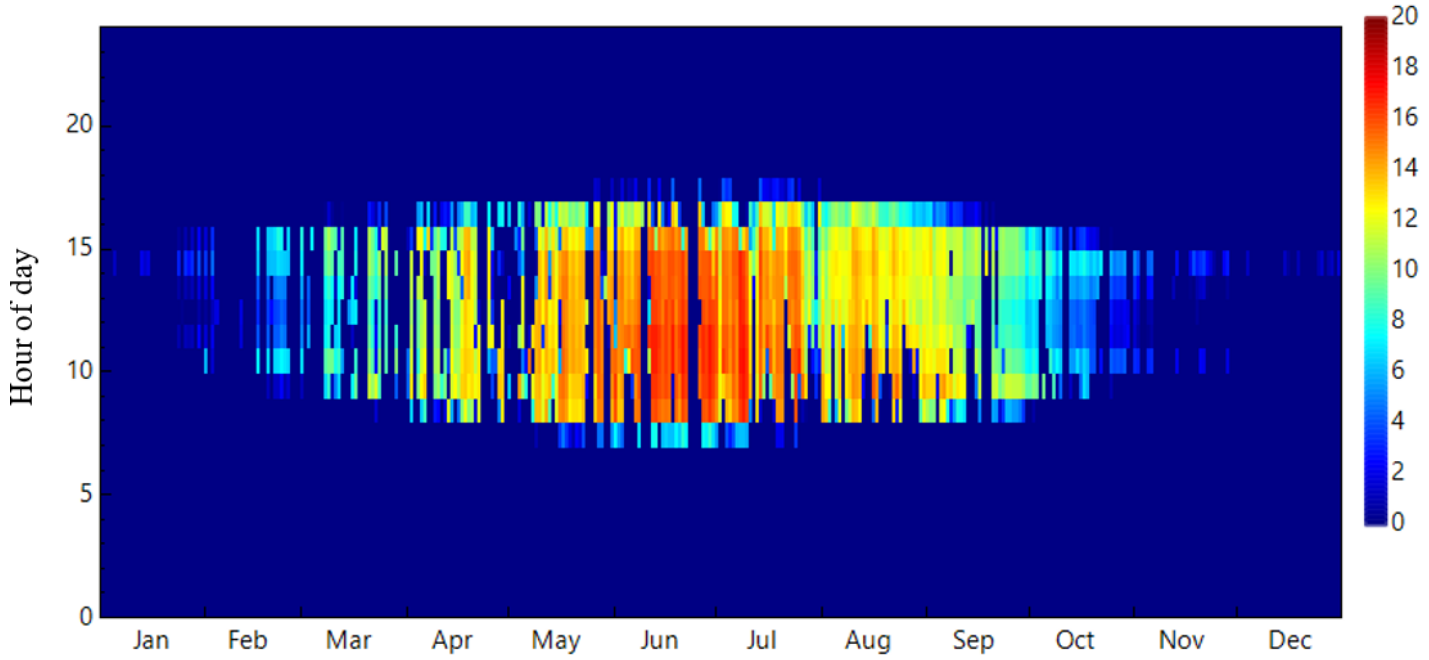

Figure 5.26 Thermal energy storage charging mass flow rate during the year (kg/s)

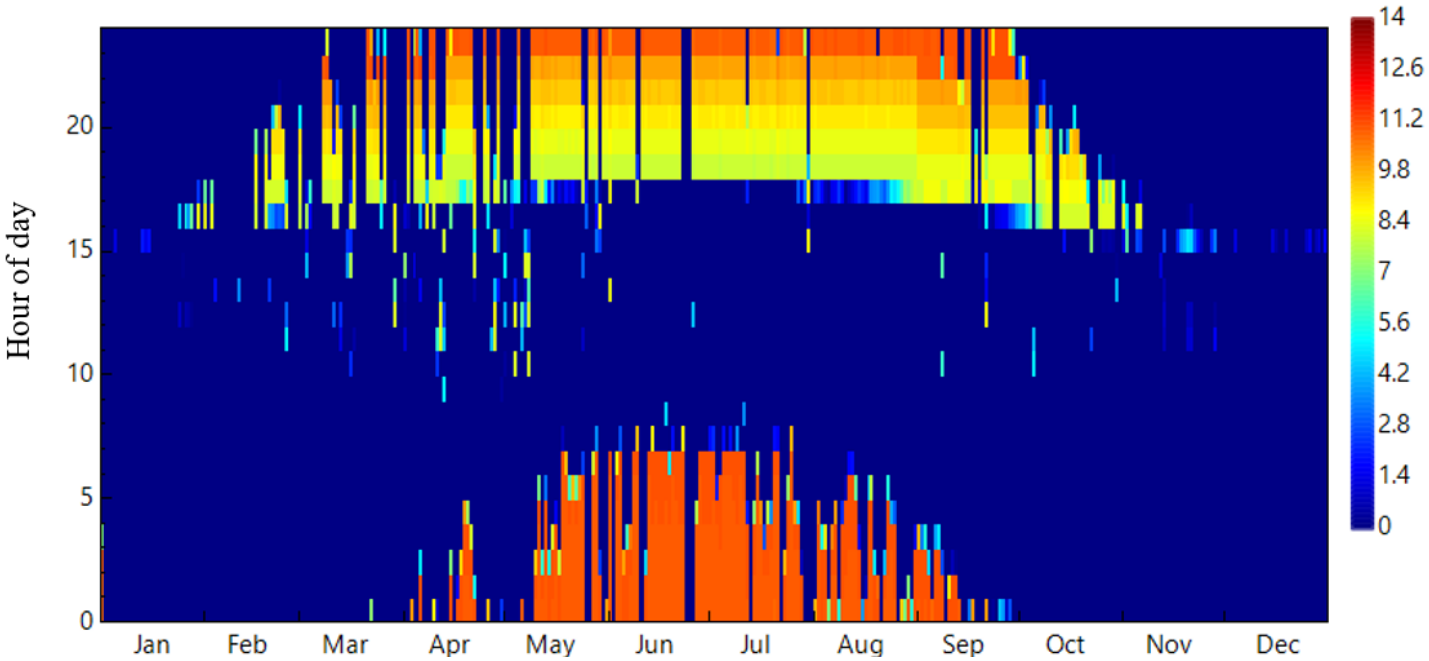

Figure 5.27 Thermal energy storage discharging mass flow rate during the year (kg/s)

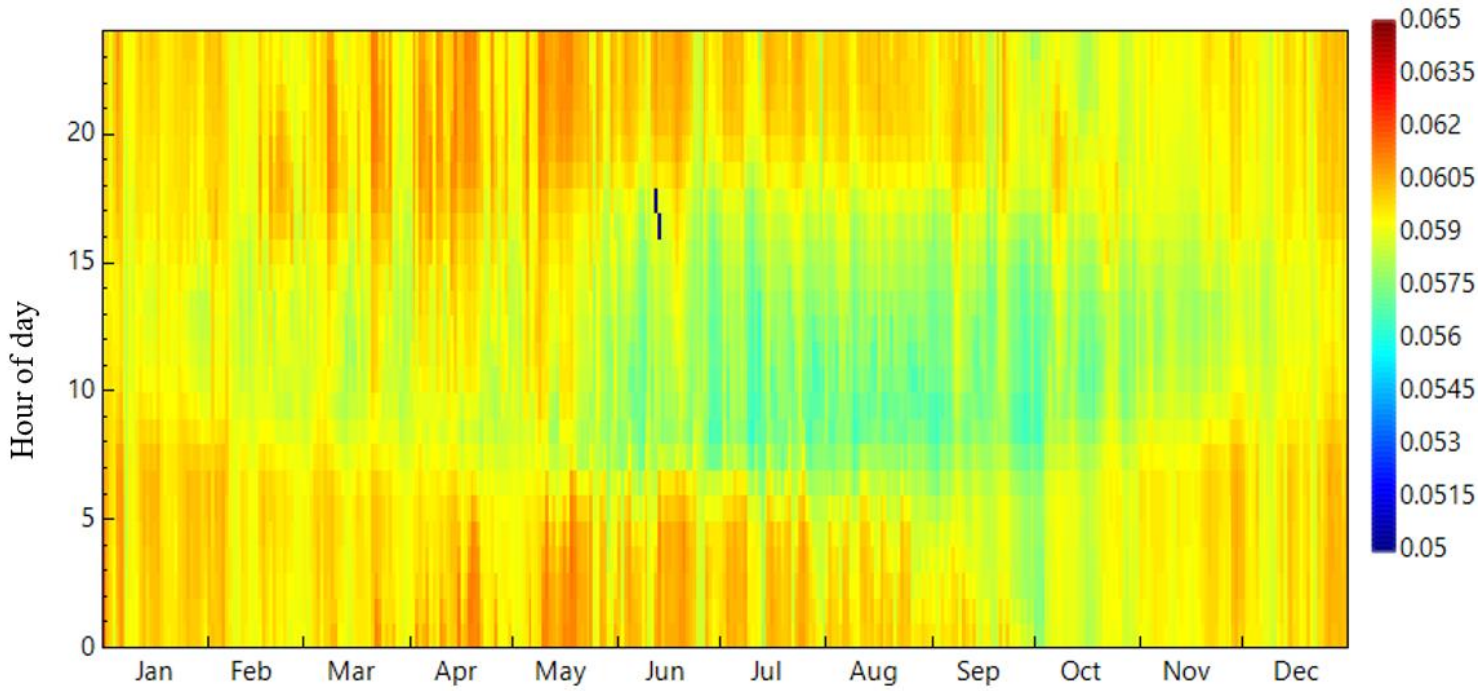

Figure 5.28 Thermal energy storage system heat losses during the year (MWt)

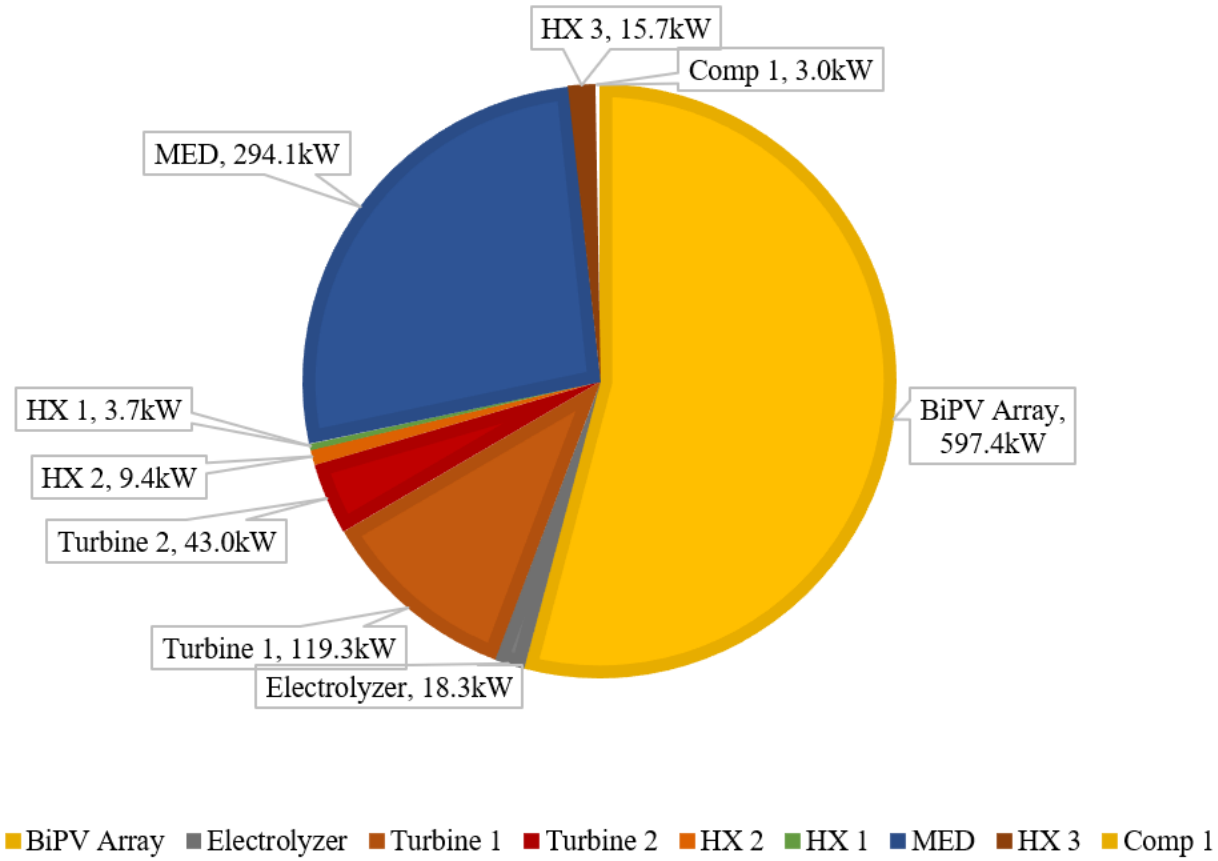

Figure 5.29 Exergy destruction rates for multigeneration system 1

For multigeneration system 1, the largest exergy destruction has occurred in the BiPV array which followed by the desalination unit and the first turbine. Exergy destructions are shown in Figure 5.29. Figure 5.30 shows how geothermal water mass flow rate influence on freshwater output and power of main electricity generator components. Between 18kg/h and 12 kg/h geothermal feed availability, the fuel cell is able to compensate for the power deficit. However, lower geothermal feed availability causes power deficits which cannot be compensated by the multigeneration system. HOMER pro feasibility simulation is employed to determine optimum fuel cell capacity for compensation purposes. 200kW PEM fuel cell unit is determined according to feasibility analysis. More than 21000 kg of freshwater production capacity is used in the simulated case as 14551 kg for daily freshwater production. Therefore, a 69% capacity factor is calculated for the MED desalination unit.

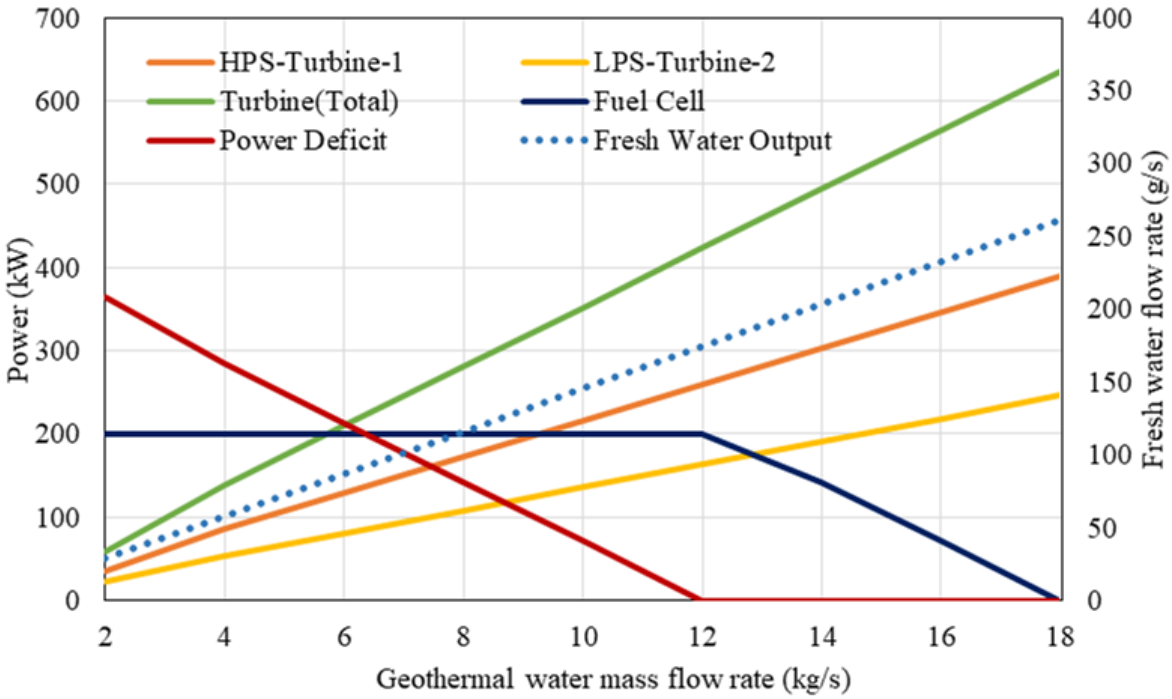

Figure 5.30 Turbines and fuel cell power rates, power deficit, and freshwater output due to geothermal water mass flow rate

Thermophysical properties of multigeneration system 1 can be seen in Table 5.1. Hydrogen production ratios are lower than multigeneration systems 2 and 3. The electrolyzer worked at a 9.6% capacity factor to produce hydrogen for a year.

Table 5.1 Thermophysical properties of state points in multigeneration system 1

State Point	Substance	Mass flow rate (kg/s)	Temperature (°C)	Pressure (kPa)	h (kJ/kg)	s (kj/kg.K)	ex (kJ/kg)
1	Water	11.600	180.0	1002.0	763.2	2.140	132.8
2	Water	11.600	147.5	444.7	763.2	2.153	129.0
3	Water	0.777	147.5	444.7	2743.0	6.861	713.3
4	Brine	10.822	147.5	444.7	621.5	1.817	86.9
5	Brine	10.822	121.0	204.9	621.5	1.826	84.2
6	Brine	0.558	121.0	204.9	2708.0	7.119	601.9
7	Water	10.264	121.0	204.9	508.0	1.539	55.8
8	Water	10.264	76.0	40.2	508.0	1.571	46.3
9	Water	9.423	76.0	40.2	318.1	1.028	17.3
10	R-134a	0.778	22.0	608.3	162.0	0.580	41.4
11	R-134a	0.778	22.0	608.3	262.6	0.922	40.6
12	R-134a	0.778	65.0	1600.0	287.0	0.935	61.1
13	R-134a	0.778	57.8	1600.0	162.0	0.558	47.9
14	Water	0.168	37.0	101.0	155.1	0.532	1.3
15	Brine	9.423	74.0	40.0	309.8	1.003	16.4
16	Brine	9.423	30.0	40.0	125.7	0.437	0.2
17	Brine	11.60	41.2	94.3	172.4	0.588	2.2
18	Hydrogen	0.00023	25.0	100.0	3549.3	48.120	1413.7
19	Hydrogen	0.00023	26.0	36300.0	4138.0	28.900	7463.1
20	Hydrogen	0.00014	26.0	35000.0	4129.0	29.050	7645.8
21	Hydrogen	0.00009	26.0	36000.0	4136.0	28.930	7688.3
22	Hydrogen	0.00009	26.0	35000.0	4129.0	29.050	7645.8
23	Seawater	1.583	34.0	102.0	142.5	0.492	0.7
24	Seawater	1.751	25.0	101.0	104.9	0.367	0.0
25	Seawater	1.751	26.0	103.0	109.1	0.381	0.0
27	Hydrogen	0.00023	25.0	100.0	3932.0	53.430	222.5
28	Hydrogen	0.00023	26.0	36875.0	4142.0	28.830	7724.0
29	Water	0.840	76.0	40.2	2636.0	7.667	367.4
30	Water	0.840	76.0	40.2	318.1	1.028	17.3
31	Water	0.777	98.0	94.3	2464.0	7.379	280.8
32	Water	0.558	98.0	94.3	2464.0	7.379	280.8
33	Water	1.335	98.0	94.3	2464.0	7.379	280.8
34	Brine	10.264	33.8	40.2	141.4	0.488	0.6
35	Brine	10.264	33.8	94.3	141.5	0.488	0.7

Thermophysical properties of multigeneration system 2 can be seen in Table 5.2 and Table 5.4. The Cu-Cl cycle in multigeneration system 2 is analyzed separately. 4.67 mol/s average molar flow rate hydrogen production is performed by the Cu-Cl cycle in a multigeneration system. 2208.91kW average thermal energy rate and 607.1kW average electrical power are consumed by the Cu-Cl hydrogen production subsystem.

Table 5.2 Thermophysical properties of state points in multigeneration system 2

State Point	Substance	Mass flow rate (kg/s)	Temperature (°C)	Pressure (kPa)	h (kJ/kg)	s (kj/kg.K)	ex (kJ/kg)
1	Water	310.000	180.0	1002.0	763.2	2.140	132.8
2	Water	310.000	147.5	444.7	763.2	2.153	129.0
3	Ammonia	35.580	29.7	1157.0	340.3	1.483	312.8
4	Ammonia	35.580	30.6	5066.3	345.0	1.118	425.7
5	Ammonia	35.580	140.0	5066.3	1677.0	5.195	549.3
6	Ammonia	35.580	90.0	2533.1	1602.0	5.288	446.7
7	Ammonia	35.580	127.0	2533.1	1709.0	5.571	469.8
8	Ammonia	35.580	80.0	1157.0	1628.0	5.700	350.6
9	Water	284.596	50.7	94.3	212.4	0.713	5.0
10	R-134a	227.800	22.0	608.3	162.0	0.580	41.4
11	R-134a	227.800	22.0	608.3	262.6	0.922	40.6
12	R-134a	227.800	65.0	1600.0	287.0	0.935	61.1
13	R-134a	227.800	57.8	1600.0	162.0	0.558	47.9
14	Water	5.086	37.0	101.0	155.1	0.532	1.3
16	Brine	284.596	30.0	94.3	125.8	0.437	0.3
43	Hydrogen	0.009	23.0	100.0	3549.3	48.120	1177.6
46	Hydrogen	0.009	25.0	100.0	3932.0	53.350	10.1
47	Hydrogen	0.009	26.0	36875.0	4142.0	28.830	7487.9
23	Seawater	47.809	34.0	102.0	142.5	0.492	0.7
24	Seawater	52.895	25.0	101.0	104.9	0.367	0.0
25	Seawater	52.895	26.0	103.0	109.1	0.381	0.0
29	Water	25.388	76.0	40.2	2636.0	7.667	367.4
50	Water	25.388	76.0	40.2	318.1	1.028	17.3
51	Water	310.000	98.0	444.7	410.9	1.284	34.2
52	Brine	310.000	33.8	94.3	141.5	0.488	0.8
53	Brine	310.000	34.0	94.3	141.5	0.488	0.8

Table 5.3 Thermophysical properties of state points in multigeneration system 3

State Point	Substance	Mass flow rate (kg/s)	Temperature (°C)	Pressure (kPa)	h (kJ/kg)	s (kj/kg.K)	ex (kJ/kg)
1	Water	11.600	550.4	10000.0	3502.0	6.757	1503.2
2	Water	11.600	533.8	6000.0	3502.0	6.982	1436.5
3	Water	0.777	147.5	444.7	2743.0	6.861	713.3
4	Brine	10.823	147.5	444.7	621.5	1.817	86.9
5	Brine	10.823	121.0	204.9	621.5	1.826	84.2
6	Water	0.558	121.0	204.9	2708.0	7.119	601.9
7	Brine	10.264	121.0	204.9	508.0	1.539	55.8
8	Brine	10.264	76.0	40.2	508.0	1.571	46.3
9	Brine	9.424	76.0	40.2	318.1	1.028	17.3
10	R-134a	0.778	22.0	608.3	162.0	0.580	41.4
11	R-134a	0.778	22.0	608.3	262.6	0.922	40.6
12	R-134a	0.778	65.0	1600.0	287.0	0.935	61.1
13	R-134a	0.778	57.8	1600.0	162.0	0.558	47.9
14	Water	0.168	37.0	101.0	155.1	0.532	1.3
15	Brine	9.424	74.0	40.0	309.8	1.003	16.4
16	Brine	9.424	32.0	40.0	134.1	0.464	0.5
17	Brine	11.600	43.1	94.3	180.1	0.612	2.6
23	Seawater	1.583	34.0	102.0	142.5	0.492	0.7
24	Seawater	1.752	25.0	101.0	104.9	0.367	0.0
25	Seawater	1.752	26.0	103.0	109.1	0.381	0.0
26	Water	11.600	180.0	1002.0	763.2	2.140	132.8
27	Water	0.000	180.0	1002.0	763.2	2.140	132.8
43	Hydrogen	0.068	23.0	100.0	3549.3	48.120	1177.6
46	Hydrogen	0.068	25.0	100.0	3932.0	53.350	10.1
47	Hydrogen	0.068	26.0	36875.0	4142.0	28.830	7487.9
29	Water	0.841	76.0	40.2	2636.0	7.667	367.4
50	Water	0.841	76.0	40.2	318.1	1.028	17.3
51	Water	0.777	98.0	94.3	2464.0	7.379	280.8
52	Water	0.558	98.0	94.3	2464.0	7.379	280.8
53	Water	1.336	98.0	94.3	2464.0	7.379	280.8
54	Brine	10.264	35.6	40.2	150.8	0.519	1.0
55	Brine	10.264	36.0	94.3	151.0	0.519	1.1
56	Brine	11.600	43.1	94.3	180.1	0.612	2.6

Table 5.4 Thermophysical properties of Cu-Cl cycle in multigeneration system 2

State Point	Substance	Mass flow rate (kg/s)	Temperature (°C)	Pressure (kPa)	h (kJ/kg)	s (kj/kg.K)	ex (kJ/kg)
30	H_2O	0.042	23.0	100.0	-15872.7	-9.086	0.0
31	H_2O	0.084	23.0	100.0	-15872.7	-9.086	0.0
31b	H_2O	0.084	390.0	100.0	-12711.5	-0.912	724.3
32	$CuCl_2$	1.255	85.0	100.0	363.4	5.290	-293.1
32b	$CUCL_2$	1.255	390.0	100.0	673.5	8.116	-825.7
33	Cu_2OCl_2+HCl	1.339	390.0	100.0	-1903.3	4.654	24.0
34	Cu_2OCl_2	0.999	390.0	100.0	-1789.3	5.926	-2.6
35	Cu_2OCl_2	0.999	510.0	100.0	-1791.8	5.922	-4.1
36	HCl	0.340	390.0	100.0	-2238.1	0.920	101.3
37	HCl	0.340	80.0	100.0	-2487.8	0.413	2.7
38	CuCl+O_2	0.999	510.0	100.0	526.6	1.162	384.9
39	O_2	0.074	510.0	100.0	477.0	0.942	196.0
40	CuCl	0.924	510.0	100.0	530.0	1.179	399.7
41	CuCl	0.924	420.0	100.0	469.1	1.179	338.9
42	$CuCl_2$+H_2	1.265	23.0	100.0	304.0	4.045	11.9
43	H_2	0.009	23.0	100.0	-28.5	-0.042	-16.1
44	$CuCl_2$+H_2O	1.255	23.0	100.0	304.7	4.069	12.1
45	$CuCl_2$+H_2O	1.255	85.0	100.0	363.4	5.290	-293.1

Thermophysical properties of multigeneration system 3 can be seen in Table 5.3 and Table 5.5.

The Cu-Cl cycle in multigeneration system 3 is analyzed separately. 33.58 mol/s average molar flow rate hydrogen production is performed by the Cu-Cl cycle in multigeneration system 3. 15885kW average thermal energy rate and 5239kW average electrical power are consumed by the Cu-Cl hydrogen production subsystem.

Figure 5.31 shows how temperature affects energy and exergy efficiencies. According to parametric studies, temperature affected exergy efficiency due to the thermal systems and their exergies.

Table 5.5 Thermophysical properties of Cu-Cl cycle in multigeneration system 3

State Point	Substance	Mass flow rate (kg/s)	Temperature (°C)	Pressure (kPa)	h (kJ/kg)	s (kj/kg.K)	ex (kJ/kg)
30	H_2O	0.302	23.0	100.0	-15872.7	-9.086	0.0
31	H_2O	0.604	23.0	100.0	-15872.7	-9.086	0.0
31b	H_2O	0.604	380.0	100.0	-12732.0	-0.943	713.0
32	$CuCl_2$	9.029	23.0	100.0	304.7	4.069	12.1
32b	$CUCL_2$	9.029	380.0	100.0	662.9	8.062	-820.2
33	Cu_2OCl_2+HCl	9.634	380.0	100.0	-1905.3	4.651	22.9
34	Cu_2OCl_2	7.186	380.0	100.0	-1789.1	5.926	-2.5
35	Cu_2OCl_2	7.186	515.0	100.0	-1791.9	5.922	-4.1
36	HCl	2.448	390.0	100.0	-2246.2	0.908	96.8
37	HCl	2.448	80.0	100.0	-2487.8	0.413	2.7
38	CuCl+O_2	7.186	515.0	100.0	530.1	1.163	388.1
39	O_2	0.537	515.0	100.0	482.2	0.949	199.3
40	CuCl	6.648	515.0	100.0	533.4	1.179	403.0
41	CuCl	6.648	100.0	100.0	252.7	1.308	84.0
42	$CuCl_2$+H_2	9.097	23.0	100.0	304.0	4.045	11.9
43	H_2	0.067	23.0	100.0	-28.5	-0.042	-16.1
44	$CuCl_2$+H_2O	9.029	23.0	100.0	304.7	4.069	12.1
45	$CuCl_2$+H_2O	9.029	23.0	100.0	304.7	4.069	12.1

Hydrogen production in multigeneration system 1 is linked with PV electricity production since the PEM electrolyzer connected with the BiPV plant is employed for hydrogen production purposes. Before midday, hydrogen production rates are higher in contrast with after midday. There are different causes for this particular result. One of them is the feasibility study did not agree with high capacity hydrogen tanks. Therefore, a 200 kg hydrogen tank is obtained for multigeneration system 1. The tank capacity is limited the hydrogen production rates. There is also a hydrogen load in the system which represents hydrogen-fueled vehicles in the community. However, even the hydrogen load was not able to run the electrolyzer in full capacity once the sun is available. Therefore, the electrolyzer worked at a 9.66% capacity factor. 3695 hours operated in a year. Hydrogen production rates can be seen in Figure 5.32

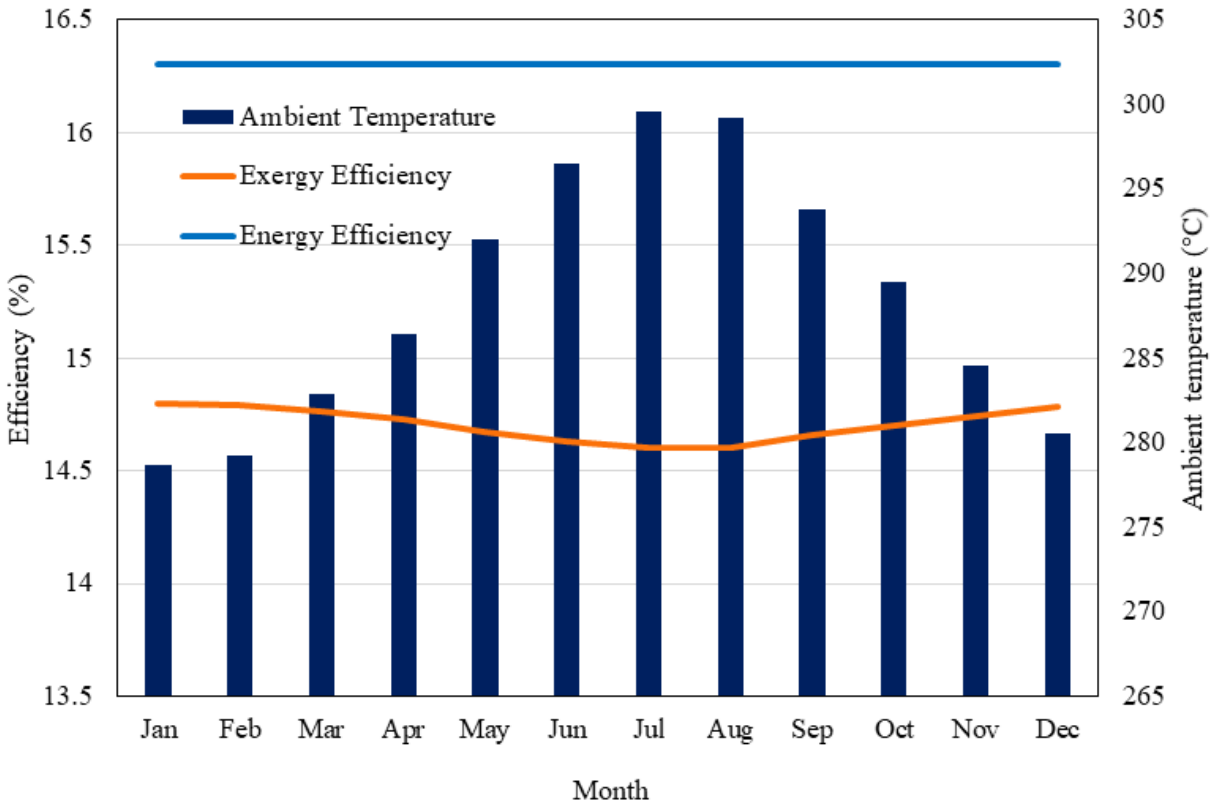

Figure 5.31 Energy and exergy efficiencies for overall multigeneration system 1

In multigeneration system 2, the Cu-Cl cycle is linked with parabolic through CSP plant. The molten salt storage system is integrated with a CSP, to provide a continuous hydrogen source. CSP plant is designed to run the Cu-Cl cycle continuously. However, production rates were not the same according to solar radiation. Since the temperatures should be stable in the Cu-Cl cycle and CSP plant, mass flow rates are changed. This change is led to varying mass flow rate for the Cu-Cl cycle and CSP. Therefore, 4.67 mol/s average hydrogen production rate is obtained. 10.8 mol/s maximum hydrogen production rate is obtained due to calculations. Figure 5.33 shows the detailed production rates of various compounds and heat consumption.

Required thermal and electrical energy for hydrogen production in the Cu-Cl thermochemical cycle can be seen in Figure 5.34 and Figure 5.35 for multigeneration systems 2 and 3 respectively. Hydrogen is produced in the various molar flow rates due to the solar availability during the year as it mentioned and showed before. Different thermal

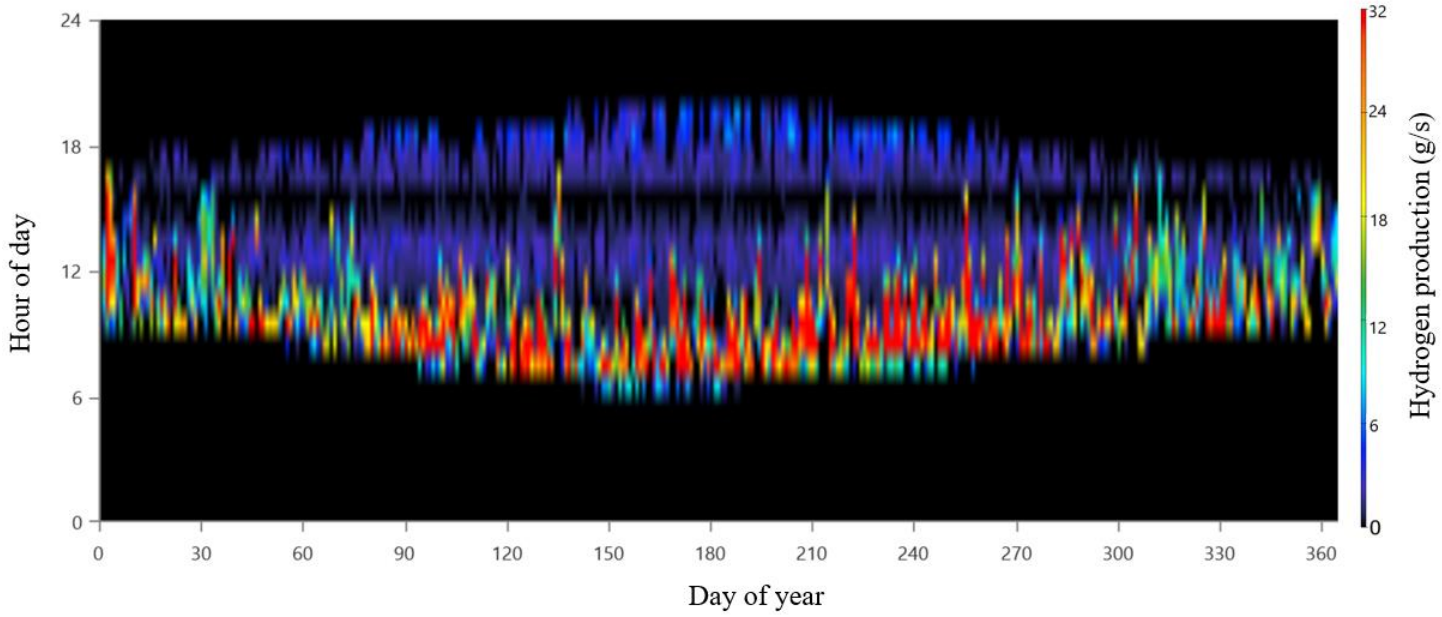

Figure 5.32 Hydrogen production rates during the year for multigeneration system 1

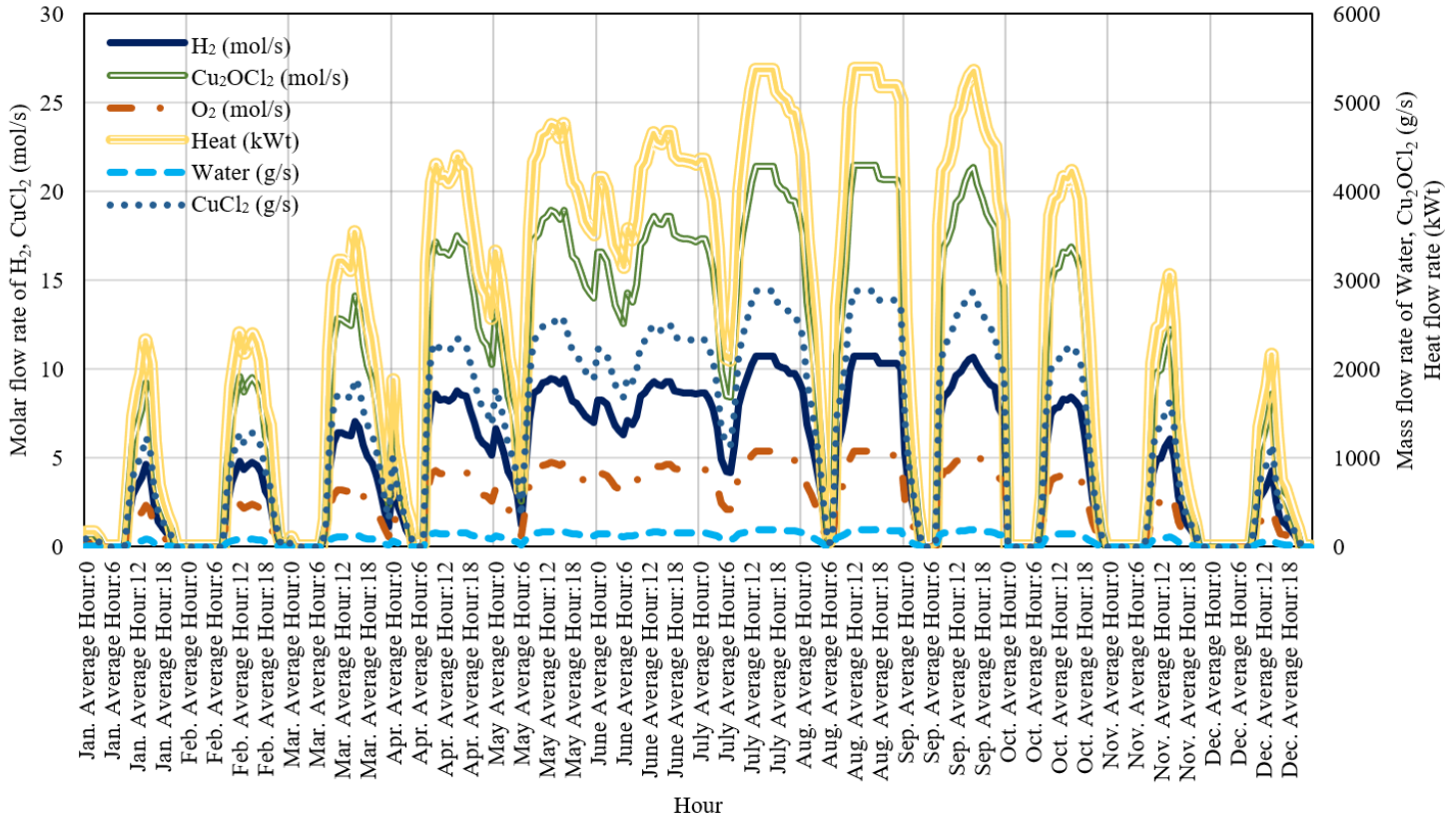

Figure 5.33 Consumption and production of various chemical compounds and heat of the Cu-Cl cycle in multigeneration system 2 for average days during the year

and electrical energy is required for different hydrogen molar production rates. Both of the Cu-Cl cycles in multigeneration systems 2 and 3 have similar systems besides their capacities. The thermal energy side required thermal energy for the cycle is calculated as 473kW to produce 1mol/s hydrogen. With the thermal energy, electrical energy is required both from electrolyzer and auxiliary systems. 130kW electrical required electrical energy to produce hydrogen at 1mol/s rate is calculated for multigeneration system 2. This electrical energy is calculated as 156kW for 1mol/s hydrogen production in multigeneration system 3.

The production rates of different compounds of the Cu-Cl cycle can be shown in Figure 5.36. This is the base figure that shows how Figure 5.33 is obtained in detail. Production of various chemical compounds of the Cu-Cl cycle can be seen there.

For multigeneration system 2, overall energy and exergy efficiencies under the effect of different ambient temperatures are shown in Figure 5.37. Overall energy efficiency is calculated as 27.4% for multigeneration system 2 where overall exergy efficiency is calculated as 17.3%. Exergy destruction rates can be seen in Figure 5.38 for major components.

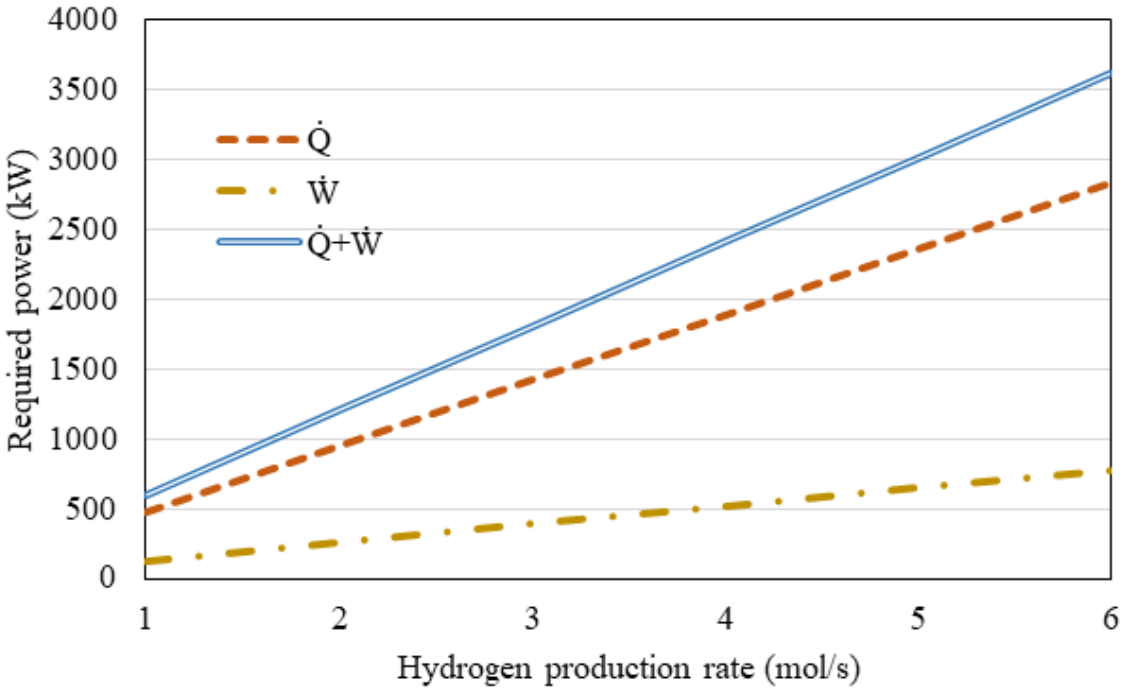

Figure 5.34 Power requirement by hydrogen production rate for the Cu-Cl cycle in multigeneration system 2

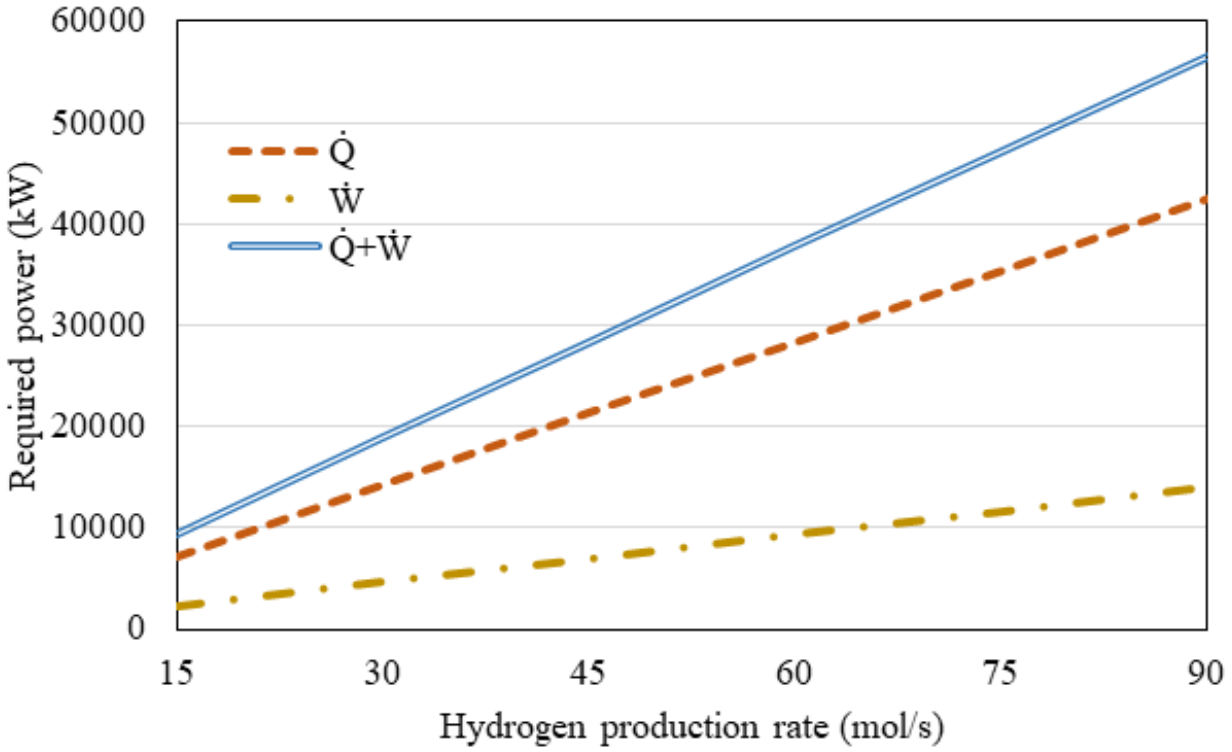

Figure 5.35 Power requirement by hydrogen production rate for the Cu-Cl cycle in multigeneration system 3

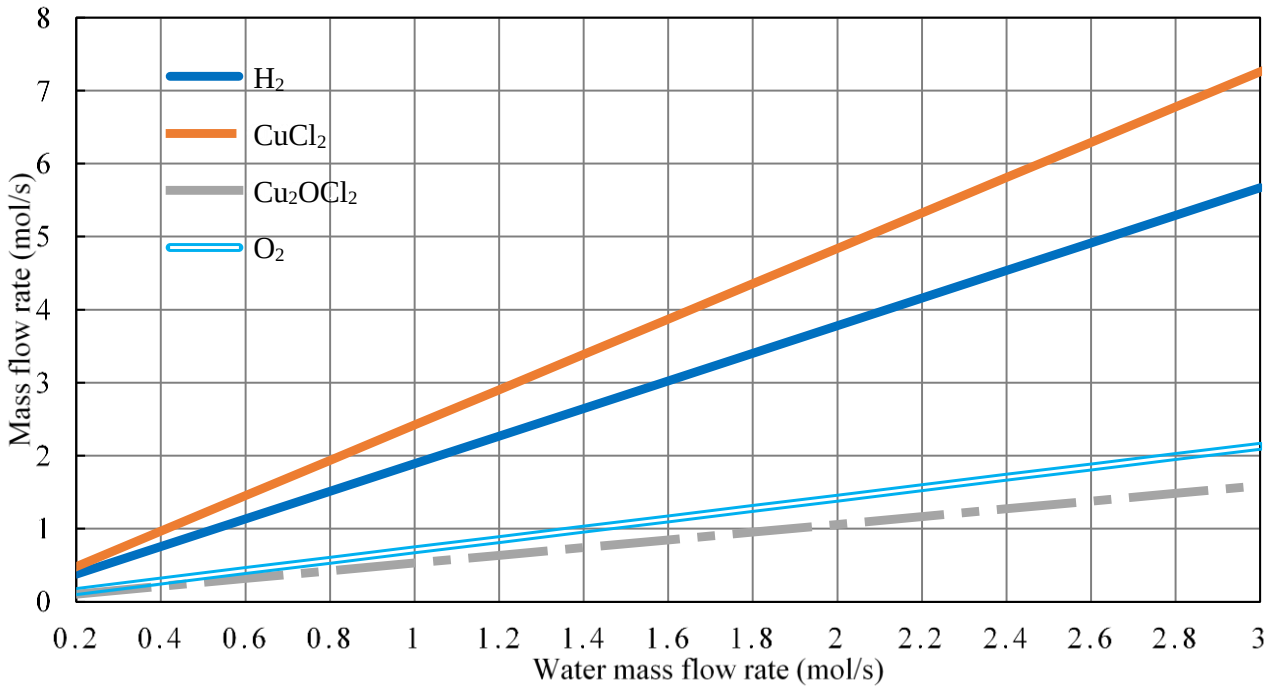

Figure 5.36 The production rates of various chemical compounds of the Cu-Cl thermochemical cycle

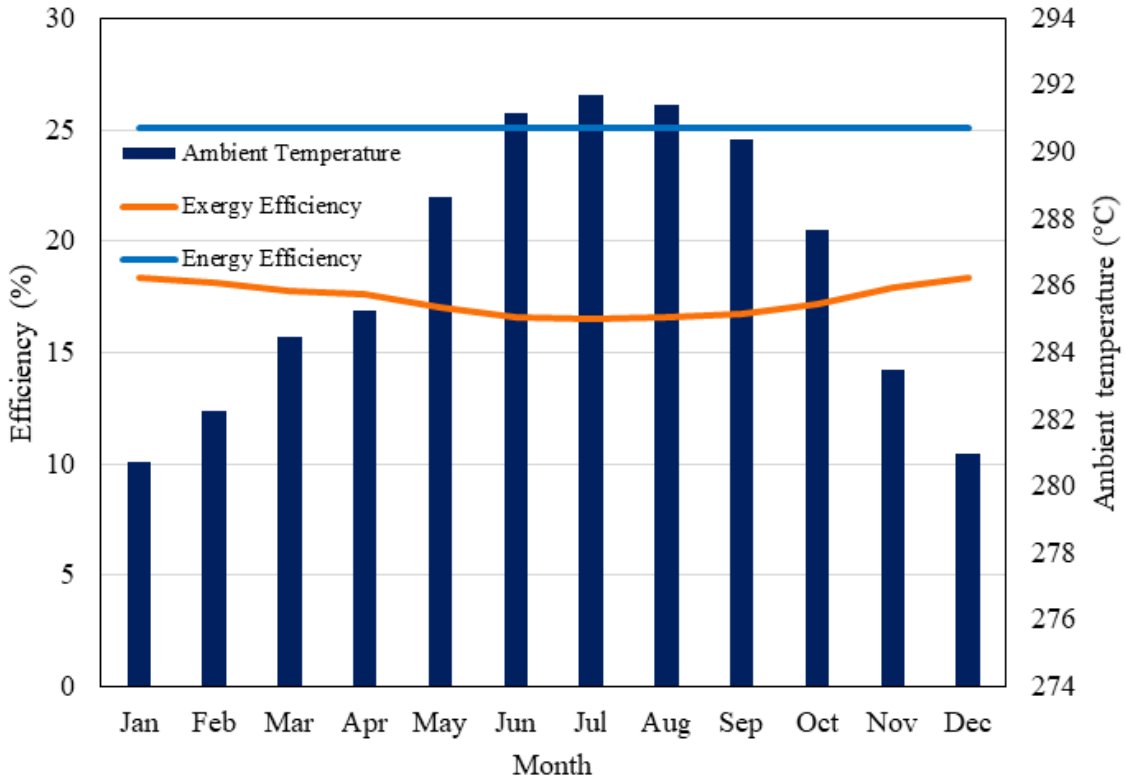

Figure 5.37 Energy and exergy efficiencies for overall multigeneration system 2

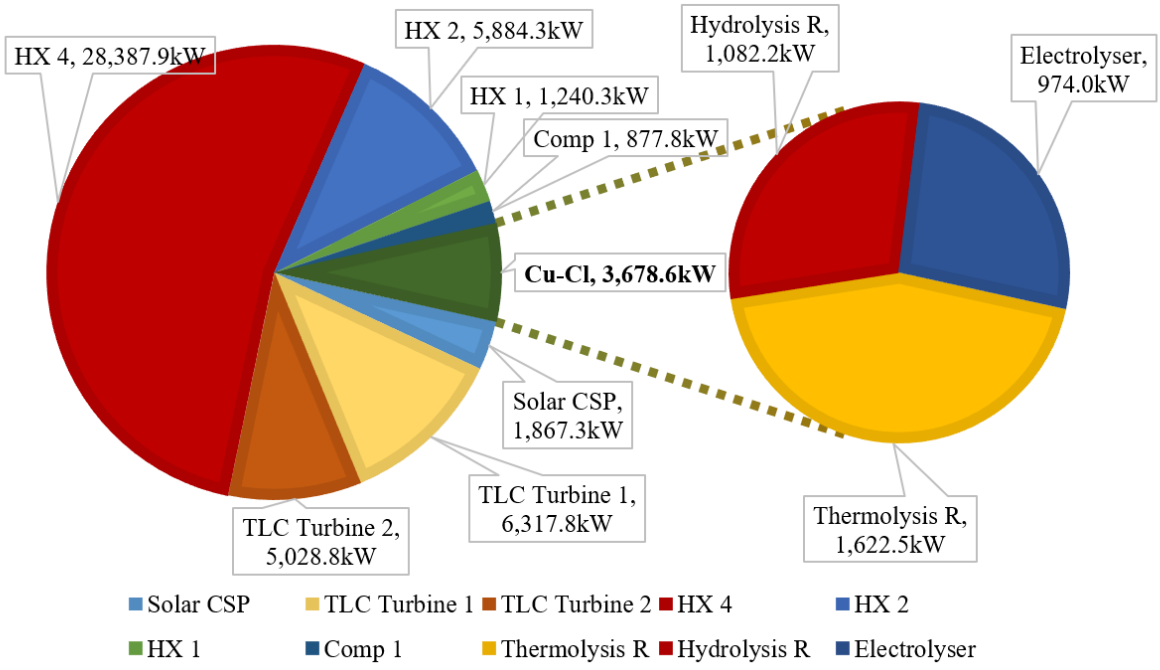

Figure 5.38 Exergy destruction rates of major components in multigeneration system 2

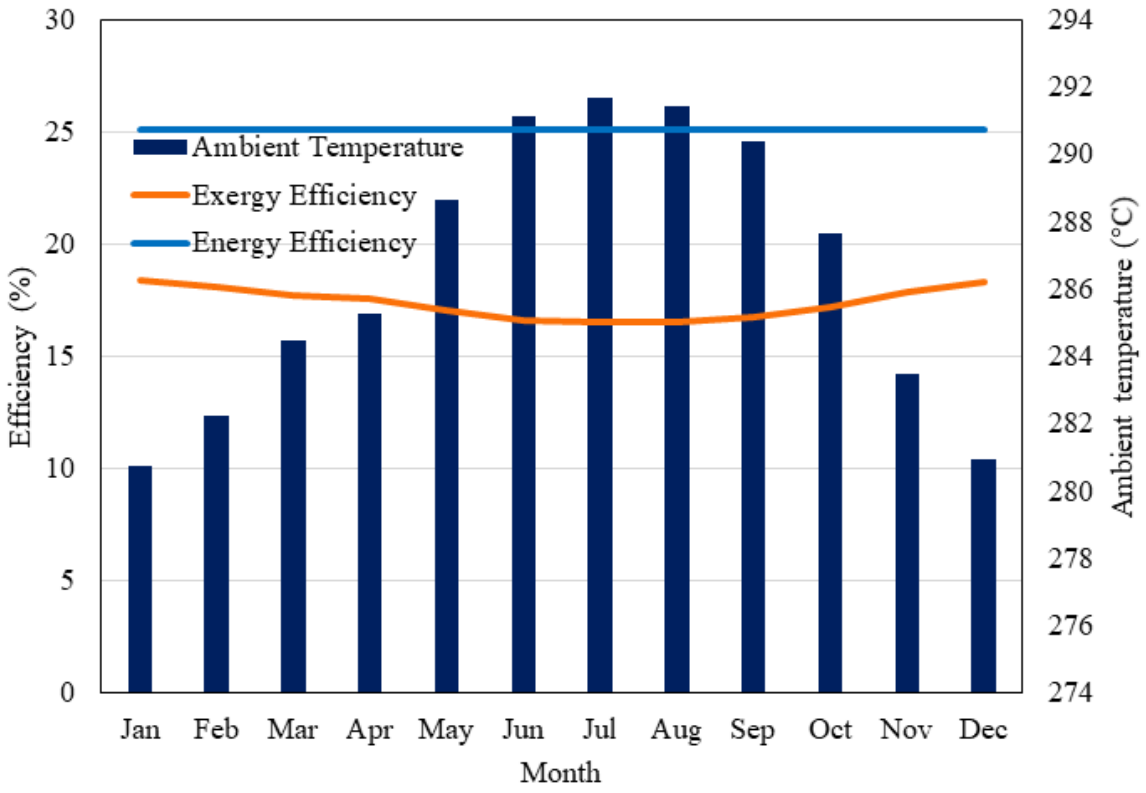

Figure 5.39 Energy and exergy efficiencies for overall multigeneration system 3

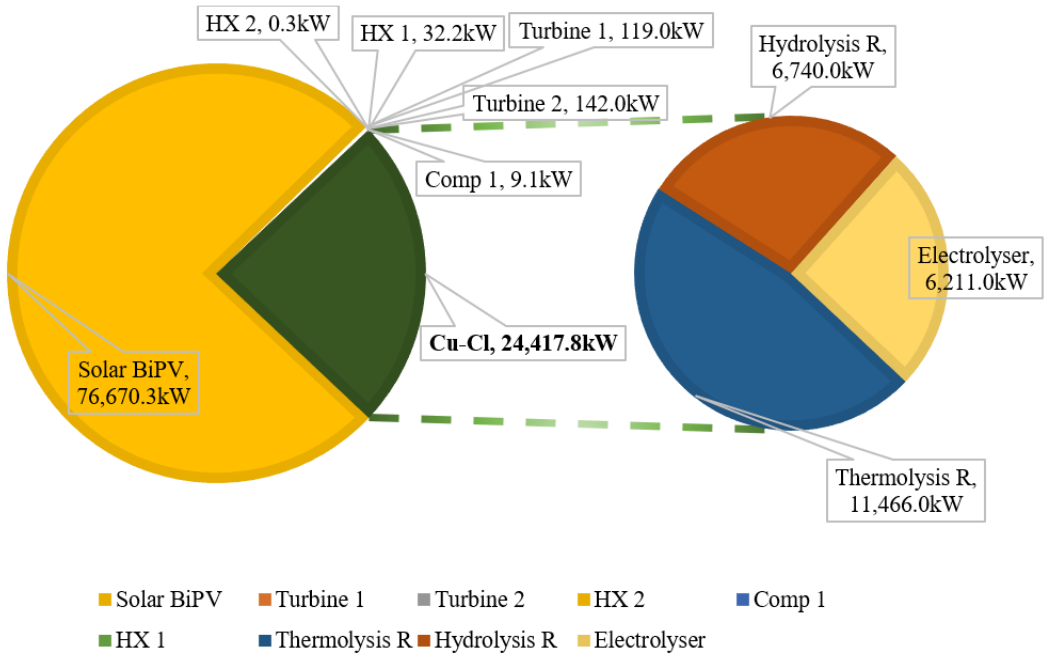

Figure 5.40 Exergy destruction rates for multigeneration system 3

For multigeneration system 3, the temperature effect on energy and exergy efficiencies can be seen in Figure 5.39. Since the BiPV plant is employed in the proposed system, the temperature coefficient is affected by energy efficiency as well. However, this effect was limited since the BiPV plant in multigeneration system 3 is an auxiliary system and the major energy resource is considered as a supercritical geothermal field. Therefore, the temperature effect on energy efficiency is not significantly visible. Overall energy efficiency is calculated as 22.8% for multigeneration system 2 where overall exergy efficiency is calculated as 18.58%. Exergy destruction rates can be seen in Figure 5.40 for major components of multigeneration system 3.

A brief summary is provided in Table 5.6. In terms of energy efficiency, the most efficient overall system is obtained as multigeneration system 2 with 27.4% energy efficiency. On the other hand, multigeneration system 3 is performed 18.6% exergy efficiency as an exergetically most efficient system in comparison with multigeneration systems 1 and 2.

Cost comparison methods are applied to determine the commercial viabilities of the proposed multigeneration systems. Each useful output is represented as a unit. Costs are shared between outputs if there is more than one product produced in a particular system. In multigeneration system 1, heating possessed the most viable application due to its IRR, NPV, and PBP results. On the other hand, the MED system possessed the least viable application. The overall system paid off itself in 8.54 years. 14% IRR and 8.8M$ NPV are calculated for the overall system. Table 5.7 shows the cost comparison results for system 1.

In multigeneration system 2, electricity and hydrogen facilities possessed better feasibility in comparison with multigeneration system1. On the electric side, fuel cells increased the costs in multigeneration system 1. In the hydrogen side, Cu-Cl integration increased the commercial viability. Also, large scale application is helped to decrease overall costs. Cu-Cl cycle is paid back in 6 years, in comparison with 12 years in multigeneration system 1. The unit cost of electricity and heating also affected the hydrogen prices. Overall system PBP is calculated as 6.77 years in multigeneration system

2. 14% IRR and 237M$ NPV are calculated. Table 5.8 shows the cost comparison results for multigeneration system 2.

Multigeneration system 3 performed the most feasible results in electricity and hydrogen sides and overall. The overall system is paid back in 5.15 years. Electricity possessed the most aggressive application with 25% IRR, 333.4M$ NPV, and 4.56 years PBP. The main reason for this, the net metering model with the Japanese national electricity grid is considered for the calculations. This incentive helped to increase the commercial viability of the system. Hydrogen possessed very similar results with multigeneration system 2. Lower unit electricity prices and high efficiency of a supercritical geothermal system are contributed to decrease costs in hydrogen production systems. Table 5.9 shows the cost comparison results for multigeneration system 3.

Table 5.6 Results summary of the proposed systems.

Details	**Multigeneration System 1**	**Multigeneration System 2**	**Multigeneration System 3**	**Unit**
Useful electricity production	5115.8	47649.8	271209.6	kWh/year
Useful heat production	13153.1	452857.0	12450.2	kWh/year
Fresh water production	5298.1	160392.1	5314.7	ton/year
H_2 production	6307.2	296876.4	2144448.0	kg/year
H_2 LHV rate	27.4	1120.8	8059.2	kW
Cu-Cl cycle heat input	-	2211.3	15885.0	kW
Electrolyzer work input	45.6	607.8	5239.0	kW
H_2 conversion efficiency	59.9	39.8	38.2	%
H_2 storage pressure	363.0	368.0	368.0	bar
H_2 temperature	26.0	23.0	23.0	°C
Exergy destruction rate	3.0	55.2	101.4	MW
Nr. of houses in the community	150.0	3841.3	204.3	#
Thermal energy capacity	0.1	53.9	16.1	MW
Geothermal power capacity	0.4	5.5	0.5	MW
Solar power capacity	1.0	-	149.0	MWp
Solar thermal energy capacity	-	13.0	-	MW
Solar GHI	1511.0	1792.2	1251.7	kWh/m^2.year
Solar area	5058.0	20640.0	788760.0	m^2
Solar GHI on array	7642.6	36990.0	987290.9	MWh/year
Converted solar energy	2033.0	19370.8	264758.7	MWh/year
Solar energy conversion ratio	26.6	52.4	26.8	%
Overall energy efficiency	25.6	27.4	22.8	%
Overall exergy efficiency	12.7	17.3	18.6	%

Table 5.7 Multigeneration system 1 cash flow projection and cost comparison results

.	Electricity	Heating	Hydrogen	Water	Total
Year	**Cash flow ($)**	**Cash flow ($)**	**Cash flow ($)**	**Cash flow ($)**	**Cash flow ($)**
0	(5,221,180.00)	(3,278,000.00)	(779,974.69)	(62,196.76)	(9,341,351.45)
1	680,406.72	578,738.16	88,237.73	4,938.84	1,352,321.45
2	678,365.50	577,407.06	88,052.43	4,927.97	1,348,752.97
3	676,324.28	576,075.96	87,867.13	4,917.11	1,345,184.48
4	674,283.06	574,744.87	87,681.83	4,906.24	1,341,616.00
5	672,241.84	573,413.77	87,496.53	4,895.38	1,338,047.52
6	670,200.62	572,082.67	87,311.23	4,884.51	1,334,479.04
7	668,159.40	570,751.57	87,125.93	4,873.65	1,330,910.55
8	666,118.18	569,420.48	86,940.63	4,862.78	1,327,342.07
9	664,076.96	568,089.38	86,755.33	4,851.92	1,323,773.59
10	662,035.74	566,758.28	86,570.03	4,841.05	1,320,205.10
11	659,994.52	565,427.18	86,384.74	4,830.19	1,316,636.62
12	657,953.30	564,096.08	86,199.44	4,819.32	1,313,068.14
13	655,912.08	562,764.99	86,014.14	4,808.45	1,309,499.66
14	653,870.86	561,433.89	85,828.84	4,797.59	1,305,931.17
15	651,829.64	560,102.79	85,643.54	4,786.72	1,302,362.69
16	649,788.42	558,771.69	85,458.24	4,775.86	1,298,794.21
17	647,747.20	557,440.60	85,272.94	4,764.99	1,295,225.73
18	645,705.98	556,109.50	85,087.64	4,754.13	1,291,657.24
19	643,664.76	554,778.40	84,902.34	4,743.26	1,288,088.76
20	641,623.54	553,447.30	84,717.04	4,732.40	1,284,520.28
21	639,582.32	552,116.20	84,531.74	4,721.53	1,280,951.80
22	637,541.10	550,785.11	84,346.44	4,710.67	1,277,383.31
23	635,499.88	549,454.01	84,161.14	4,699.80	1,273,814.83
24	633,458.66	548,122.91	83,975.85	4,688.94	1,270,246.35
25	631,417.44	546,791.81	83,790.55	4,678.07	1,266,677.87
IRR	12%	17%	10%	6%	14%
NPV ($)	3,899,473.05	4,476,222.49	417,876.86	5,669.09	8,799,241.49
PBP	10.07 Years	6.84 Years	12.12 Years	21.01 Years	8.54 Years
Unit Cost	0.041 $/kWh	0.012$/kWh	4.95$/kg	0.47$/$m^3$	

Table 5.8 Multigeneration system 2 cash flow projection and cost comparison results.

	Electricity	Heating	Hydrogen	Water	Total
Year	**Cash flow ($)**	**Cash flow ($)**	**Cash flow ($)**	**Cash flow ($)**	**Cash flow ($)**
0	(32,048,437.50)	(116,835,872.85)	(21,081,566.20)	(1,648,000.00)	(171,613,876.55)
1	6,337,417.71	19,925,706.24	4,153,300.84	149,517.51	30,565,942.30
2	6,318,405.45	19,879,877.12	4,144,578.90	149,188.57	30,492,050.05
3	6,299,393.20	19,834,047.99	4,135,856.97	148,859.63	30,418,157.80
4	6,280,380.95	19,788,218.87	4,127,135.04	148,530.70	30,344,265.55
5	6,261,368.70	19,742,389.74	4,118,413.11	148,201.76	30,270,373.30
6	6,242,356.44	19,696,560.62	4,109,691.18	147,872.82	30,196,481.06
7	6,223,344.19	19,650,731.49	4,100,969.25	147,543.88	30,122,588.81
8	6,204,331.94	19,604,902.37	4,092,247.31	147,214.94	30,048,696.56
9	6,185,319.68	19,559,073.25	4,083,525.38	146,886.00	29,974,804.31
10	6,166,307.43	19,513,244.12	4,074,803.45	146,557.07	29,900,912.07
11	6,147,295.18	19,467,415.00	4,066,081.52	146,228.13	29,827,019.82
12	6,128,282.92	19,421,585.87	4,057,359.59	145,899.19	29,753,127.57
13	6,109,270.67	19,375,756.75	4,048,637.65	145,570.25	29,679,235.32
14	6,090,258.42	19,329,927.62	4,039,915.72	145,241.31	29,605,343.07
15	6,071,246.16	19,284,098.50	4,031,193.79	144,912.37	29,531,450.83
16	6,052,233.91	19,238,269.37	4,022,471.86	144,583.43	29,457,558.58
17	6,033,221.66	19,192,440.25	4,013,749.93	144,254.50	29,383,666.33
18	6,014,209.40	19,146,611.13	4,005,028.00	143,925.56	29,309,774.08
19	5,995,197.15	19,100,782.00	3,996,306.06	143,596.62	29,235,881.84
20	5,976,184.90	19,054,952.88	3,987,584.13	143,267.68	29,161,989.59
21	5,957,172.65	19,009,123.75	3,978,862.20	142,938.74	29,088,097.34
22	5,938,160.39	18,963,294.63	3,970,140.27	142,609.80	29,014,205.09
23	5,919,148.14	18,917,465.50	3,961,418.34	142,280.86	28,940,312.84
24	5,900,135.89	18,871,636.38	3,952,696.41	141,951.93	28,866,420.60
25	5,881,123.63	18,825,807.26	3,943,974.47	141,622.99	28,792,528.35
IRR	19%	16%	19%	7%	17%
NPV ($)	52,113,151.48	150,327,997.42	34,556,288.01	395,370.41	237,392,807.49
PBP	6.02 Years	7.11 Years	6.03 Years	16.77 Years	6.77 Years
Unit Cost	0.029 $/kWh	0.010$/kWh	2.84$/kg	0.41$/$m^3$	

Table 5.9 Multigeneration system 3 cash flow projection and cost comparison results.

	Electricity	Heating	Hydrogen	Water	Total
Year	**Cash flow ($)**	**Cash flow ($)**	**Cash flow ($)**	**Cash flow ($)**	**Cash flow ($)**
0	(143,770,000.00)	(4,798,300.00)	(146,509,336.06)	(62,196.76)	(295,139,832.82)
1	36,070,876.80	547,806.60	30,000,827.52	4,954.40	66,624,465.32
2	35,962,664.17	546,546.64	29,937,825.78	4,943.50	66,451,980.10
3	35,854,451.54	545,286.69	29,874,824.04	4,932.60	66,279,494.88
4	35,746,238.91	544,026.73	29,811,822.31	4,921.70	66,107,009.65
5	35,638,026.28	542,766.78	29,748,820.57	4,910.80	65,934,524.43
6	35,529,813.65	541,506.82	29,685,818.83	4,899.90	65,762,039.21
7	35,421,601.02	540,246.87	29,622,817.09	4,889.00	65,589,553.98
8	35,313,388.39	538,986.91	29,559,815.36	4,878.10	65,417,068.76
9	35,205,175.76	537,726.96	29,496,813.62	4,867.20	65,244,583.54
10	35,096,963.13	536,467.00	29,433,811.88	4,856.31	65,072,098.31
11	34,988,750.50	535,207.05	29,370,810.14	4,845.41	64,899,613.09
12	34,880,537.87	533,947.09	29,307,808.40	4,834.51	64,727,127.87
13	34,772,325.24	532,687.14	29,244,806.67	4,823.61	64,554,642.65
14	34,664,112.60	531,427.18	29,181,804.93	4,812.71	64,382,157.42
15	34,555,899.97	530,167.23	29,118,803.19	4,801.81	64,209,672.20
16	34,447,687.34	528,907.27	29,055,801.45	4,790.91	64,037,186.98
17	34,339,474.71	527,647.32	28,992,799.72	4,780.01	63,864,701.75
18	34,231,262.08	526,387.36	28,929,797.98	4,769.11	63,692,216.53
19	34,123,049.45	525,127.41	28,866,796.24	4,758.21	63,519,731.31
20	34,014,836.82	523,867.45	28,803,794.50	4,747.31	63,347,246.08
21	33,906,624.19	522,607.50	28,740,792.76	4,736.41	63,174,760.86
22	33,798,411.56	521,347.54	28,677,791.03	4,725.51	63,002,275.64
23	33,690,198.93	520,087.59	28,614,789.29	4,714.61	62,829,790.41
24	33,581,986.30	518,827.63	28,551,787.55	4,703.71	62,657,305.19
25	33,473,773.67	517,567.68	28,488,785.81	4,692.81	62,484,819.97
IRR	25%	10%	20%	6%	22%
NPV ($)	333,415,072.98	2,622,224.01	255,108,664.61	5,873.59	591,151,835.19
PBP	4.56 Years	11.06 Years	5.73 Years	20.85 Years	5.15 Years
Unit Cost	0.023 $/kWh	0.015$/kWh	2.73$/kg	0.47$/$m^3$	

Chapter 6. Conclusions and Recommendations

6.1 Conclusions

Solar and geothermal based multigeneration systems integrated with the Cu-Cl thermochemical hydrogen production cycle are proposed. Three multigeneration systems are considered to be materialized in Turkey, the United States, and Japan with different scenarios. Multigeneration system 1 is proposed with a PEM type electrolyzer which utilizes electrical energy as the excess electricity of the BiPV plant. Cu-Cl thermochemical hydrogen production cycle subsystem is integrated with the CSP system in multigeneration system 2 and supercritical geothermal system in multigeneration system 3 due to its high-grade heat requirements. The supercritical heating fluid has been utilized to give desired temperatures at high-temperature reactors in the Cu-Cl cycle namely thermolysis and hydrolysis reactors. The top priority of multigeneration systems 2 and 3 is to perform the Cu-Cl cycle safely and reliably.

Therefore, major energy sources are fed to the Cu-Cl cycle primarily, thereafter, excess energy and minor energy sources are exploited to produce several useful outputs as electricity, space heating, and freshwater, and to run auxiliary systems such as tracker systems of the parabolic trough collector, electrolyzer component of Cu-Cl cycle, pumps and compressors.

Recent technologies are employed to enhance commercial viability, sustainability, and feasibility of overall systems. BiPV plants in the enhanced albedo field are utilized in multigeneration systems 1 and 2. The supercritical geotherm field is utilized in multigeneration system 3.

Parametric studies are performed to determine optimum operating conditions and to find the effects of different parameters on system performance. For this reason, different types of albedo and PV modules are used to calculate the BiPV plant's energy gain in three different locations. In multigeneration system 1 in Gokcebayir, bifacial energy gain is found as 23.60%. Conventional PV plant with a tracker system and conventional monocrystalline PV modules in the regular field is found to annually produce 2322MWh of electricity. In contrast, the fourth BiPV plant with a tracker system and bifacial monocrystalline PV modules in the enhanced albedo field is found to annually produce

2870MWH of electricity in Gokcebayir. In Geysers in the United States, bifacial energy gain is found as 21.51%. Conventional PV plant with a tracker system and conventional monocrystalline PV modules in the regular field is found to annually produce 2873MWh of electricity. In contrast, the fourth BiPV plant with a tracker system and bifacial monocrystalline PV modules in the enhanced albedo field is found to annually produce 3491MWH of electricity in Geysers. In multigeneration system 3 in Shinozaki in Japan, bifacial energy gain is found as 25.49%. Conventional PV plant with a tracker system and conventional monocrystalline PV modules in the regular is found to annually produce 1930MWh of electricity. In contrast, the fourth BiPV plant with a tracker system and bifacial monocrystalline PV modules in the enhanced albedo field is found to annually produce 2422MWH of electricity in Shinozaki. BiPV plant simulation has been made for comparison purposes in Geysers location since there is no PV application in multigeneration system 2.

Thermodynamic analyses are conducted for all systems and subsystems. One of the most significant integrations was the integration of the Cu-Cl cycle with a supercritical geothermal system and concentrated solar system. Therefore, more complex analyses are conducted around this cycle in multigeneration system 2 and 3. Cu-Cl cycle conversion efficiency was calculated between 38.1% and 39.8% for multigeneration systems 2 and 3. While multigeneration system 1 is performed at 25.6% energetic efficiency and 12.7% exergetic efficiency, multigeneration system 2 is performed at 27.4% energetic and 17.3% exergetic efficiencies. In multigeneration system 3, 22.8% energetic, and 18.6% exergetic efficiencies are calculated. The climatic differences are also affected by exergetic efficiencies between Shinozaki in Japan and Geysers in the United States. While BSh warm semi-arid climate is effective in Shinozaki in Japan, Dfa warm continental-humid continental climate is effective in Geysers in the United States, according to Köppen–Geiger climatic classification.

The proposed multigeneration systems are suitable for particular locations. Especially multigeneration system 3 has a critical constrain. Multigeneration system 1 can be implemented to all three locations, namely Geysers Geothermal Field, Gokcebayir, and Shinozaki. Multigeneration system 2 can be built in all of these locations; however, it might

be less feasible in lower solar radiation availability. With minimum system change, nuclear integration may create a multigeneration system that covers all over the earth.

The main findings of this thesis study are listed as follows:

- Multigeneration system 1 results in an overall energy efficiency of 25.6% and an overall exergy efficiency of 12.7%. It produces 6,307.2 kg/year of hydrogen. The bifacial gain in multigeneration system 1 is simulated as 23.6% of total PV electricity production.
- In multigeneration system 2, 27.4% energy and 17.3% exergy efficiencies are calculated for the overall system. Cu-Cl thermochemical cycle in multigeneration system 2 produces 296,876 kg/year of hydrogen at 4.67mol/s average molar flow rate. Conversion efficiency is calculated to be 39.8% for the Cu-Cl cycle. 2.208MW average thermal energy rate, and 0.607MW average electrical power rate is calculated as the average loads in the Cu-Cl cycle. Although there is no BiPV plant in multigeneration system 2, for comparison purposes, bifacial gain in Geysers in the United States location is calculated as 21.51% of the total PV electricity production.
- In multigeneration system 3, 22.8% energy and 18.6% exergy efficiencies are calculated for the overall system. Cu-Cl thermochemical cycle in multigeneration system 2 produces 2,144,448 kg/year of hydrogen at 33.58mol/s average molar flow rate. Conversion efficiency is calculated by 38.1% for the Cu-Cl cycle. Cu-Cl cycle as a thermal and electric load in multigeneration system 3, 15.885MW average thermal energy rate, and 5.239MW average electrical power rate is calculated as the loads. Bifacial gain of BiPV application in Shinozaki is calculated as 25.49% of total PV electricity production.
- In multigeneration system 1, the overall system paid off itself in 8.54 years. 14% IRR and 8.8M$ NPV are calculated for the overall system.
- In multigeneration system 2 hydrogen, PBP is calculated as 6 years. It decreased in comparison with 12 years for the hydrogen unit in multigeneration system 1. Overall system PBP is calculated as 6.77 years in the second system. 14% IRR and 237M$ NPV are calculated.

- Among the systems proposed, multigeneration system 3 is found to be the most feasible based on the obtained results with an overall payback period of 5.15 years. Electricity is possessed the best results with 25% IRR, 333.4M$ NPV, and 4.56 years PBP. Hydrogen possessed similar results with multigeneration system 2 in terms of IRR and PBP.

6.2 Recommendations

Three different multigeneration systems are proposed in the current thesis. Cu-Cl thermochemical cycle is integrated with geothermal and solar based systems. As it is mentioned before, technologies and techniques that are studied in this thesis are promising according to reliable projections by 2030 or 2040. Solar and geothermal systems are already having momentum in terms of their growing amount of installed capacities. There is a fast implementation of modern technologies and techniques for solar and geothermal systems. However, the implementation of modern hydrogen techniques and technologies are slower in comparison with solar and geothermal, due to its high requirements at the infrastructural side. However modern societies will require another fuel soon or late. Hydrogen as an environmentally benign fuel will take over the dominancy of fossil-based fuels. Therefore, the transition process is momentous. Implementation of the Cu-Cl thermochemical hydrogen production cycle with a high-temperature heat source is an important step due to its promising results, such as in this thesis.

Recommendations are listed as follows:

- There is a need for, these systems should be experimentally built and tested. Lab-scale and commercial-scale implementations of the proposed systems should be assessed in order to address the practical issues in the real-world environment with all of the real aspects.
- Comprehensive life cycle assessments of these developed systems are necessary in order to understand the total costs and emissions of each proposed multigeneration system and unit. Global warming potential should be determined in order to understand its harmful impacts.
- Developing and investigating of utilization techniques for all useful commodities in the proposed systems are necessary. Various applications should be comparatively

assessed such as fuel cell technologies, hydrogen internal combustion engines, feedstock applications, industrial steel and iron production applications, and chemical substance applications. Fuel cell engines and internal combustion engines should be considered for domestic usage in mobility purposes for residential applications.

- A comprehensive economic analysis including state subsidies and tax incentives should be carried out.

References

[1] Smil V. Energy and civilization: A history. The MIT Press; 2017. doi:10.1353/tech.2018.0067.

[2] Scott H. Whale Oil Culture, Consumerism, and Modern Conservation. Oil Culture 2014:3–18.

[3] Lüthi D, Le Floch M, Bereiter B, Blunier T, Barnola JM, Siegenthaler U, et al. High-resolution carbon dioxide concentration record 650,000-800,000 years before present. Nature 2008;453:379–82. doi:10.1038/nature06949.

[4] International Energy Agency (IEA). The Future of Cooling. Paris: OECD; 2018. doi:10.1787/9789264301993-en.

[5] van Ruijven BJ, De Cian E, Sue Wing I. Amplification of future energy demand growth due to climate change. Nature Communications 2019;10. doi:10.1038/s41467-019-10399-3.

[6] International Energy Agency (IEA). World Energy Outlook 2019. Paris: 2019.

[7] Ballard JR. U.S. Energy Infrastructure: Climate Change Vulnerabilities and Adaptation Efforts. 2015.

[8] Meyer JE. The Renewable Energy Transition. vol. 71. Cham: Springer International Publishing; 2020. doi:10.1007/978-3-030-29115-0.

[9] Demirkan H, Spohrer JC, Welser JJ. Digital Innovation and Strategic Transformation. IT Professional 2016;18:14–8. doi:10.1109/MITP.2016.115.

[10] Butti K, Perlin J. A golden thread: 2500 years of solar architecture and technology. Cheshire books; 1980.

[11] International Energy Agency (IEA). Renewables 2019 2019:1–15. doi:10.1787/b3911209-en.

[12] SolarPower Europe. Global Market Outlook for Solar Power 2020-2024. Global Market Outlook 2020-2024 2020. https://www.solarpowereurope.org/global-market-outlook-2020-2024/ (accessed June 24, 2020).

[13] Dincer I. Green methods for hydrogen production. International Journal of Hydrogen Energy 2012;37:1954–71. doi:10.1016/j.ijhydene.2011.03.173.

[14] Pamela S., Margaret K. ., Life Cycle Assessment of Hydrogen Production via Natural Gas Steam Reforming, Technical Report (NREL/TP-570-27637). National Renewable Energy Laboratory 2001.

[15] Muradov NZ, Veziroğlu TN. From hydrocarbon to hydrogen-carbon to hydrogen

economy. International Journal of Hydrogen Energy 2005;30:225–37. doi:10.1016/j.ijhydene.2004.03.033.

[16] World Energy Outlook 2018. OECD; 2018. doi:10.1787/weo-2018-en.

[17] Veziroglu TN. 21st Century's energy: Hydrogen energy system. NATO Security through Science Series C: Environmental Security, Springer, Dordrecht; 2007, p. 9–31. doi:10.1007/978-1-4020-6442-5_2.

[18] Dincer I. Renewable energy and sustainable development: A crucial review. Renewable & Sustainable Energy Reviews 2000;4:157–75. doi:10.1016/S1364-0321(99)00011-8.

[19] Dincer I, Acar C. A review on clean energy solutions for better sustainability. International Journal of Energy Research 2015;39:585–606. doi:10.1002/er.3329.

[20] Joshi AS, Dincer I, Reddy B V. Performance analysis of photovoltaic systems: A review. Renewable and Sustainable Energy Reviews 2009;13:1884–97. doi:10.1016/j.rser.2009.01.009.

[21] Zhang HL, Baeyens J, Degrève J, Cacères G. Concentrated solar power plants: Review and design methodology. Renewable and Sustainable Energy Reviews 2013;22:466–81. doi:10.1016/j.rser.2013.01.032.

[22] Guerrero-Lemus R, Vega R, Kim T, Kimm A, Shephard LE. Bifacial solar photovoltaics - A technology review. Renewable and Sustainable Energy Reviews 2016;60:1533–49. doi:10.1016/j.rser.2016.03.041.

[23] Branker K, Pathak MJM, Pearce JM. A review of solar photovoltaic levelized cost of electricity. Renewable and Sustainable Energy Reviews 2011;15:4470–82. doi:10.1016/j.rser.2011.07.104.

[24] Fuqiang W, Ziming C, Jianyu T, Yuan Y, Yong S, Linhua L. Progress in concentrated solar power technology with parabolic trough collector system: A comprehensive review. Renewable and Sustainable Energy Reviews 2017;79:1314–28. doi:10.1016/j.rser.2017.05.174.

[25] González-Roubaud E, Pérez-Osorio D, Prieto C. Review of commercial thermal energy storage in concentrated solar power plants: Steam vs. molten salts. Renewable and Sustainable Energy Reviews 2017;80:133–48. doi:10.1016/j.rser.2017.05.084.

[26] Prieto C, Cooper P, Fernández AI, Cabeza LF. Review of technology: Thermochemical energy storage for concentrated solar power plants. Renewable and Sustainable Energy Reviews 2016;60:909–29. doi:10.1016/j.rser.2015.12.364.

[27] Breede K, Dzebisashvili K, Liu X, Falcone G. A systematic review of enhanced (or engineered) geothermal systems: past, present and future. Geothermal Energy 2013;1:4. doi:10.1186/2195-9706-1-4.

[28] Olasolo P, Juárez MC, Morales MP, Damico S, Liarte IA. Enhanced geothermal systems (EGS): A review. Renewable and Sustainable Energy Reviews 2016;56:133–44. doi:10.1016/j.rser.2015.11.031.

[29] Carnot S. Réflexions sur la puissance motrice du feu et sur les machines propres à développer cette puissance. Annales Scientifiques de l'École Normale Supérieure 1872;1:393–457. doi:10.24033/asens.88.

[30] Clausius R. Ueber die Anwendung der mechanischen Wärmetheorie auf die Dampfmaschine. Annalen Der Physik Und Chemie 1856;173:441–76. doi:10.1002/andp.18561730306.

[31] Hutchison K. W. J. M. Rankine and the Rise of Thermodynamics. The British Journal for the History of Science n.d.;14:1–26. doi:10.2307/4026070.

[32] Smith IK. Development of the Trilateral Flash Cycle System: Part 1: Fundamental Considerations. Proceedings of the Institution of Mechanical Engineers, Part A: Journal of Power and Energy 1993;207:179–94. doi:10.1243/pime_proc_1993_207_032_02.

[33] Smith IK, da Silva RPM. Development of the Trilateral Flash Cycle System Part 2: Increasing Power Output with Working Fluid Mixtures. Proceedings of the Institution of Mechanical Engineers, Part A: Journal of Power and Energy 1994;208:135–44. doi:10.1243/pime_proc_1994_208_022_02.

[34] Smith IK, Stošić N, Aldis CA. Development of the trilateral flash cycle system. Part 3: The design of high-efficiency two-phase screw expanders. Proceedings of the Institution of Mechanical Engineers, Part A: Journal of Power and Energy 1996;210:75–92. doi:10.1243/pime_proc_1996_210_010_02.

[35] Fischer J. Comparison of trilateral cycles and organic Rankine cycles. Energy 2011;36:6208–19. doi:10.1016/j.energy.2011.07.041.

[36] Zamfirescu C, Dincer I. Thermodynamic analysis of a novel ammonia-water trilateral Rankine cycle. Thermochimica Acta 2008;477:7–15. doi:10.1016/j.tca.2008.08.002.

[37] Dincer I, Acar C. Review and evaluation of hydrogen production methods for better sustainability. International Journal of Hydrogen Energy 2014;40:11094–111. doi:10.1016/j.ijhydene.2014.12.035.

[38] Rosen MA. Advances in hydrogen production by thermochemical water

decomposition: A review. Energy 2010;35:1068–76. doi:10.1016/j.energy.2009.06.018.

[39] Shah A, Torres P, Tscharner R, Wyrsch N, Keppner H. Photovoltaic technology: The case for thin-film solar cells. Science 1999;285:692–8. doi:10.1126/science.285.5428.692.

[40] Razykov TM, Ferekides CS, Morel D, Stefanakos E, Ullal HS, Upadhyaya HM. Solar photovoltaic electricity: Current status and future prospects. Solar Energy 2011;85:1580–608. doi:10.1016/j.solener.2010.12.002.

[41] Kumar R, Rosen MA. A critical review of photovoltaic-thermal solar collectors for air heating. Applied Energy 2011;88:3603–14. doi:10.1016/j.apenergy.2011.04.044.

[42] Joshi AS, Dincer I, Reddy B V. Analysis of energy and exergy efficiencies for hybrid PV/T systems. International Journal of Low-Carbon Technologies 2011;6:64–9. doi:10.1093/ijlct/ctq045.

[43] Joshi AS, Tiwari A, Tiwari GN, Dincer I, Reddy B V. Performance evaluation of a hybrid photovoltaic thermal (PV/T) (glass-to-glass) system. International Journal of Thermal Sciences 2009;48:154–64. doi:10.1016/j.ijthermalsci.2008.05.001.

[44] Rosell JI, Vallverdú X, Lechón MA, Ibáñez M. Design and simulation of a low concentrating photovoltaic/thermal system. Energy Conversion and Management 2005;46:3034–46. doi:10.1016/j.enconman.2005.01.012.

[45] Zhao J, Song Y, Lam WH, Liu W, Liu Y, Zhang Y, et al. Solar radiation transfer and performance analysis of an optimum photovoltaic/thermal system. Energy Conversion and Management 2011;52:1343–53. doi:10.1016/j.enconman.2010.09.032.

[46] Agrawal B, Tiwari GN. Optimizing the energy and exergy of building integrated photovoltaic thermal (BIPVT) systems under cold climatic conditions. Applied Energy 2010;87:417–26. doi:10.1016/j.apenergy.2009.06.011.

[47] Liang TS, Pravettoni M, Deline C, Stein JS, Kopecek R, Singh JP, et al. A review of crystalline silicon bifacial photovoltaic performance characterisation and simulation. Energy and Environmental Science 2019;12:116–48. doi:10.1039/c8ee02184h.

[48] Castillo-Aguilella JE, Hauser PS. Multi-Variable Bifacial Photovoltaic Module Test Results and Best-Fit Annual Bifacial Energy Yield Model. IEEE Access 2016;4:498–506. doi:10.1109/access.2016.2518399.

[49] Stein JS, Riley D, Lave M, Hansen C, Deline C, Toor F. Outdoor Field

Performance from Bifacial Photovoltaic Modules and Systems, Institute of Electrical and Electronics Engineers (IEEE); 2018, p. 3184–9. doi:10.1109/pvsc.2017.8366042.

[50] Chudinzow D, Haas J, Díaz-Ferrán G, Moreno-Leiva S, Eltrop L. Simulating the energy yield of a bifacial photovoltaic power plant. Solar Energy 2019;183:812–22. doi:10.1016/j.solener.2019.03.071.

[51] Wang S, Wilkie O, Lam J, Steeman R, Zhang W, Khoo KS, et al. Bifacial Photovoltaic Systems Energy Yield Modelling. Energy Procedia, vol. 77, Elsevier Ltd; 2015, p. 428–33. doi:10.1016/j.egypro.2015.07.060.

[52] Valdivia CE, Li CT, Russell A, Haysom JE, Li R, Lekx D, et al. Bifacial Photovoltaic Module Energy Yield Calculation and Analysis. 2017 IEEE 44th Photovoltaic Specialist Conference (PVSC), 2017, p. 1094–9. doi:10.1109/pvsc.2017.8366206.

[53] Appelbaum J. Bifacial photovoltaic panels field. Renewable Energy 2016;85:338–43. doi:10.1016/j.renene.2015.06.050.

[54] Guo S, Walsh TM, Peters M. Vertically mounted bifacial photovoltaic modules: A global analysis. Energy 2013;61:447–54. doi:10.1016/j.energy.2013.08.040.

[55] Deline C, Macalpine S, Marion B, Toor F, Asgharzadeh A, Stein JS. Assessment of Bifacial Photovoltaic Module Power Rating Methodologies-Inside and Out. IEEE Journal of Photovoltaics 2017;7:575–80. doi:10.1109/jphotov.2017.2650565.

[56] Castillo-Aguilella JE, Hauser PS. Bifacial photovoltaic module best-fit annual energy yield model with azimuthal correction. Conference Record of the IEEE Photovoltaic Specialists Conference, vol. 2016- November, Institute of Electrical and Electronics Engineers Inc.; 2016, p. 3109–12. doi:10.1109/pvsc.2016.7750238.

[57] Drury E, Lopez A, Denholm P, Margolis R. Relative performance of tracking versus fixed tilt photovoltaic systems in the USA. Progress in Photovoltaics: Research and Applications 2013;22:n/a-n/a. doi:10.1002/pip.2373.

[58] AL-Rousan N, Isa NAM, Desa MKM. Advances in solar photovoltaic tracking systems: A review. Renewable and Sustainable Energy Reviews 2018;82:2548–69. doi:10.1016/j.rser.2017.09.077.

[59] Kaur T, Mahajan S, Verma S, Priyanka, Gambhir J. Arduino based low cost active dual axis solar tracker. 1st IEEE International Conference on Power Electronics, Intelligent Control and Energy Systems, ICPEICES 2016, Institute of Electrical and Electronics Engineers Inc.; 2017. doi:10.1109/icpeices.2016.7853398.

[60] Morón C, Ferrández D, Saiz P, Vega G, Díaz J. New Prototype of Photovoltaic Solar Tracker Based on Arduino. Energies 2017;10:1298. doi:10.3390/en10091298.

[61] Ferroudji F, Ouattas T, Khelifi C. Design, modeling and finite element static analysis of a new two axis solar tracker using SolidWorks/COSMOSWorks. Applied Mechanics and Materials, vol. 446, Trans Tech Publ; 2014, p. 738–43.

[62] Sahu A, Yadav N, Sudhakar K. Floating photovoltaic power plant: A review. Renewable and Sustainable Energy Reviews 2016;66:815–24. doi:10.1016/j.rser.2016.08.051.

[63] Trapani K, Redón Santafé M. A review of floating photovoltaic installations: 2007–2013. Progress in Photovoltaics: Research Applications 2015;23:524–32. doi:10.1002/pip.2466.

[64] Cazzaniga R, Cicu M, Rosa-Clot M, Rosa-Clot P, Tina GM, Ventura C. Floating photovoltaic plants: Performance analysis and design solutions. Renewable and Sustainable Energy Reviews 2018;81:1730–41. doi:10.1016/j.rser.2017.05.269.

[65] Liu L, Wang Q, Lin H, Li H, Sun Q, Wennersten R. Power Generation Efficiency and Prospects of Floating Photovoltaic Systems. Energy Procedia, vol. 105, Elsevier Ltd; 2017, p. 1136–42. doi:10.1016/j.egypro.2017.03.483.

[66] Choi Y-K, Lee N-H, Lee A-K, Kim K-J. A study on major design elements of tracking-type floating photovoltaic systems. International Journal of Smart Grid and Clean Energy 2014;3:70–4. doi:10.12720/sgce.3.1.70-74.

[67] Redón Santafé M, Torregrosa Soler JB, Sánchez Romero FJ, Ferrer Gisbert PS, Ferrán Gozálvez JJ, Ferrer Gisbert CM. Theoretical and experimental analysis of a floating photovoltaic cover for water irrigation reservoirs. Energy 2014;67:246–55. doi:10.1016/j.energy.2014.01.083.

[68] Temiz M, Javani N. Design and analysis of a combined floating photovoltaic system for electricity and hydrogen production. International Journal of Hydrogen Energy 2020;45:3457–69. doi:10.1016/j.ijhydene.2018.12.226.

[69] Henemann A. BIPV: Built-in solar energy. Renewable Energy Focus 2008;9:14–9. doi:10.1016/S1471-0846(08)70179-3.

[70] Peng C, Huang Y, Wu Z. Building-integrated photovoltaics (BIPV) in architectural design in China. Energy and Buildings 2011;43:3592–8. doi:10.1016/j.enbuild.2011.09.032.

[71] Yoon JH, Song J, Lee SJ. Practical application of building integrated photovoltaic (BIPV) system using transparent amorphous silicon thin-film PV module. Solar

Energy 2011;85:723–33. doi:10.1016/j.solener.2010.12.026.

[72] Heinstein P, Ballif C, Perret-Aebi LE. Building integrated photovoltaics (BIPV): Review, potentials, barriers and myths. Green 2013;3:125–56. doi:10.1515/green-2013-0020.

[73] Shukla AK, Sudhakar K, Baredar P. Recent advancement in BIPV product technologies: A review. Energy and Buildings 2017;140:188–95. doi:10.1016/j.enbuild.2017.02.015.

[74] Biyik E, Araz M, Hepbasli A, Shahrestani M, Yao R, Shao L, et al. A key review of building integrated photovoltaic (BIPV) systems. Engineering Science and Technology, an International Journal 2017;20:833–58. doi:10.1016/j.jestch.2017.01.009.

[75] Liu B, Duan S, Cai T. Photovoltaic DC-building-module-based BIPV system-concept and design considerations. IEEE Transactions on Power Electronics 2011;26:1418–29. doi:10.1109/tpel.2010.2085087.

[76] Yang T, Athienitis AK. A review of research and developments of building-integrated photovoltaic/thermal (BIPV/T) systems. Renewable and Sustainable Energy Reviews 2016;66:886–912. doi:10.1016/j.rser.2016.07.011.

[77] Chae YT, Kim J, Park H, Shin B. Building energy performance evaluation of building integrated photovoltaic (BIPV) window with semi-transparent solar cells. Applied Energy 2014;129:217–27. doi:10.1016/j.apenergy.2014.04.106.

[78] Stein WH, Buck R. Advanced power cycles for concentrated solar power. Solar Energy 2017;152:91–105. doi:10.1016/j.solener.2017.04.054.

[79] Pikra G, Salim A, Prawara B, Purwanto AJ, Admono T, Eddy Z. Development of small scale concentrated solar power plant using organic Rankine cycle for isolated region in Indonesia. Energy Procedia, vol. 32, Elsevier Ltd; 2013, p. 122–8. doi:10.1016/j.egypro.2013.05.016.

[80] Dunham MT, Iverson BD. High-efficiency thermodynamic power cycles for concentrated solar power systems. Renewable and Sustainable Energy Reviews 2014;30:758–70. doi:10.1016/j.rser.2013.11.010.

[81] Carlino S, Somma R, Troiano A, Di Giuseppe MG, Troise C, De Natale G. The geothermal system of Ischia Island (southern Italy): Critical review and sustainability analysis of geothermal resource for electricity generation. Renewable Energy 2014;62:177–96. doi:10.1016/j.renene.2013.06.052.

[82] Zhai H, Shi L, An Q. Influence of working fluid properties on system performance and screen evaluation indicators for geothermal ORC (organic Rankine cycle)

system. Energy 2014;74:2–11. doi:10.1016/j.energy.2013.12.030.

[83] Campos Rodríguez CE, Escobar Palacio JC, Venturini OJ, Silva Lora EE, Cobas VM, Marques Dos Santos D, et al. Exergetic and economic comparison of ORC and Kalina cycle for low temperature enhanced geothermal system in Brazil. Applied Thermal Engineering 2013;52:109–19. doi:10.1016/j.applthermaleng.2012.11.012.

[84] Fallah M, Mahmoudi SMS, Yari M, Akbarpour Ghiasi R. Advanced exergy analysis of the Kalina cycle applied for low temperature enhanced geothermal system. Energy Conversion and Management 2016;108:190–201. doi:10.1016/j.enconman.2015.11.017.

[85] Calise F, D'Accadia MD, MacAluso A, Piacentino A, Vanoli L. Exergetic and exergoeconomic analysis of a novel hybrid solar-geothermal polygeneration system producing energy and water. Energy Conversion and Management 2016;115:200–20. doi:10.1016/j.enconman.2016.02.029.

[86] Al-Ali M, Dincer I. Energetic and exergetic studies of a multigeneration solar-geothermal system. Applied Thermal Engineering 2014;71:16–23. doi:10.1016/j.applthermaleng.2014.06.033.

[87] Lund JW, Bjelm L, Bloomquist G, Mortensen and AK. Characteristics, development and utilization of geothermal resources – a Nordic perspective. Episodes 2008;31:140–7.

[88] Lu SM. A global review of enhanced geothermal system (EGS). Renewable and Sustainable Energy Reviews 2018;81:2902–21. doi:10.1016/j.rser.2017.06.097.

[89] Reinsch T, Dobson P, Asanuma H, Huenges E, Poletto F, Sanjuan B. Utilizing supercritical geothermal systems: a review of past ventures and ongoing research activities. Geothermal Energy 2017;5:1–25. doi:10.1186/s40517-017-0075-y.

[90] Elders WA, Frioleifsson GO, Albertsson A. Drilling into magma and the implications of the Iceland Deep Drilling Project (IDDP) for high-temperature geothermal systems worldwide. Geothermics 2014;49:111–8. doi:10.1016/j.geothermics.2013.05.001.

[91] Friðleifsson GÓ, Elders WA. Successful drilling for supercritical geothermal resources at Reykjanes in SW Iceland. Trans Geotherm Resour Council 2017;41:1095–106.

[92] Ásmundsson R, Pezard P, Sanjuan B, Henninges J, Deltombe JL, Halladay N, et al. High temperature instruments and methods developed for supercritical geothermal reservoir characterisation and exploitation-The HiTI project.

Geothermics 2014;49:90–8. doi:10.1016/j.geothermics.2013.07.008.

[93] Shnell J, Elders WA, Orcutt J, Osborn WL. Exploration and development of supercritical geothermal resources on the ocean floor. Proceedings, 2019.

[94] Scott S, Driesner T, Weis P. Geologic controls on supercritical geothermal resources above magmatic intrusions. Nature Communications 2015;6:7837. doi:10.1038/ncomms8837.

[95] Stimac J, Wilmarth M, Mandeno PE, Dobson P, Winick J. Review of Exploitable Supercritical Geothermal Resources to 5 km at Geysers-Clear Lake, Salton Sea, and Coso. Geothermal Resources Council Transactions 2017;41.

[96] Tsuchiya N, Yamada R, Uno M. Supercritical geothermal reservoir revealed by a granite–porphyry system. Geothermics 2016;63:182–94. doi:10.1016/j.geothermics.2015.12.011.

[97] Radulovic J, Beleno Castaneda NI. On the potential of zeotropic mixtures in supercritical ORC powered by geothermal energy source. Energy Conversion and Management 2014;88:365–71. doi:10.1016/j.enconman.2014.08.048.

[98] Turner JA. Sustainable Hydrogen Production. Science 2004;305:972 LP – 974. doi:10.1126/science.1103197.

[99] Acar C, Dincer I. Comparative assessment of hydrogen production methods from renewable and non-renewable sources. International Journal of Hydrogen Energy 2014;39:1–12. doi:10.1016/j.ijhydene.2013.10.060.

[100] Bolton JR. Solar photoproduction of hydrogen: A review. Solar Energy 1996;57:37–50. doi:10.1016/0038-092X(96)00032-1.

[101] Turner J, Sverdrup G, Mann MK, Maness PC, Kroposki B, Ghirardi M, et al. Renewable hydrogen production. International Journal of Energy Research 2008;32:379–407. doi:10.1002/er.1372.

[102] Holladay JD, Hu J, King DL, Wang Y. An overview of hydrogen production technologies. Catalysis Today 2009;139:244–60. doi:10.1016/j.cattod.2008.08.039.

[103] Sherif SA, Barbir F, Veziroglu TN. Wind energy and the hydrogen economy-review of the technology. Solar Energy 2005;78:647–60. doi:10.1016/j.solener.2005.01.002.

[104] Wentorf RH, Hanneman RE. Thermochemical hydrogen generation. Science 1974;185:311–9. doi:10.1126/science.185.4148.311.

[105] Steinfeld A. Solar thermochemical production of hydrogen - A review. Solar

Energy 2005;78:603–15. doi:10.1016/j.solener.2003.12.012.

[106] Naterer GF, Suppiah S, Stolberg L, Lewis M, Wang Z, Daggupati V, et al. Canada's program on nuclear hydrogen production and the thermochemical Cu-Cl cycle. International Journal of Hydrogen Energy 2010;35:10905–26. doi:10.1016/j.ijhydene.2010.07.087.

[107] Funk JE. Thermochemical hydrogen production: Past and present. International Journal of Hydrogen Energy 2001;26:185–90. doi:10.1016/S0360-3199(00)00062-8.

[108] Beghi GE. A decade of research on thermochemical hydrogen at the Joint Research Centre, Ispra. International Journal of Hydrogen Energy 1986;11:761–71. doi:10.1016/0360-3199(86)90172-2.

[109] Ozbilen A, Dincer I, Rosen MA. Development of a four-step Cu-Cl cycle for hydrogen production - Part I: Exergoeconomic and exergoenvironmental analyses. International Journal of Hydrogen Energy 2016;41:7814–25. doi:10.1016/j.ijhydene.2015.12.184.

[110] Ozbilen A, Dincer I, Rosen MA. Development of a four-step Cu-Cl cycle for hydrogen production - Part II: Multi-objective optimization. International Journal of Hydrogen Energy 2016;41:7826–34. doi:10.1016/j.ijhydene.2015.12.104.

[111] Guo XM, Trably E, Latrille E, Carrre H, Steyer JP. Hydrogen production from agricultural waste by dark fermentation: A review. International Journal of Hydrogen Energy 2010;35:10660–73. doi:10.1016/j.ijhydene.2010.03.008.

[112] Yilmaz C, Kanoglu M, Abusoglu A. Exergetic cost evaluation of hydrogen production powered by combined flash-binary geothermal power plant. International Journal of Hydrogen Energy 2015;40:14021–30. doi:10.1016/j.ijhydene.2015.07.031.

[113] Yuksel YE, Ozturk M. Thermodynamic and thermoeconomic analyses of a geothermal energy based integrated system for hydrogen production. International Journal of Hydrogen Energy 2017;42:2530–46. doi:10.1016/j.ijhydene.2016.04.172.

[114] Yilmaz C, Kanoglu M. Thermodynamic evaluation of geothermal energy powered hydrogen production by PEM water electrolysis. Energy 2014;69:592–602. doi:10.1016/j.energy.2014.03.054.

[115] Ratlamwala TAH, Dincer I. Comparative energy and exergy analyses of two solar-based integrated hydrogen production systems. International Journal of Hydrogen Energy 2015;40:7568–78. doi:10.1016/j.ijhydene.2014.10.123.

[116] Meteonorm V 7.2 – PVsyst n.d. https://www.pvsyst.com/meteo-data-source/ (accessed June 10, 2020).

[117] Uihlein, Andreas (2018): JRC Geothermal Power Plant Dataset. European Commission, Joint Research Centre (JRC) [Dataset] PID: http://data.europa.eu/89h/jrc-10128-10001. n.d.

[118] Global Solar Atlas 2.0, a free, web-based application is developed and operated by the company Solargis s.r.o. on behalf of the World Bank Group, utilizing Solargis data.